

Alma Mater Studiorum – Università di Bologna

DOTTORATO DI RICERCA IN  
ONCOLOGIA E PATOLOGIA SPERIMENTALE

Ciclo XXVII

**Settore Concorsuale di afferenza: 06/A2**

**Settore Scientifico disciplinare: MED/04**

RIBOSOME-INACTIVATING PROTEINS AND THEIR  
IMMUNOTOXINS FOR CANCER THERAPY:  
INSIGHTS INTO THE MECHANISM OF CELL DEATH

**Presentata da: Dott. Daniele Mercatelli**

**Coordinatore Dottorato**

**Relatore**

**Chiar.mo Prof. Pier Luigi Lollini**

**Chiar.mo Prof. Andrea Bolognesi**

**Esame finale anno 2015**



## TABLE OF CONTENTS

<b>ABBREVIATIONS</b>	III
<b>SUMMARY</b>	V
<b>CHAPTER I: INTRODUCTION</b>	1
INTRODUCTION	3
1. Ribosome-inactivating proteins (RIPs)	3
2. Classification of RIPs	4
2.1 Type 1 RIPs	5
2.2 Type 2 RIPs	8
2.3 Type 3 RIPs	11
3. Interaction of RIPs with cells: mechanism of entry	11
4. Biological activities of RIPs	12
4.1 Glycosylase activity	12
4.2 RIPs and apoptosis	14
4.2.1 <i>Apoptosis induction by ribotoxic stress response</i>	14
4.2.2 <i>RIP-induced ER-stress and the activation of UPR genes</i>	16
4.2.3 <i>Oxidative stress</i>	17
4.3 Antiviral activity	18
5. RIPs employment in experimental and clinical medicine	19
5.1 RIP-containing immunotoxins in anti-tumor therapy	19
5.2 Clinical Trials in cancer diseases	21
5.3 Immunotoxins in autoimmune disorders	22
<b>CHAPTER II: MATERIALS AND METHODS</b>	24
2.1 Materials	26
2.2 Methods	30

<b>CHAPTER III: <i>IN VITRO</i> COMPARISON OF ANTITUMOR ACTIVITY OF SAPORIN-BASED IMMUNOTOXINS</b>	36
BACKGROUND	38
AIM OF THE PROJECT	41
RESULTS	43
DISCUSSION	61
<b>CHAPTER IV: EVALUATION OF EARLY CHANGES INDUCED BY STENODACTYLIN IN AML CELLS</b>	65
BACKGROUND	67
AIM OF THE PROJECT	69
RESULTS	70
DISCUSSION	92
<b>CHAPTER V: REFERENCES</b>	95
REFERENCES	97

## ABBREVIATIONS

ADCC	Antibody-dependent cellular cytotoxicity
AML	Acute monocytic leukemia
AOP-1	Antioxidant protein-1
AP-1	Activator protein-1
ATF	Activating transcription factor
B-CLL	B-cell lymphoblastic leukemia
BiP	Binding immunoglobulin protein (also GRP78)
CA	Correspondece analysis
CDC	Complement-dependent cytotoxicity
CHOP	Cyclophosphamide, adriamycin, oncovin, prednisone
CRE	cAMP-responsive element
CTCL	Cutaneous T-cell lymphoma
DUSP1	Dual specificity protein phosphatase 1
EF1	Elongation factor 1
EF2	Elongation factor 2
EGR-1	Early growth response-1
eIF2 $\alpha$	Eukaryotic translation initiation factor two subunit $\alpha$
ER	Endoplasmic reticulum
ERAD	ER-associated degradation pathway
ERK	Extracellular signal-regulated kinase
FDA	Food and Drug administration
FDR	False discovery rate
FLU	Fludarabine
GO	Gene-onthology
GVHD	Graft-versus host disease
Hck	Hematopoietic cell kinase
HCMV	Human DNA virus cytomegalovirus
HTLV-1	Human T-cell leukemia virus 1
IL-1B	Interleukin-1B
IL-8	Interleukin-8

IRE1	Inositol-requiring ER to nucleus signal kinase-1
IT	Immunotoxin
JNK	c-Jun NH2-terminal
mAb	Monoclonal antibody
MAPK	Mitogen-activated protein kinase
MCMV	Murine cytomegalovirus
MCL	mantle cell lymphoma
MLII	Mistletoe lectin II
NAC	N-Acetyl-l-cysteine
NHL	Non-Hodgkin's lymphoma
PAP	Pokeweed antiviral protein
PBS	Phosphate-buffered saline
PCI	Photochemical internalization
PERK	Protein kinase-like ER kinase
PKR	Double-stranded RNA activated protein kinase
RCA	<i>Ricinus communis</i> agglutinin
RIP	Ribosome-inactivating protein
ROS	Reactive oxygen species
SAM	Significance analysis of microarrays
scFv	Single-chain variable fragment
SRL	Sarcin/ricin loop
UPR	Unfolded protein response
UPS	Ubiquitin-proteasome system
VLS	Vascular leak syndrome
XBP-1	X-box binding protein 1
ZAK	Zipper sterile alpha motif kinase

## SUMMARY

Ribosome-inactivating proteins (RIPs) are a family of plant toxic enzymes that permanently damage ribosomes and possibly other cellular substrates, thus causing cell death involving different and still not completely understood pathways. The high cytotoxic activity showed by many RIPs makes them ideal candidates for the production of immunotoxins (ITs), chimeric proteins designed for the selective elimination of unwanted or malignant cells. Saporin-S6, a type 1 RIP extracted from *Saponaria officinalis* L. seeds, has been extensively utilized to construct anticancer conjugates because of its high enzymatic activity, stability and resistance to conjugation procedures, resulting in the efficient killing of target cells.

This thesis investigates the anticancer properties of two saporin-based ITs, anti-CD20 RTX/S6 and anti-CD22 OM124/S6, designed for the experimental treatment of B-cell NHLs, and the possibility to enhance their cytotoxic effects using proteasome inhibitors or fludarabine. The experiments demonstrate that both ITs shows high cytotoxicity towards CD20-positive B-cells, and their antitumor efficacy might be enhanced synergistically by a combined treatment with proteasome inhibitors or fludarabine. Furthermore, the two ITs show differences in potency and ability to activate effector caspases, and a different behavior in the presence of ROS scavenger catalase. Taken together, these results suggest that the different carriers employed to target saporin might influence saporin intracellular routing and saporin-induced cell death mechanisms.

We also investigate the early cellular response to stenodactylin, a recently discovered highly toxic type 2 RIP which represents an interesting candidate for the design and production of a new IT for the experimental treatment of cancer. The gene expression microarray analysis shows an enhanced transcription of genes regulating cellular processes like cellular response to stress and cell death in stenodactylin-treated acute monocytic leukemia cells and the activation of p38 and JNK MAPKs signaling. These informations could be useful to design a highly specific stenodactylin-based IT for the experimental treatment of hematological malignancies and to design combination therapies to further enhance ITs cytotoxicity.



*Chapter I*

**INTRODUCTION**



## INTRODUCTION

### 1. Ribosome-inactivating proteins (RIPs)

The term “ribosome-inactivating proteins” (RIPs) was introduced to designate plant proteins that inactivate animal ribosomes. Firstly discovered over a century ago in the castor oil plant *Ricinus communis* after the characterization of ricin, RIPs have become of great scientific interest due to their importance in human health, either as pathogens or as potential therapeutics. RIPs form a family of well-characterized toxins that specifically and irreversibly inhibit protein synthesis in eukaryotic cells by altering the 28S rRNA of the large 60S ribosomal subunit. The term RIPs was introduced by Stirpe to define plant proteins that inactivate animal ribosomes, in a period when the details of their enzymatic activity and structure were still unknown (Stirpe *et al.*, 1982). The designation “RIP” can be associated with their enzymatic activity, namely RNA *N*-glycosylase activity. Widely distributed in nature, RIPs have been found predominantly in plants, bacteria and fungi, often in multiple isoforms (Stirpe, 2013). Most of them are produced by plants, where their physiological role is still controversial. It has been hypothesized that plants accumulate RIPs in some of their tissues as a defensive mechanism against biotic and abiotic stresses (Nielsen *et al.*, 2001; Polito *et al.*, 2013b). Well-known examples of plant-derived RIPs include ricin, abrin, ebulin, nigrin, saporin, trichosanthin and volkensin. Bacterial RIPs include Shiga and Shiga-like toxins, which are part of the AB<sub>5</sub> enterotoxin family and are produced by gram-negative pathogenic bacteria as virulence factors in order to aid their survival and replication in the host organism (Walsh *et al.*, 2013). RIPs have been also purified from several mushroom species, including *Calvatia caelata*, *Flammulina velutipes*, *Hypsizigus marmoreus*, *Lyophyllum shimeiji*, and *Pleurotus tuber-regium* (Xu *et al.*, 2011). Notable example of RIP from mushrooms is represented by  $\alpha$ -sarcin, isolated from *Aspergillus giganteus*.

Small doses of some of these toxins can be lethal through injection, ingestion or inhalation and can trigger irreversible inhibition of host cellular protein synthesis accompanied by diffuse inflammation and acute necrosis of affected tissues. RIPs elevated cytotoxic activity together with the development of monoclonal antibodies (mAbs) as tools for the identification and targeting of specific cell surface marker, made

this class of proteins of great interest as possible candidates for the production of immunotoxins (ITs). ITs are chimeric proteins that consists of a targeting portion (usually a mAb) linked to a toxin, designed for the selective elimination of unwanted or malignant cells.

Furthermore, RIPs also possess antiviral and antifungal properties that can be exploited in human therapy and agriculture. For these reasons, current biotechnological research into RIPs is focused into the better understanding and subsequent improvement of the cell entry mechanism, reducing RIP antigenicity, prolonging their plasma half-life and elucidating the mechanism of RIP-induced cell death (Puri *et al.*, 2012).

## 2. Classification of RIPs

Plant RIPs are currently classified into three groups based on their physical properties and the presence or absence of a lectin-like chain. A schematic representation showing a comparison of the characteristic primary structure of the three groups is given in fig. 1.

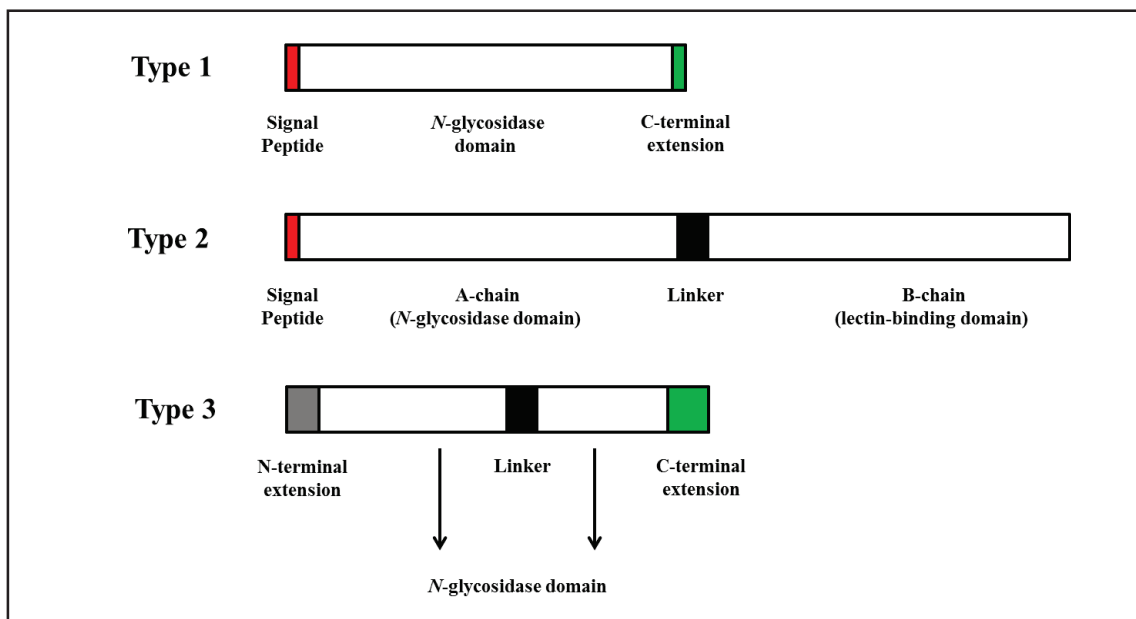


**Fig. 1** Schematic representation showing a comparison primary structure of the three RIP groups. Blank boxes show regions present in the mature form of the enzymes. Modified from Van Damme *et al.*, 2001.

## 2.1 Type 1 RIPs

The majority of RIPs discovered so far actually belong to type 1 and are preferentially distributed within particular plant families such as *Caryophyllaceae*, *Cucurbitaceae* and *Euphorbiaceae* (Stirpe, 2004). Notably examples of type 1 RIPs are pokeweed antiviral protein (PAP, (from *Phytolacca Americana*)), saporin (from *Saponaria officinalis* L.), dianthin (from *Dianthus caryophyllus*), momordin (from *Momordica charantia*) and gelonin (from *Gelonium multiflorum*). Type 1 RIPs are single-chain basic enzymes (usually showing a  $pI \geq 9$ ) with an approximate molecular weight of 30 kDa. Most of them are synthesized as pre-proteins composed of a signal peptide, the mature protein and a C-terminal extension (Fig. 1), as demonstrated by different studies on protein and DNA sequences (Nielsen *et al.*, 2001). It is likely that the synthesis of type 1 RIPs follows the secretory pathway, so that these cytotoxic proteins are segregated into the vacuoles or other extra-cytoplasmatic compartment, but detailed localization studies are available only for a few type 1 RIPs (Van Damme *et al.*, 2001). It has been shown that in pokeweed leaves, for example, PAP is primarily located in the cell wall matrix and a small amount in the vacuole (Ready *et al.*, 1986); while in *Saponaria officinalis* seeds, saporin is mainly located in the intercellular spaces, between the primary cell wall and the plasmalemma and the vacuole of the periplasmic cells (Carzaniga *et al.*, 1994).

Type 1 RIPs are generally purified from plant tissues by cation-exchange chromatography on carboxymethyl or sulfopropyl-derivatized matrices, taking advantage of their  $pI$  in the alkaline region (Barbieri *et al.*, 1987).

**Table 1:** type 1 RIPs from plant, modified from Gilabert-Oriol *et al.*, 2014.

Plant	RIP	Absolute molecular mass (kDa)
<i>Abelmoschus esculentus</i> (L.) Moench	Abelesculin	30
<i>Adenia ellenbeckii</i> Harms	<i>Adenia ellenbeckii</i> RIP	30
<i>Adenia goetzii</i> Burt-Davy	<i>Adenia goetzii</i> RIP	30

<i>Adenia racemosa</i> W.J. de Wilde	<i>Adenia racemosa</i> RIP	30
<i>Adenia venenata</i> Forssk.	<i>Adenia venenata</i> RIP	30
<i>Agrostemma githago</i> L.	Agrostin-2; agrostin-5; agrostin 6	30.6; 29.5; 29.6
<i>Amaranthus caudatus</i> L.	Amaranthin ( <i>Amaranthus caudatus</i> agglutinin, ACA)	33-36
<i>Amaranthus tricolor</i> L.	<i>Amaranthus tricolor</i> antiviral protein-27 (AAP-27)	27
<i>Amaranthus viridis</i> L.	Amaranthin	30
<i>Asparagus officinalis</i> L.	<i>Asparagus officinalis</i> RIP; asparin 1; asparin 2	32.5; 30.5; 29.8
<i>Basella rubra</i> Roxb.	<i>Basella rubra</i> RIP 2a; <i>Basella rubra</i> RIP 2b; <i>Basella rubra</i> RIP 3	30.6; 31.2; 31.2
<i>Benincasa hispida</i> (Thunb.) Cogn.	Hispin	21
<i>Beta vulgaris</i> L.	Betavulgin; beetin 27; beetin 29	28; 27; 29
<i>Bougainvillea spectabilis</i> Willd.	Bouganin ( <i>Bougainvillea spectabilis</i> RIP)	26.2
<i>Bougainvillea xbuttiana</i> Willd.	<i>Bougainvillea xbuttiana</i> antiviral protein	35.5
<i>Bryonia dioica</i> Jacq.	Bryodin-L; bryodin-1 (BD-1); bryodin-2 (BD-2)	28.8; 30; 27
<i>Celosia cristata</i> L.	<i>Celosia cristata</i> antiviral protein 25 (CCP-25); <i>Celosia cristata</i> antiviral protein 27 (CCP-27)	25; 27
<i>Charybdis maritima</i> L.	Charybdin	29
<i>Chenopodium album</i> L.	<i>Chenopodium album</i> antiviral RIP (CAP30)	30
<i>Cinnamomum camphora</i> (L.) J. Presl.	Camphorin	23
<i>Citrullus colocynthis</i> Schrad.	Colocin 1; colocin2	26.3; 26.3
<i>Clerodendrum inerme</i> (L.) Gaertn	CIP-29; CIP-34	29; 34
<i>Croton tiglium</i> L.	Croton I; croton II	ND; 34
<i>Cucumis figarei</i> Naud.	<i>Cucumis figarei</i> RIP (CF-RIP)	31.8
<i>Cucumis melo</i> L.	Melonin	23.5
<i>Cucurbita moschata</i> Duchesne ex Poir.	Moschatin; cucurmosin (CUS); cucurmosin 2; <i>Cucurbita moschata</i> RIP	29; 27; 27.2; 30.7
<i>Cucurbita pepo</i> L.	Pepocin	26
<i>Cucurbita texana</i> (Scheele) A. Gray	Texanin	29.7
<i>Dianthus barbatus</i> L.	Dianthin-29	29
<i>Dianthus caryophyllus</i> L.	Dianthin-30; dianthin-32	29.5; 31.7
<i>Dianthus sinensis</i> L.	<i>Dianthus sinensis</i> RIP (DsRIP)	33.3
<i>Gelonium multiflorum</i> A. Juss.	Gelonin (GAP31)	31
<i>Gynostemma pentaphyllum</i> (Thunb.) Makino	Gynostemmin	27
<i>Gypsophila elegans</i> Bieb.	Gypsophilin	28
<i>Hordeum vulgare</i> L.	Barley translation inhibitor (barley toxinI, BRIP); barley toxin II; barley toxin III	31; 30; 30
<i>Hura crepitans</i> L.	<i>Hura crepitans</i> RIP	28
<i>Iris hollandica</i> L.	<i>Iris</i> RIP A1 (IRIP A1); <i>Iris</i> RIP A2 (IRIP A2); <i>Iris</i>	30.9; 31; 30.9

	RIP A3 (IRIP A3)	
<i>Jatropha curcas</i> L.	Curcin; Jc-SCRIP	28.2; 38.9
<i>Lagenaria siceraria</i> Molina	Lagenin	20
<i>Luffa acutangula</i> Roxb.	Luffaculin-1; luffaculin-2	28; 28
<i>Luffa aegyptiaca</i> Mill.	Luffin-c; <i>Luffa</i> ribosomal inhibitory protein (LRIP)	ND; 30
<i>Luffa cylindrica</i> Mill.	Luffin-A (alpha-luffin); luffin-B (beta-luffin)	27; 28
<i>Lychnis chalconica</i> L.	Lychnin	26.1
<i>Manihot palmate</i> Mill.	Mapalmin	32.3
<i>Manihot utilissima</i> Mill.	Manutin	30.7
<i>Marah oreganus</i> (Torr. Ex S. Wats.) Howell	MOR-I ( <i>Marah oreganus</i> RIP-I); MOR-II ( <i>Marah oreganus</i> RIP-II)	28; 27.6
<i>Mesembryanthemum crystallinum</i> L.	RIP1	32.7
<i>Mirabilis expansa</i> Standl.	ME1; ME2	27; 27.5
<i>Mirabilis jalapa</i> L.	<i>Mirabilis</i> antiviral protein (MAP); MAP-2; MAP-3; MAP-4	27.8; 30.4; 29.7; 29.3
<i>Momordica balsamina</i> L.	<i>Momordica balsamina</i> RIP-1 (MbRIP-1); momordin II; balsamin	30; 32; 28
<i>Momordica charantia</i> L.	Momordin ( <i>Momordica charantia</i> inhibitor, momordin-a); alpha-momorcharin (alpha-MMc); beta-momorcharin (beta-MMc); delta-momorcharin; epsilon-momorcharin; momordin I ( <i>Momordica charantia</i> inhibitor)	23; 29; 28; 30; 24; 31
<i>Momordica cochinchinensis</i> Spreng	Momorcochin-S; momorcochin; cochinin B	30; 32; 28
<i>Momordica grosvernoria</i> Swingle	Momorgrosvin	27.7
<i>Muscari armeniacum</i> Leichtlin ex Baker	Musarmim-1 (MU-1); musarmin-2 (MU-2); musarmin-3 (MU-3)	28.7; 30; 27.6
<i>Nicotiana tabacum</i> L.	Tobacco RIP (TRIP); CIP31	26; 31
<i>Oryza sativa</i> L.	<i>Oryza sativa</i> RIP; <i>Oryza sativa</i> cultivar Kazemi RIP	33; 29
<i>Petrocoptis glaucifolia</i> (Lag.) Boiss.	Petroglaucin-1; petroglaucin-2	26.7; 27.5
<i>Peterocoptis grandiflora</i> Rothm.	Petrograndin	28.6
<i>Phytolacca americana</i> L.	PAP (pokeweed antiviral protein, <i>Phytolacca</i> antiviral protein); PAP II (pokeweed antiviral protein II); PAP III (pokeweed antiviral protein III); PAP-S; PAP-C; PAP-R; PAP-H	30; 30; 30; 29; 29.8; 29.5
<i>Phytolacca dioica</i> L.	PD-S1 ( <i>Phytolacca dioica</i> RIP1); PD-S2 ( <i>Phytolacca dioica</i> RIP2); PD-S3 ( <i>Phytolacca dioica</i> RIP3); PD-L1; PD-L2; PD-L3; PD-L4; dioicin 1; dioicin 2	30; 32.7; 31.5; 30.4; 29.2; 30; 29.9
<i>Phytolacca dodecandra</i> L'Herrit	Dodecandrin	29
<i>Phytolacca heteropala</i> H. Walter	Heterotepalin-4 (Mexican pokeweed RIP-4,	29.3; 30.5

	<i>Phytolacca heteropala</i> anti-viral protein PAP); Heterotepalin-5b (Mexican pokeweed RIP-5b)	
<i>Phytolacca insularis</i> Nakai	<i>Phytolacca insularis</i> antiviral protein (PIP, insularin); <i>Phytolacca insularis</i> antiviral protein 2 (PIP2)	35; 35.7
<i>Pisum sativum</i> L.	Alpha-pisavin; beta-pisavin; sativin	20.5; 18.7; 38
<i>Sambucus ebulus</i> L.	Alpha-ebulitin; beta-ebulitin; gamma-ebulitin	32; 29; 29
<i>Sambucus nigra</i> L.	Nigritin f1; nigritin f2	24.1; 23.6
<i>Saponaria ocymoides</i> L.	Ocymoidine	30.2
<i>Saponaria officinalis</i> L.	Saporin-6; saporin-9; saporin-L1; saporin-L2; saporin-R1; saporin-R2; saporin-R3; saporin-S5; Saporin-S6; saporin-S8; saporin-S9	29.5; 29.5; 31.6; 31.6; 30.2; 30.9; 30.9; 30.9; 31.6; 29.5; 29.5
<i>Secale cereale</i> L.	<i>Secale cereale</i> RIP	31
<i>Sechium edule</i> (Jacq.) Sw.	Sechiumin	27
<i>Spinacia oleracea</i> L.	<i>Spinacia oleracea</i> RIP1 (SoRIP1, BP31); <i>Spinacia</i> <i>oleracea</i> RIP2 (SoRIP2)	31; 29
<i>Stellaria aquatica</i> Scop.	Stellarin	ND
<i>Stellaria media</i> (L.) Vill.	RIP Q3	28.2
<i>Trichosantes anguina</i> L.	Trichoanguin	35
<i>Trichosanthes cucumeroides</i> Maxim.	Beta-trichosanthin	28
<i>Trichosantes kirilowii</i> Maxim.	Alpha-kirilowin; beta-kirilowin; Trichosanthin (TCS); TAP-29 ( <i>Trichosanthes</i> anti-HIV protein 29 kDa); Trichobitacin; alpha-trichosanthin; karasurin-A; karasurin-B; karasurin-C; trichomislin; trichokirin	28.8; 27.5; 25-26; 29; 27.2; 31.7; 27.1; 27.2; 27.4; 27.2; 27
<i>Trichosantehes lepiniate</i> Maxim.	Trichomaglin	24.7
<i>Trichosantes sp. Bac Kan 8-98</i>	Trichobakin	27
<i>Triticum aestivum</i> L.	Tritin	30
<i>Vaccaria pyramidata</i> Medik.	Pyramidatine	28
<i>Zea mays</i> L.	Maize seed RIP (b-32, corn RIP)	32.4

## 2.2 Type 2 RIPs

Type 2 RIPs can be composed of two or four polypeptide chains, with an approximate molecular weight of 60 kDa or 120 kDa, respectively. At least one chain possess enzymatic activity and is therefore called A-chain (A, active). The A-chain is linked by disulphide bonds and other non-covalent bonds to a galactose-specific lectin B-chain. The majority of type 2 RIPs known are heterodimers composed of one A-chain linked to a B-chain, like abrin, modeccin, ricin, volkensin and stenodactylin. The

tetrameric structure is typical of the *Ricinus communis* agglutinin (RCA), and also viscumin form tetramers in concentrate solutions (Van Damme *et al.*, 2001).

Most of the knowledge about type 2 RIPs biosynthesis has been obtained by studies on ricin in castor bean seeds. Ricin, and probably most of type 2 RIPs, is synthesized as a preprotein formed by a signal peptide, the mature A-chain and the mature B-chain linked by a 12-residue linker peptide (Fig. 1). The pre-proRIP is co-translationally translocated into the endoplasmic reticulum (ER) lumen, where the signal peptide is cleaved and four exposed asparagine residues are *N*-glycosylated. The formation of disulfide bonds between A-chain and B-chain, and also within the B-chain, occurs in the ER. The pro-RIP is subsequently transported via the ER and the Golgi complex into protein storage vacuoles, where the excision of the internal 12-residue linker yields mature protein. This maturation step implies that the protein becomes active only after its arrival in the storage compartment, probably a mechanism to prevent unwanted activation of the toxin in the cytoplasm (Lord *et al.*, 1994).

Type 2 RIPs are generally more cytotoxic than type 1 RIPs. The presence of the lectin B-chain facilitates the translocation of the A chain into the cytosol binding to galactosyl moieties of glycoproteins and/or glycolipids that are present on the surface of eukaryotic cells. However, several non-toxic type 2 RIPs have been described. Despite strong anti-ribosomal molecular activity *in vitro*, non-toxic type 2 RIPs lack the high toxicity in cultured animals cells and *in vivo* rodents, maybe because of individual changes in the high-affinity sugar binding sites of the B-chains, which alter their intracellular trafficking (Ferrerias *et al.*, 2011).

The purification of type 2 RIPs takes advantage of the lectin properties of their B-chains and it is performed by affinity chromatography on Sepharose, acid-treated Sepharose or other galactose-containing stationary phases. Elution of bound protein is obtained with galactose or lactose.

**Table 2:** type 2 RIPs from plant, modified from Gilabert-Oriol *et al.*, 2014.

Plant	RIP	Absolute molecular mass (kDa)
<i>Abrus precatorius</i> L.	Abrin-a; abrin-b; abrin-c; abrin-d; abrin-I; abrin-II; abrin-III; APA-I; APA-II; <i>Abrus</i> agglutinin; <i>Abrus</i> agglutinin	63; 67; 63; 67; 64; 63; 63; 130; 128; 67; 134
<i>Abrus pulchellus</i> L.	Pulchellin	61.5-63
<i>Adenia digitata</i> Burt-Davy	Modeccin	57
<i>Adenia ellenbeckii</i> Harms.	<i>Adenia ellenbeckii</i> RIP	60
<i>Adenia goetzii</i> Burt-Davy	<i>Adenia goetzii</i> RIP	60
<i>Adenia keramanthus</i> Harms.	<i>Adenia keramanthus</i> RIP	60-65
<i>Adenia lanceolata</i> Engl.	<i>Adenia lanceolata</i> RIP; lanceolin	60; 61.2
<i>Adenia stenodactyla</i> Harms.	<i>Adenia stenodactyla</i> RIP; stenodactylin	60; 63.1
<i>Adenia venenata</i> Forssk.	<i>Adenia venenata</i> RIP	60
<i>Adenia volkensis</i> Harms.	Volkensin	62
<i>Aralia elata</i> (Miq.) Seem	Aralin ( <i>Aralia elata</i> lectin)	61.3
<i>Camellia sinensis</i> (L.) Kuntze	<i>Camellia sinensis</i> RIP (CS-RIP)	63.6
<i>Cinnamomum camphora</i> (L.) J. Presl.	Cinnamomin	61
<i>Cinnamomum porrectum</i> L.	Porrectin	64.5
<i>Cucurbita foetidissima</i> Kunth	Foetidissima; foetidissimin II	63; 61
<i>Eranthis hyemalis</i> Salisb.	<i>Eranthis hyemalis</i> lectin (EHL)	62
<i>Iris hollandica</i> L.	<i>Iris</i> agglutinin b (IRAb); <i>Iris</i> agglutinin r (IRAr)	65; 65
<i>Malania oleifera</i>	Malanin	61.9
<i>Momordica charantia</i> L.	<i>Momordica charantia</i> lectin (MCL)	130
<i>Phoradendron californicum</i> Nutt.	<i>Phoradendron californicum</i> lectin (PCL)	69
<i>Polygonatum multiflorum</i> Kunth.	<i>Polygonatum multiflorum</i> RIP monomer (PMRIPm); <i>Polygonatum multiflorum</i> RIP tetramer (PMRIPt)	60; 240
<i>Ricinus communis</i> L.	Ricin; ricin 1; ricin 2; ricin 3; ricin D; ricin E; <i>Ricinus</i> agglutinin (RCA 120); <i>Ricinus</i> agglutinin 1 (RCA 1); <i>Ricinus</i> agglutinin 2	62; 64; 67; 66; 60; 60; 120; 134; 140
<i>Ricinus sanguineus</i> Hort. ex Groenland	Ricin R2; ricin R11; ricin R12; <i>Ricinus sanguineus</i> agglutinin	63.1; 57.8; 62.2; 120
<i>Sambucus ebulus</i> L.	Ebulin r; ebulin I (ebulin 1)	56; 56
<i>Sambucus nigra</i> L.	Nigrin b; <i>Sambucus nigra</i> agglutinin I (SNAI); SNLRP	58; 140; 60-62
<i>Sambucus racemosa</i> L.	Basic racemosin b	58
<i>Sambucus sieboldiana</i> L.	Sieboldin-b	59.4

<i>Viscum album</i> L.	Viscumin (mistletoe lectin I)	60
<i>Viscum articulatum</i> Burm. F.	Articulatin-D	66
<i>Ximenia americana</i> L.	Riproximin	63

### 2.3 Type 3 RIPs

Type 3 RIPs are a group that comprises two proteins characterized only from maize and barley (b-32 and JIP60, respectively). Type 3 RIPs are synthesized as single-chain inactive precursors (proRIPs) that require proteolytic processing events to produce two noncovalently linked chains equivalent to a type 1 RIP. The absence of a signal peptide in the gene encoding type 3 RIPs indicates that these proteins are synthesized on free-polysomes in the cytoplasm. The function of the extra domains in the type 3 RIPs is not known (Van Damme *et al.*, 2001).

**Table 3:** type 3 RIPs from plant, modified from Gilabert-Oriol *et al.*, 2014.

<b>Plant</b>	<b>RIP</b>	<b>Absolute molecular mass (kDa)</b>
<i>Hordeum vulgare</i> L.	JIP60 (60 kDa jasmonate-induced protein)	60
<i>Zea mays</i> L.	Maize proRIP	34

### 3. Interaction of RIPs with cells: mechanism of entry

A general mechanism of cell entry could be depicted for all RIPs: after binding to cell surface, RIPs are endocytosed and follow retrograde transport through the Golgi apparatus to the endoplasmic-reticulum (ER), then enter the cytosol possibly exploiting the ER-associated degradation pathway (ERAD). Differences in cytotoxicity between type 1 and type 2 RIPs are due to the presence of a lectin B-chain in the latter, which facilitates cell entry. The B-chain of type 2 RIPs possesses galactose-specific lectin activity, which allows its interaction with galactose-containing glycoproteins and glycolipids on the cell surface. Interactions between mannose cell receptors and RIPs carbohydrate side chains also occur (Stirpe, 2004).

Most of the knowledge on type 2 RIPs endocytic mechanism comes from studies on ricin. It has been shown that, after binding to cell surface, ricin and possibly other type 2 RIPs reach the endosomal compartment through clathrin-dependent or clathrin-independent pathways. Once in the cell, RIPs could be recycled to cell surface or transported to lysosomes for degradation. The majority of RIPs entered translocate to the Golgi apparatus, then to the ER, where they can gain access to cytosol interacting with the ERAD machinery (Sandvig *et al.*, 2005). Since translocation through the ER membranes implies the unfolding of the protein and subsequent loss of activity, RIPs are thought to escape degradation because of the low number of lysines that they contain (Johannes *et al.*, 2008).

The mechanism of cell entry of type 1 RIPs have been examined in various studies, but some questions remain unanswered. It has been proposed that type 1 RIPs could be endocytosed by pinocytosis or after binding to either the galactosyl residues or the mannose receptor on the cell membrane. A comparison between the endocytosis of ricin and saporin indicated that the type 1 RIP follows a Golgi-independent pathway to the cytosol and does not require a low pH for membrane translocation which allows the internalization of the toxin without receptor binding (Vago *et al.*, 2005). Type 1 RIP intracellular routing seems to present some diversity within the group or depending on the cell type: while saporin seems to follow a Golgi-independent pathway and to localize also in the cell nucleus (Bolognesi *et al.*, 2012); PAP presents a type 2 RIP-similar retro-translocation mechanism from the ER into the cytosol (Parikh *et al.*, 2005). The latter observation suggests that type 1 RIPs may also be able to follow the intracellular route of misfolded proteins without being degraded by the proteasome.

#### **4. Biological activities of RIPs**

##### 4.1 Glycosylase activity

RIPs are officially classified as rRNA N-glycosylases (EC 3.2.2.22). They recognize a specific and highly conserved region in the large subunit of rRNA and cleave a specific *N*-glycosidic bond between an adenine and the nucleotide on the rRNA. The first description of the mechanism underlying RIP-induced ribosomal damage was described by Endo and co-workers (Fig. 2). Using ricin and rat liver ribosomes as substrate, they showed that the adenine cleavage was highly selective and

that the specific adenine removed (A<sub>4324</sub>) lies in a highly conserved sequence, GAGA, that is present in a universally conserved loop (termed sarcin/ricin loop, SRL) located at the top of a stem region in the 28S rRNA (Endo *et al.*, 1987). The SRL is important for binding and GTPase activation of the translational GTPases, which include the elongation factor 1 (EF1) and the elongation factor 2 (EF2), by the ribosome. The irreversible removal of this adenine from GAGA sequence prevents the binding of EF2 to ribosomes and affects both the EF1- and EF2-dependent GTPase activities with subsequent arrest of protein synthesis at the translocation step, thus inhibiting irreversibly cellular protein synthesis. All RIPs known are able to deadenylate larger rRNA, but marked differences in efficiency and substrate specificity exist between different RIPs. For example, ricin shows activity on mammalian and yeast ribosomes, but not on bacterial or plant ones. Conversely, PAP is able to deadenylate ribosomes from bacteria, plant and yeast. This differential sensitivity may be accounted to a different interaction with ribosomal proteins that may limit accessibility to the substrate (Tumer *et al.*, 2012).

Some RIPs were found to be catalytically active *in vitro* also on other nucleotide substrates, such as herring sperm DNA, poly(A) and RNAs from different sources. Following these observation, the redefinition of RIPs as polynucleotide: adenosine glycosidases was proposed (Barbieri *et al.*, 1997).

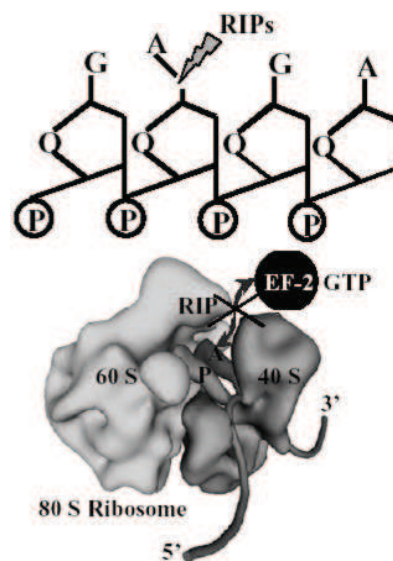


**Fig. 2** RIPs mechanism of action on larger rRNA, modified from Girbés *et al.*, 2004.

## 4.2 RIPs and apoptosis

It was initially thought that RIPs cytotoxicity depended solely on their ability to arrest cellular protein synthesis, thus causing intoxicated cells to undergo necrosis. However, a rich series of experimental evidences and reports support the notion that RIPs are able to induce apoptosis in intoxicated cells, but very little progress has been made on elucidating the mechanism and pathways of RIP-induced apoptosis. RIP-treated cells undergo apoptosis via different mechanisms including the loss of mitochondrial membrane potential, caspases activation and modulation of regulator proteins (Narayan *et al.*, 2005), but the relationship between apoptosis induction and RIPs *N*-glycosylase activity remains an open question. There are contradictory reports on the importance of translation inhibition by RIPs in apoptosis induction: some authors indicate that protein synthesis inhibition activity is necessary for triggering apoptosis, while others suggest that induction of apoptosis by RIPs is not necessarily consequent to the translation inhibition (Sikriwal *et al.*, 2010). Even if all RIPs share a common activity on 28S rRNA, it is becoming clear that they not share a single common pathway for the induction of apoptosis, instead, it is likely that RIPs are able to induce multiple cell death pathways in different cell types. In addition to the inhibition of translation, alternative mechanisms were proposed to explain how RIPs induce apoptosis, such as (a) the ribotoxic stress response; (b) ER-stress and the activation of unfolded protein response (UPR) genes; (c) interactions with anti-oxidant proteins and the production of reactive oxygen species. All these mechanisms could cooperate in RIP-induced apoptosis at different levels and in different ways depending on cell type.

### *4.2.1 Apoptosis induction by ribotoxic stress response*

It was shown for the first time by Jordanov *et al.*, 1997, that ricin,  $\alpha$ -sarcin and anisomycin were able to activate signaling through the c-Jun NH<sub>2</sub>-terminal (JNK) mitogen-activated protein kinase (MAPK) pathway in response to specific damage to 28S rRNA. They provided evidence that the peptidyl transferase reaction center of eukaryotic ribosomes could function as a sensor of translational stress and that activation of SAPK/JNK1 was not simply due to protein synthesis arrest, but to specific signaling starting from damaged 28S rRNA. This novel pathway of kinase activation was then termed “ribotoxic stress response”. Initiation of the ribotoxic stress response

required actively translating ribosomes at the time of ribosome damage, and activation of p38 and extracellular signal-regulated kinases (ERKs) together with JNKs can also occur. Activation of the ribotoxic stress response was observed to increase the expression of pro-inflammatory proteins, such as IL-8, GRO- $\alpha$ , IL-1 $\beta$  and TNF- $\alpha$ , as well as pro-apoptotic genes like FasL (Jandhyala *et al.*, 2012).

Signaling through the ribotoxic stress response has been linked to RIP-induced apoptosis. In the immortalized, non-transformed epithelial cell line, MAC-T, inhibition of the JNK pathway reduced ricin-induced caspase activation and poly(ADP-ribose) polymerase cleavage, suggesting the requirement of JNK for apoptosis induction (Jetzt *et al.*, 2009). In ricin-treated RAW 264.7 cells, inhibition of p38 MAPK strongly inhibited the release of TNF- $\alpha$  and reduced ricin-induced apoptosis. Similar observations were obtained with modeccin, suggesting that ribotoxic stress response may trigger the multiple signal transduction pathways through the activation of p38 MAP kinase, which in turn leads to TNF- $\alpha$  release and apoptosis (Higuchi *et al.*, 2003). Similarly, the blocking of the p38 and JNK activation prevented intestinal epithelial cell line HCT-8 death and diminished Shiga toxin 1-associated caspase 3 cleavage (Smith *et al.*, 2003). An interesting observation was made in shiga toxin-treated Burkitt's lymphoma cell line Ramos, where inhibitors of p38 actually increased apoptosis. The authors suggested that persistent p38 MAPK activation in lymphoid cells may induce survival pathways that render those cells less sensitive to the toxin (Garibal *et al.*, 2010).

How cells sense 28S damage and trigger signalling through the ribotoxic stress response is not fully understood, but three upstream effectors have been described: the double-stranded RNA activated protein kinase (PKR); hematopoietic cell kinase (Hck); and the zipper sterile alpha motif kinase (ZAK).

Zhou *et al.* (2014) proposed a role for PKR as a ribosome guardian, as it was found to associate with 18S and 28S rRNA sequences in a region-specific manner and to be phosphorylate upon ricin and other ribotoxins addition in a concentration-dependent way, suggesting that PKR is able to rapidly respond to subtle alterations in secondary and/or tertiary rRNA structure. This would result in recruitment and activation of MAPKs to the ribosome thereby initiating downstream signalling (Bae *et al.*, 2010). Treatment of RAW 264.7 cells with PKR inhibitors or antisense knockdown of PKR resulted in a decrease of ribotoxic insult-driven MAPK activation as well

apoptosis (Zhou *et al.*, 2003). Furthermore, expression of a dominant-negative PKR in human monocytic U937 blocked ricin-induced IL-8 expression (Gray *et al.*, 2008).

Hck was also shown to play a potential role in ribotoxic stress response, as knockdown of Hck was found to decreased both TNF- $\alpha$  production, ERKs, p38, JNKs activation and apoptosis following ribotoxic insult (Zhou *et al.*, 2005). Both PKR and Hck were found to interact with 40S rRNA subunit, but knocking down of PKR expression suppress interaction between Hck and 40S subunit (Bae *et al.*, 2010).

The MAP3K ZAK was considered as a third upstream mediator of the ribotoxic stress response. ZAK was shown to transduce activation of JNKs and p38 by ricin and shiga-toxin 2. Treatment with ZAK inhibitors or siRNA blocked SAPK activation in COS-7, Vero and HCT-8 cells and resulted in a modest but statistically significant improvement of cell viability (Jandhyala *et al.*, 2008).

#### *4.2.2 RIP-induced ER-stress and the activation of UPR genes*

The ER is the intracellular site functioning as Ca<sup>2+</sup> storage and represents the site for correct folding and post-translational processing of proteins. Three proteins, RNA-dependent protein kinase-like ER kinase (PERK), inositol-requiring ER to nucleus signal kinase-1 (IRE1) and activating transcription factor-6 (ATF6), serve as sensors of unfolded proteins. The unfolded protein response (UPR) acts by halting protein translation and transcription of genes to restore ER function. If ER homeostasis is compromised, UPR activates apoptotic signaling cascade. The central activator of UPR is the chaperone binding immunoglobulin protein BiP (also named GRP78), which in the presence of unfolded proteins starts UPR signalling by dissociating from PERK, IRE-1 and ATF-6. Once BiP is titrated away by unfolded proteins, PERK and IRE-1 are activated: PERK phosphorylates and inhibits eukaryotic translation initiation factor two subunit  $\alpha$  (eIF2 $\alpha$ ) that produce a general translational arrest, while enhancing the transcription of activating transcription factor 4 (ATF4). After BiP detachment, ATF6 re-localizes to the Golgi apparatus to activate UPR and ERAD genes, including X-box binding protein 1 (XBP-1), whose mRNA is alternatively spliced by activated IRE-1 whose product activates ERAD components as well as several chaperones and foldases (Yadav *et al.*, 2014).

UPR is another stress response that may contribute to RIPs-induced pro-apoptotic signaling. Ricin was shown to induce Bip degradation, starting ER-stress which in turn triggered IL-6 production (Shi *et al.*, 2009). RIP-treated human adenocarcinoma cell lines MDA-MB-231 and HCT116 were shown to activate in a concentration-dependent manner the PERK and ATF6 branches of UPR, but not the branch involving XBP-1 alternative splicing by IRE1 (Horrix *et al.*, 2011). Similarly, Shiga toxin 1 treatment was found to increase activation of the ER stress sensors IRE1, PERK and ATF6 in human monocytic cells, leading to apoptosis (Lee *et al.*, 2008).

#### 4.2.3 Oxidative stress

RIPs were found to induce apoptosis by increasing the reactive oxygen species (ROS) and intracellular calcium levels. Trichosanthin causes ROS production in human choriocarcinoma cells (JAR cells) after its interaction with a membrane-bound receptor. ROS production in trichosanthin-treated cells might be a consequence of calcium signaling, as ROS levels were shown to increase in parallel with calcium levels (Zhang *et al.*, 2001). In U937 cells, mistletoe lectin II (MLII) toxin generated high levels of hydrogen peroxide, which in turn activated the intracellular stress signaling and JNK/SAPK pathways, concomitant with apoptosis. Treatment with a ROS scavenger was successful in reducing apoptosis (Kim *et al.*, 2003). The same cell line treated with a low dose of abrin showed an increase in ROS levels, followed by DNA damage (Bhaskar *et al.*, 2008); while N-Acetyl-L-cysteine (NAC) and Trolox were found to confer significant protection in Jurkat cells by restoring antioxidant molecules depleted by abrin treatment (Saxena *et al.*, 2014).

Abrin was also found to interact with antioxidant protein-1 (AOP-1). AOP-1 is located in the mitochondria protecting them from the action of ROS. Direct binding of abrin to AOP-1 promotes apoptosis by inhibiting the mitochondrial AOP-1, resulting in the increase of intracellular ROS and the release of cytochrome c from the mitochondria to the cytosol, which in turn activates caspase-9 and caspase-3 (Shih *et al.*, 2001).

### 4.3 Antiviral activity

Type 1 and some type 2 RIPS have been shown to be active against plant, fungal and animal viruses, but the exact mechanism of their broad-spectrum anti-viral activity is still not clear. Some of the first studies showed that RIPS were effective against viruses as broad as poliovirus, influenza and herpes simplex virus (Parikh *et al.*, 2004). Initially it was thought that RIPS could come in contact with and damage ribosomes of the infected cells, with consequent death of the cells and arrest of viral proliferation. However, with the help of recombinant techniques, mutated RIPS were produced and it was possible to ascertain that the ribosome-inactivating and antiviral activities can be separated (Stirpe *et al.*, 2006). For example, two non-toxic recombinant mutants of PAP from *Phytolacca americana* depurinate HIV-1 RNA much better than cellular rRNA (Uckun *et al.*, 2003). PAP was also shown to inhibit the production of the human T-cell leukemia virus 1 (HTLV-1) (Mansouri *et al.*, 2009).

RIPs inhibit replication of RNA as well as DNA viruses. This activity appears to exhibit some specificity, as not all the substrates are equally affected. For example, PAP has been shown to inhibit the translation of capped but not of uncapped viral RNAs (Hudak *et al.*, RNA 2000). Barnett *et al.*, 1995, described the activity of single-chain RIP gelonin on human DNA virus cytomegalovirus, (HCMV). These authors evaluated the antiviral activity of gelonin after its chemical linkage to a polyclonal human IgG specific for infected cells. In uninfected cells, there was no difference in [<sup>35</sup>S]methionine incorporation between untreated cultures and cultures treated with immunotoxin at 100 micrograms/ml. In HCMV-infected cells, there was a significant decrease in [<sup>35</sup>S]methionine incorporation in the immunotoxin-treated cultures, suggesting a selective cytotoxic effect on the virus-infected cells. An immunotoxin specific for murine cytomegalovirus (MCMV) was prepared by linking gelonin to a polyclonal anti-MCMV IgG. Protein synthesis inhibition-based cytotoxic assay showed that the anti-MCMV immunotoxin had a 50% cytotoxic concentration of 35 micrograms/ml in MCMV-infected cells and greater than 200 micrograms/ml in uninfected cells. MCMV yields measured at 7 days post-inoculation were reduced by 2 log in cultures treated with immunotoxin at 20 micrograms/ml at 1 day post-inoculation (Barnett *et al.*, 1996). Following first observations by McGrath *et al.*, 1989; the antiviral efficacy of RIPS were also tested in some phase I/II clinical trials using RIPS and RIP-

based immunotoxins, especially to treat HIV patients, unfortunately without success (Kaur *et al.*, 2011).

## **5. RIPs employment in experimental and clinical medicine**

Many efforts have been spent to exploit cytotoxicity and antiviral properties of RIPs in medicine. Clinical employment of unmodified type 1 RIPs have been very limited: inhibitory effects of RIPs on HIV proliferation in cells were tested in clinical trials involving AIDS patients, but the results were unfortunately too poor (Kaur *et al.*, 2011). On the other hand, the lack of cell-binding specificity of type 2 B-chain renders the use of these proteins unsafe in clinical practice. Most of the interest in RIPs in the biomedical field has been the possibility of directing their high cytotoxicity in a selective manner to deplete populations of undesired cells, as for example malignant, virus infected or autoreactive cells. This was achieved by linking them to molecules, in particular monoclonal antibodies (mAbs), but also lectins, hormones, growth factors, to form “immunotoxins” (ITs) or other cell-binding conjugates capable of selective killing of unwanted cells (Madhumathi *et al.*, 2012). To date, RIP-based ITs have been employed to treat cancer and also autoimmune disorders (Madhumathi *et al.*, 2012).

### 5.1 RIP-containing immunotoxins in anti-tumor therapy

The term immunotoxin is generally referred to a toxin targeted by an antibody, while toxins linked to other carriers are commonly referred to as “chimeric toxins” or “conjugates”. After the IT targeting moiety binds to the target cell surface, the payload is internalized to the endocytic compartment. Processing and trafficking of these molecules is target- and toxin-specific, but converge in the delivery of the toxic cargo to appropriate cellular compartment.

The efficiency of ITs in killing the target cells have been shown with excellent results in numerous pre-clinical models (Fracasso *et al.*, 2010) and clinical trials (Polito *et al.*, 2011; Palanca-Wessels *et al.*, 2014), with the best results obtained in the experimental treatment of hematological malignancies. The cell-killing efficiency of an IT mainly depends on the cell type, antigen availability, binding affinity and intracellular routing. First ITs produced were obtained by chemical coupling of native toxins to antibody moieties by the formation of disulphide bonds between the toxin and

the carrier. Despite great advantages like good stability and ease of production, the resulting product was heterogeneous and poorly suitable for commercialization. New generation ITs are produced using recombinant DNA techniques, using modified toxins and antibody fragments (as single-chain variable fragments, scFvs). The production of these ITs could be achieved using different expression hosts, such as bacteria (Wang *et al.*, 1997), yeasts (Lombardi *et al.*, 2010) and algae (Mayfield, 2013), however yields are often very poor and sometimes with low stability.

Main issues reported by clinical trials which have had limited ITs development and expansion in clinical practice are immunogenicity and vascular leak syndrome (VLS). Approximately 90% of IT-treated patients with solid tumors develop anti-toxin antibodies after 1 or 2 cycles of treatment, while better results were achieved with hematologic cancer: end-stage onco-hematological patients are often heavily immunosuppressed, and several cycles of therapy were needed to observe formation of anti-toxin antibodies (Fitzgerald *et al.*, 2011). A patient could either develop antibodies against the mAb portion or the toxin part. Host antibodies against the antibody portion of the IT can be avoided for example by humanizing this portion of the molecule, while several immunosuppressive regimen were tested to reduce IT-associated immune response, often with poor results (Alewine *et al.*, 2015). Recently, the pentostatin plus cyclophosphamide nonmyeloablative regimen was found to be effectively immunosuppressive, resulting in a marked durable suppression of T-cell effector function (Mariotti *et al.*, 2011). The efficacy of the combination of pentostatin plus cyclophosphamide in reducing ITs immunogenicity was confirmed in a preclinical mice model (Mossoba *et al.*, 2011) and then tested in a pilot clinical study achieving promising results. In fact, after induction therapy with pentostatin plus cyclophosphamide regimen, 8 of 10 patients could receive repeated cycles of IT before development of anti-IT neutralizing antibodies, delaying markedly anti-IT antibodies formation (Hassan *et al.*, 2013).

VLS is caused by an endothelial damage which cause an increase in vascular permeability associated with edema, hypotension and, in severe form, signs of pulmonary and cardiovascular failure. VLS often sets the major dose-limiting toxicity in IT therapy, and several attempts were made to limit this side effect (Wang *et al.*, 2007; Wang *et al.*, 2008; Liu *et al.*, 2012). Ricin and other toxins were shown to contain short

aminoacid motifs that bind endothelial cells and initiate VLS (Baluna *et al.*, 1999). Modification or deletion of these sequences were shown to be effective in reducing toxin-induced VLS (Wang *et al.*, 2007; Weldon *et al.*, 2013).

Beside modification of the carrier and toxic moieties to reduce immunogenicity of ITs (i.e. PEGylation or removal of B cell epitopes), some efforts have been made to enhance the toxicity of ITs, in order to reduce the dose *in vivo*. The use of photochemical internalization (PCI) technology could increase the efficacy of ITs. PCI is a drug delivery technology which allows the cytosolic release of drugs from the endocytic compartment. This method utilizes photosensitizers that localize to the membrane of endocytic vesicle and can cause controlled membrane breakage after light exposure. As ITs are taken up by receptor-mediated endocytosis, PCI could allow controlled release of the drug inside the tumor. In several studies, PCI was found to effectively enhance ITs efficacy in tumor treatment (Weyergang *et al.*, 2011).

Another strategy followed to improve ITs efficacy resulted from the employment of a mixture of saponins in combination with ITs. Saponins are in general tenside-like compounds able to interact with cholesterol within membranes, they were found to enhance endosomal escape of the toxin moiety, which in turn resulted in apoptosis. The concomitant use of saponins from *Saponaria officinalis* L. and *Gypsophila paniculata* L. was shown to synergistically enhance the toxicity of saporin-EGF and dianthin-EGF (Gilalbert-Oriol *et al.*, 2014).

## 5.2 Clinical Trials in cancer diseases

Several ITs have been investigated in recent or ongoing trials. Moxetumomab pasudotox is a recombinant IT that combines an anti-CD22-Fv with a 38-kDa fragment of *Pseudomonas* exotoxin A. It is currently in clinical trials for the treatment of hairy cell leukemia (phase III, NCT01829711); adult acute lymphoblastic leukemia (ALL) (phase I/II, NCT01891981); and childhood ALL or non-Hodgkin's lymphoma (NHL) (phase I, NCT00659425). Anti-CD25 recombinant immunotoxin LMB-2 is in a phase II trial for hairy cell leukemia as single agent (NCT00321555) and for adult T-cell leukemia in combination with fludarabine and cyclophosphamide (NCT00924170). SS1P is another *Pseudomonas* exotoxin A-based IT designed for the treatment of mesothelioma currently in a phase II clinical trial in combination with fludarabine and

cyclophosphamide (NCT01362790). Two diphtheria toxin-based ITs are currently in phase I and I/II, clinical trials as single agents, A-dmDT390-bisFv(UCHT1) and DT2219ARL (NCT00611208; NCT00889408, respectively). An anti-CD33 IT that contains type I RIP gelonin recently successfully completed a phase I clinical trial in patients with advanced myeloid malignancies as a single agent (Borthakur et al., 2013). To date, the only FDA approved ITs are denileukin diftitox and gemtuzumab ozogamicin. However, the latter was approved in 2000 as a single agent under the category of "accelerated" approval in patients with relapsed acute myelogenous leukemia, but the lack of evidence to confirm clinical benefit and safety concerns have altered the benefit/risk assessment unfavorably for gemtuzumab ozogamicin and have led to the decision to withdraw the accelerated approval.

### 5.3 Immunotoxins in autoimmune disorders

The ability to target specific cells taking advantage of surface markers was also exploited in the experimental treatment of some autoimmune diseases, showing promising results. In 1999, the FDA approved the use of an engineered IT combining interleukin-2 and diphtheria toxin known as denileukin diftitox for patients with persistent or relapsed CD25-positive cutaneous T-cell lymphoma (CTCL). Denileukin diftitox was subsequently reported to be an effective therapy for other non-neoplastic conditions, such as autoimmune disorders like psoriasis, rheumatoid arthritis, systemic lupus, scleroderma and vasculitis (Manoukian *et al.*, 2009). Similarly, a *Pseudomonas* exotoxin A-based IT to folate receptor beta was effective in the intra-articular treatment of antigen-induced arthritis in a rat model of disease (Nagai *et al.*, 2012). The same IT have had previously shown efficacy on the activation and proliferation of rheumatoid arthritis synovial cells. (Nagai *et al.*, 2006). Type 1 RIP gelonin was conjugated to amino acids 4-181 of the extracellular domain of the alpha-subunit of the human muscle acetylcholine receptor and used in the experimental treatment of Myasthenia gravis. This approach was found to be also useful for the therapy of further autoimmune diseases by substituting other autoantigens for the AchR fragment in the fusion protein. (Hossann *et al.*, 2006). RIPs-based ITs, such as ATG-saporin-S6 (Polito *et al.*, 2009b) and CTLA-4-saporin-S6 (Tazzari *et al.*, 2001), have been also utilized for the

prevention and treatment of graft-versus host disease (GVHD), showing promising efficacy *in vitro* and in animals, respectively.

*Chapter II*

**MATERIALS AND METHODS**



## 2.1 Materials

### RIPs

Stenodactylin was purified from the caudex of *Adenia stenodactyla* as described by Stirpe *et al.*, 2007. Saporin was purified from the seeds of *Saponaria officinalis* as described by Barbieri *et al.*, 1987. Ricin was purified from the seeds of *Ricinus communis* as described by Nicolson *et al.*, 1974.

### Immunotoxins

Anti-CD20 monoclonal antibody (mAb) rituximab-S6 immunotoxin (RTX-S6) and anti-CD22 OM124-S6 immunotoxin were produced as described in Polito *et al.*, 2004 and Bolognesi *et al.*, 1998, respectively. Briefly, mAbs and saporin-S6 were dissolved in 50 mM sodium borate buffer, pH 9.0, and were derivatized by adding 2-iminothiolane (Sigma-Aldrich, St.Louis, MO, USA). mAbs and the reduced RIP were allowed to react for 16 h (RTX/S6) or 24 h (OM124/S6) at room temperature. The resulting conjugates were separated from RIP homopolymers and free antibody by gel filtration on a Sephacryl S200 high-resolution column (100 cm × 2.5 cm) (GE-Healthcare, Buckinghamshire, UK), equilibrated and eluted with phosphate-buffered saline (PBS, 0.14 M sodium chloride in 5 mM sodium phosphate buffer, pH 7.4). The immunoconjugates were analyzed by sodium dodecyl sulfate-polyacrylamide gel electrophoresis (SDS-PAGE) under non-reducing conditions. Proteins were incubated in sample buffer (40 mM Tris-HCl pH 6.8, 2% SDS, 0.005% bromophenol blue) containing 1 mg/ml iodoacetamide, for 30 min at room temperature, analyzed on a 4–15% PhastGel gradient, and then stained with Coomassie brilliant blue, following manufacturer's instructions (Pharmacia Biotech, Uppsala, Sweden). Molecular weight markers were from Sigma: myosin (205 kDa), beta-galactosidase (116 kDa), phosphorylase B (97 kDa), bovine serum albumin (66 kDa). The RIP/antibody ratio of the immunotoxins was estimated by densitometric analysis, performed with a Kodak DC 290 apparatus, using Kodak 1D, 3.6 software version. The final immunoconjugate concentration was expressed as RIP content.

### **Cell lines and cultures**

Human anaplastic large-cell lymphoma (D430B) cells, (a kind gift from Dr. Tazzari P.L., Department of Immunohaematology and Transfusion Medicine, Sant'Orsola-Malpighi Hospital), human Burkitt's lymphoma (Raji and Ramos) cells (American Type Culture Collection), human acute monocytic leukemia (AML) (MOLM-13) cells (a kind gift from Prof. Gjertsen B.T., Department of Clinical Science, Hematology Section, University of Bergen) were maintained in RPMI 1640 medium (Sigma-Aldrich) containing 10% heat-inactivated foetal bovin serum 2 mM L-glutamine, 100U/ml penicillin and 100 µg/ml streptomycin (Sigma-Aldrich), hereafter named complete medium. All cells were cultured at 37 °C in a humidified environment with 5% CO<sub>2</sub> in a HeraCell Haereus incubator (Hanau, Germany) and routinely checked for the absence of Mycoplasma infection. Trypan blue, was obtained from BioWhittaker (Vervies, Belgium). Cytotoxicity was evaluated using L-[4,5-<sup>3</sup>H] leucine purchased by GE Healthcare (Buckingham shire, UK). Flasks and plates were from Falcon (Franklin Lakes, NJ, USA).

### **Antibodies**

Western blots were performed with rabbit antibodies against phospho-SAPK/JNK (Thr183/Tyr185), p38, phospho-p38 (Thr180/Tyr182), COX IV, horseradish peroxidase-conjugated anti-mouse or anti-rabbit IgG purchased from Cell Signaling Technology, Inc. (Danvers, MA, USA). Mouse anti-caspase 3 was purchased from Santa Cruz Biotechnology, Inc (Santa Cruz, CA, USA). Antibodies were diluted following manufacturer's instructions.

Phosflow cytometry was performed with Alexa Fluor® 647 conjugate mouse antibodies against phospho-p38 (Thr180/Tyr182), phospho-JNK (Thr183/Tyr185) and phospho-ERK1/2 (Thr202/Tyr204) purchased from BD transduction Laboratories (Heidelberg, Germany).

### **Kits**

Caspases activity was evaluated using the luminescent kit Caspase-Glo™<sup>3/7</sup> Assay, CaspaseGlo™<sup>2</sup> Assay, Caspase-Glo™<sup>8</sup> Assay, Caspase-Glo™<sup>9</sup> Assay (Promega Corporation, Wisconsin, USA)

Morphological membrane changes were detected using Annexin V-EGFP/PI detection kit (Biovision, Mt. View, CA).

Viability was measured using the colorimetric CellTiter 96® Aqueous One Solution Cell Proliferation Assay (Promega). The CellTiter 96® Aqueous One Solution Reagent contains a novel tetrazolium compound [3-(4,5-dimethylthiazol-2-yl)-5-(3-carboxymethoxyphenyl)-2-(4-sulfophenyl)-2H-tetrazolium, MTS] and an electron coupling reagent (1-methoxy phenazine methosulfate, PMS).

Total RNA was isolated using the RNeasy Plus Minikit purchased from QIAGEN (Valencia CA, USA).

### **Reagents**

The liquid scintillation was the Ready-Gel (Beckman Instrument, Fullerton, USA). The reagents and the molecular weight standard were purchased from GE Healthcare.

The pan-caspase inhibitor Z-VAD-fmk (carbobenzoxy-valyl-alanyl-aspartyl-[O-methyl]fluoromethylketone), proteasome inhibitors PS-341 and MG-132 were supplied by Vinci-Biochem (Florence, Italy).

The Immobilon Western detection Reagent and the PVDF membrane were purchased from Millipore (Milford, MA, USA).

For SDS-PAGE, precasted gels and buffer strips obtained from GE Healthcare were used.

The iScript cDNA synthesis Kit and the SsoFast™ EvaGreen® Supermix were obtained from Bio-Rad (Hercules, CA, USA).

Other reagents used were from Merck (Darmstadt, Germany), Carlo Erba (Milano, Italy) and Sigma.

### **Instruments**

Cells were maintained at 37°C in humidified atmosphere at 5% CO<sub>2</sub> in the HeraCell Haereus incubator (Hanau, Germany).

Cell-incorporated radioactivity was measured by a  $\beta$ -counter (Beckman Coulter, Fullerton, CA, USA).

Morphological cell analysis was carried out with a digital camera from Motic Microscopes, (Xiamen,China).

Absorbance at 492 nm was measured by a microtiter plate reader Multiskan EX, ThermoLabsystem, (Helsinki, Finland).

Flow cytometry analysis, was done using the FACSAria BD analyzer or FACS Fortessa (Franklin Lakes, New Jersey, USA).

The luminescence was read using the Fluoroskan Ascent FL (Labsystem, Finland).

Protein concentration was determined by UVICON 860 Spectrophotometer (Kontron Instruments, Milano, Italy).

The protein were separated on SDS-PAGE and then blotted using the Mini Protean 3 Cell electro-blotting apparatus (Bio-Rad).

The SDS-PAGE analysis of immunotoxins was conducted using the the PhastSystem (GE-Healthcare).

qRT-PCR was performed using the CFX96 Real-Time PCR System (Bio-Rad).

PCR was conducted using the thermal cycler PCR system 2400 (Perkin Elmer).

Nucleic acids were quantified using NanoDrop 1000 Spectrophotometer (Thermo Fischer Scientific, Inc. Waltham, Ma, USA ).

RNA integrity was evaluated with Agilent 2100 Bioanalyzer (Agilent Technologies, USA).

### **Statistical analysis**

Statistical analyses were conducted using the XLSTAT-Pro software, version 6.1.9 (Addinsoft 2003). Result are given as means  $\pm$  SD. Data were analyzed by ANOVA/Bonferroni, followed by a comparison with Dunnett's test.

## **2.2 Methods**

### **Cell protein synthesis inhibition assay**

The inhibitory activity of free RIPs and immunotoxins on blood-derived cell lines was evaluated as inhibition of L-[4,5-<sup>3</sup>H] leucine incorporation. Cells ( $4 \times 10^4$ /well) were seeded in 96-well microtiter plates in 100  $\mu$ l of complete medium in the presence or absence of 100  $\mu$ l of stenodactylin added to final concentrations ranging from  $10^{-9}$  to  $10^{-13}$  M, or in the presence of 100  $\mu$ l of immunotoxin added to final concentrations ranging from  $10^{-7}$  to  $10^{-11}$  M. Control samples were run with RIP alone, mAb alone, a mixture of unconjugated anti-CD20 or anti-CD22 mAb and RIP. At different time-points, 1  $\mu$ Ci of L-[4,5-<sup>3</sup>H] leucine was added to each well. After further 6 h cells were harvested with an automatic cell harvester (Skatron Instruments, Lier, Norway) onto glass-fiber diskettes. Cell-incorporated radioactivity was determined by a  $\beta$ -counter with Ready-Gel scintillation liquid containing 0.7% acetic acid. The IC<sub>50</sub> and IC<sub>100</sub> (concentration of immunotoxin or RIP required to inhibit cell protein synthesis by 50% and 100%, respectively), were calculated by regression analysis.

### **Cell viability assay**

Cell viability was evaluated with the colorimetric assay CellTiter 96® Aqueous One Solution Cell Proliferation. This colorimetric kit allows to determine the number of viable cells. The MTS tetrazolium compound is bio-reduced by cells into a colored formazan product that is soluble in RPMI medium. This conversion is presumably accomplished by NADPH or NADH produced by dehydrogenase enzymes in metabolically active cells. The quantity of formazan product is measured by the absorbance at 490 nm. Cells ( $2 \times 10^4$ /well) were seeded in 96-well microtiter plates in 100  $\mu$ l RPMI complete medium. After 24 h, cells were incubated in the absence (control culture) or in the presence of stenodactylin, ricin or ITs at desired concentrations in complete medium. After the indicated times 20  $\mu$ l/well of colorimetric kit solution were added. After 1 h of incubation at 37°C the absorbance at 492 nm was measured.

### **Cell morphology**

Cells ( $1 \times 10^5$  / 500  $\mu$ l complete RPMI medium) were incubate with stenodactylin in 24-well microtiter plates for 24 and 48 h at 37°C. Morphology was assessed by phase contrast microscopy.

### **Assessment of apoptosis**

Apoptotic cell death was examined by flow cytometry Annexin V-EGFP/PI detection kit and by luminometer measuring of caspase activation. Apoptosis inhibitor Z-VAD was added 3 h before treatment with stenodactylin or ITs.

#### *Quantification by flow cytometry*

Cells ( $2 \times 10^5$ / 1 ml complete RPMI) were seeded in 24-well microtiter plate, and after incubation with ITs or RIP, the cells were centrifuged at 400 $\times$ g for 5 min, washed in 2 ml fresh medium, centrifuged again and resuspended in 294  $\mu$ l binding buffer provided in the kit. Annexin V-EGFP (3  $\mu$ l) and propidium iodide (3  $\mu$ l) were added. Tubes were incubated for 10 min in the dark at room temperature. Cells were analyzed by flow cytometry within 30 min, using the FACS Aria BD analyzer. Data were analyzed using FlowJo software.

#### *Caspase -3/7, -8,-9,-2 activities*

The caspase-2, -8, -9 and -3/7 were assessed by the luminescent assay Caspase-Glo™, specific for each caspase. Each kit provides a luminogenic caspase substrate, which contains the tetrapeptide sequence specific for each caspase (VDVAD, LETD, LEHD, DEVD for caspase -2, -8, -9, 3/7, respectively). The caspase cleaves its substrate generating a luminescent signal, produced by luciferase. Luminescence is proportional to the amount of caspase activity present. Cells ( $2 \times 10^4$ /well) were seeded in 96-well microtiter plates in 40  $\mu$ l RPMI complete medium. Cells were treated with 40  $\mu$ l RPMI containing ITs or stenodactylin to reach desired concentration. After incubation at the indicated times, 80  $\mu$ l/well of Caspase-Glo™ 2, Caspase-Glo™ 8, Caspase-Glo™ 9, and Caspase-Glo™ 3/7 were added. Plates were shaken at 420 rpm for 1 min and then

incubated for 20 min at room temperature in the dark. The luminescence was measured by Fluoroskan Ascent FL (integration time 10 sec).

### **SDS- PAGE**

RTX/S6 and OM124/S6 were analyzed by polyacrylamide electrophoresis gels under denaturing conditions. IT was incubated in SDS-Sample Buffer (40 mM Tris-HCl pH 6.8, 0.005% bromophenol blue) for 20 min at 37°C. Then the samples were analyzed on the PhastGel 4-15% gradient using the PhastSystem instrument. The gel was stained with Coomassie Brilliant Blue G250 0.1% (w/v) in 50% methanol and 10% acetic acid.

### **Western Blot analysis**

Cells ( $3 \times 10^6$ / 15 ml RPMI complete) were seeded in 25 cm<sup>2</sup> flasks and stenodactylin ( $10^{-9}$  M) was added. At different times of incubation, ranging from 2 to 6 h, cells were harvested and collected by centrifugation at 500×g for 5 min at room temperature. Cell pellets were lysed by adding 75 µl of Cell Lytic-M (Sigma-Aldrich) supplemented with Protease inhibitor Cocktail (1:100), Phosphatase inhibitor cocktail 1 (1:100) and sodium-orthovanadate (1:500). After 45 min at 0°C, vortexing every 5 min, insoluble material (nuclear pellet plus membranes) was removed by centrifugation at 14,000×g for 25 min at 4°C. Protein supernatant (cell lysate) was collected and stored at -20°C. Protein content was quantified by spectrophotometer using Bradford assay (Bio-Rad). Protein (40 µg/lane) were separated by SDS-PAGE (10% gel or 4-15%) and blotted for 45 min at 100 V to Immobilon (polyvinylidene difluoride, PVDF) membrane (Millipore). Non-specific antibody binding sites were blocked by incubation with blocking buffer (TRIS buffered saline, 0.1% Tween 20 (TBS/T)) with 5% non-fat dry milk, for 1 h at room temperature. For phosphoepitopes, 5% bovine serum albumin (BSA) was used as blocking reagent. After 5 washes with TBS/T, membranes were incubated overnight at 4°C with various primary antibodies. COX IV was used as protein loading control. All antibodies were diluted in TBS/T with 5% bovine serum albumin. After 5 washes with TBS/T, membranes were incubated for 1 h at room temperature with horseradish peroxidase-conjugated anti-mouse or anti-rabbit antibody or secondary antibody used at 1:10000, diluted in blocking buffer with 5% non-fat dry milk. After further 5 washes, proteins were detected by incubating the membrane with

Immobilon Western detection Reagent (Millipore) according to manufacturer's protocol and the image was taken on ImageQuant imager. The level of expression of different proteins was analysed by using the public domain software Image J.

### **Intracellular phospho-specific flow cytometry**

MOLM-13 cells ( $1 \times 10^6$ /5 ml RPMI complete) 25 cm<sup>2</sup> flasks and stenodactylin ( $10^{-9}$  M) was added. At different times of incubation, ranging from 2 to 6 h, cells were harvested and collected by centrifugation at  $500\times g$  for 5 min at room temperature. Cells were fixed in 1.6% paraformaldehyde, permeabilized with 100% methanol and stored at  $-80^\circ\text{C}$  until flow cytometric analysis. PFA fixed, methanol-permeabilized cells were rehydrated by addition of 2 mL PBS, resuspension by vortexing, and then centrifugation. The cell pellet was washed once with 2 mL PBS, 1% BSA (Sigma), resuspended in 50  $\mu\text{L}$  PBS, 1% BSA, and then split evenly into new cytometry tubes for staining. To achieve high-throughput and to reduce costs, the cells were barcoded (Krutzik *et al.*, 2006). Then, 50  $\mu\text{L}$  of an antibody mix containing 0.13  $\mu\text{g}$  Alexa Fluor® 647 conjugate mouse primary phospho-specific antibody per sample was added to each tube of MOLM-13 cells and staining proceeded for 20 minutes at room temperature. Stained cells were washed by adding 2 mL PBS, 1% BSA and resuspended in 200  $\mu\text{L}$  PBS. At least 30000 live cell events were collected for each sample on a FACS Fortessa (Becton Dickinson). FCS data analysis was performed with FlowJo.

### **Microarray experiments**

#### *Sample preparation and RNA extraction*

MOLM-13 cells ( $4 \times 10^6$ / 20 ml complete medium) were seeded in 75 cm<sup>2</sup> flasks and then stenodactylin ( $10^{-9}$  M) was added. At different times of incubation, ranging from 2 to 6 h, cells were harvested and collected by centrifugation at  $500\times g$  for 5 min at room temperature. Cell pellets were frozen at  $-80^\circ\text{C}$ , then total RNA was extracted using the RNeasy Plus Minikit, following manufacturer's instructions. Amount and quality of the extracted RNA were measured by the NanoDrop® ND-1000 spectrophotometer (NanoDrop Technologies, USA) and the Agilent 2100 Bioanalyzer (Agilent Technologies, USA).

*Illumina iScan system*

A microarray study of early gene expression changes induced by  $10^{-9}$  M stenodactylin on MOLM-13 cells was conducted using the Illumina iScan, which is based upon fluorescence detection of biotin-labeled cRNA. Using the Illumina TotalPrep RNA Amplification Kit (version 280508, Applied Biosystems/Ambion, USA), 300ng of total RNA from each sample was reversely transcribed, amplified and Biotin-16-UTP-labeled. The amount (15–52  $\mu$ g) and quality of labeled cRNA were measured using both the NanoDrop spectrophotometer and Agilent 2100 Bioanalyzer. Biotin-labeled cRNA (750 ng) was hybridized to the The Illumina Sentrix BeadChip according to manufacturer's instructions. The Human HT12 v4 BeadChip targets approximately 47231 annotated RefSeq transcripts.

*Microarray data extraction and analysis*

Quality control and preprocessing

Bead summary data was imported into GenomeStudio to remove control probes and to produce a text file containing the signal and detection p-values per probe for all samples. The text file was imported into J-Express Pro 2012 (<http://jexpress.bioinfo.no>), and signal intensity values were quantile normalized (Bolstad *et al.*, 2003) and log transformed (base 2). Correspondence Analysis (CA) (Fellenberg *et al.*, 2001) and hierarchical clustering with Pearson Correlation as a distance measure were performed to look for global trends in the data. In the CA plot, the microarray data for genes and samples are projected onto a two-dimensional plane defined by the first and second principal components. The first principal component (along the x-axis) explains most of the total chi square, the second principal component explains second most of the total chi square. Samples that are close together in the plot have more similarity than samples further apart. The quality of the data in this experiment were good, with a tendency for samples to create a gradient, with control samples and samples treated with stenodactylin for 2 hours at one end, and samples treated with stenodactylin for 6 hours at the other end. No sample was excluded from analysis since no outliers were detected.

### Microarray Gene Expression Data Analysis

Correspondence analysis (CA) (Fellenberg *et al.*, 2001), significance analysis of microarrays (SAM) (Tusher *et al.*, 2001), and hierarchical clustering of samples and transcripts were performed on the sub-data sets in J-Express 2012. For pathway and gene ontology analysis, the PANTHER classification system was used (Mi *et al.*, 2013).

### **cDNA synthesis and qRT-PCR for apurinic sites**

For detection of apurinic sites in the 28S rRNA, the qRT-PCR method of Melchior *et al.*, 2010 was applied with some modifications. Briefly, 800 ng of total RNA was reverse transcribed with the iScript cDNA Synthesis kit (Bio-Rad) following the manufacturer's direction, applying 4  $\mu$ l of 5 $\times$  iScript Mix, 1  $\mu$ l of iScript reverse, the sample and Nuclease free water to a total volume of 20  $\mu$ l. The reaction mix was incubated for 5 min 25°C, followed by 30 min incubation at 42°C, then by 5 min at 85°C and then the cDNA product was stored at -20°C. The resulting cDNA was used in the real time PCR reaction. Then 3  $\mu$ l of a 1:125 dilution of the resulting cDNA was used for qRT-PCR. qRT-PCR was performed in 20  $\mu$ l of reaction mixture consisting of 10  $\mu$ l of 2 $\times$ EvaGreen Supermix (Bio-Rad), 1  $\mu$ l of each primer (final concentration of 0.4  $\mu$ M), 3  $\mu$ l of template and 6  $\mu$ l of Nuclease free water. A sequence of the 28S rRNA near the apurinic site served as internal control. The following primers were used: 28S rRNA control, 5'-GATGTCGGCTCTTCCTATCATTGT-3' (forward); 28S rRNA control, 5'-CCAGCTCACGTTCCCTATTAGTG-3' (reverse); 28S rRNA depurination, 5'-TGCCATGGTAATCCTGCTCAGTA-3' (forward); 28S rRNA depurination, 5'-TCTGAACCTGCGGTTCCACA-3' (reverse). RT-PCR was performed using the CFX96 Bio-Rad Real-Time System and the following cycling program: enzyme activation for 30 sec at 98°C, 44 cycles of denaturation for 3 sec at 98°C and annealing/extension for 8 sec at 60°C, and melt curve for 5 sec/step at 65°C-95°C (in 0.5°C increments). The relative gene expression changes (given as fold changes compared to untreated controls, which were set to 1) were calculated with BioRad CFX Manager software using the  $\Delta\Delta$ Ct method. The data represent mean  $\pm$  SE of three independent experiments, each performed in duplicate.

*Chapter III*

***IN VITRO* COMPARISON OF  
ANTITUMOR ACTIVITY OF  
SAPORIN-BASED IMMUNOTOXINS**



## BACKGROUND

Non-Hodgkin's lymphoma (NHL) consists of a large group of hematological malignancies and represents a heterogeneous group of diseases involving monoclonal expansion of both B- and T-lymphocytes. B-cell lymphomas account for over 90% of all NHLs. Nearly 70000 new cases in the United States (American Cancer Society) and approximately 37000 new cases in the European Union (European Cancer Observatory <http://eco.iarc.fr/EUCAN/>) of aggressive B-cell NHLs are diagnosed every year. The CD20 antigen is a 33-37 kDa tetra-membrane spanning protein located on chromosome 11q12-q13.1, reliably expressed on most NHL malignant B-cells and normal B-cells, but not on hematologic stem cells. In the last two decades, CD20 has emerged as an excellent target for immunotherapy as it is expressed in multimeric forms on the cell surface and it is not shed, internalized or significantly down-regulated once the binding with an antibody has occurred. Rituximab, a genetically engineered chimeric anti-CD20 monoclonal antibody, has been the first mAb approved by Food and Drug administration (FDA) in 1997 as single agent for the treatment of follicular and low-grade NHL and subsequently of untreated aggressive NHL in combination with CHOP regimen (cyclophosphamide, adriamycin, oncovin, prednisone). Rituximab cell-killing efficiency is due to the activation of effector mechanisms, such as complement-dependent cytotoxicity (CDC), antibody-dependent cellular cytotoxicity (ADCC), phagocytosis, induction of apoptosis and inhibition of proliferation (Maloney DG, 2012). Rituximab is routinely incorporated into all phases of conventional treatment, including first-line therapy, maintenance and salvage therapy, however, approximately two-thirds of lymphoma patients eventually develop disease recurrence (Siegel *et al.*, 2014), so a urgent need of novel therapeutic options exists.

Acquirement of rituximab resistance has been observed in lymphoma patients and could be reasonably attributed to the loss of expression of the CD20 antigen, even if this loss has been observed only in a small number of patients (Davis *et al.*, 1999). *In vitro* studies using rituximab-resistant cell lines have shown that the development of rituximab resistance could be attributed to significant changes that occur to the CD20 antigen, including a moderate down-regulation of CD20 and its altered reorganization

into the lipid raft domain; a possible role of the ubiquitin-proteasome system in the degradation of the COOH-terminal of CD20; abnormal CD20 promoter activity; and/or a defect in the Golgi-to-surface protein transport (Czuczman *et al.*, 2008; Tsai *et al.*, 2012). Since the up-regulation of components of the ubiquitin-proteasome system (UPS) is involved in mediating rituximab resistance, the use of proteasome inhibitors could overcome resistance and augment rituximab efficacy. It has been shown that treatment of mantle lymphoma cells with bortezomib, rituximab and cyclophosphamide were shown to act synergistically in apoptosis induction (Wang *et al.*, 2008) and rituximab + bortezomib chemotherapy was effective with low toxicity in patients with refractory or relapsed indolent B cell NHL (Yun *et al.*, 2015). However, bortezomib and other proteasome inhibitors were found to affect rituximab-mediated CDC but not ADCC. Surprisingly, treatment with bortezomib was shown to increase CD20 ubiquitination and to reduce surface CD20 levels (Bil *et al.*, 2010). In preclinical studies, additive cytotoxic effects have been reported with the combination of bortezomib and rituximab in B-cell lymphoblastic leukemia (B-CLL) and mantle cell lymphoma (MCL) (Smolewski *et al.*, 2006; Alinari *et al.*, 2009).

A strategy to improve monoclonal antibodies efficacy is to conjugate them with a cytotoxic agent to enhance their specific cell-killing properties and to broaden their action even involving different mechanisms of cytotoxicity. In the past years, several groups evaluated the efficacy of rituximab conjugated with different cytotoxic agents, such as iodine-131 (Leahy *et al.*, 2008; Wagner *et al.*, 2013), the antibiotic calicheamicin (Dijoseph *et al.*, 2007) and the type 1 RIP saporin-S6 (Polito *et al.*, 2004). In all these studies, a significant increase in cytotoxic efficacy of mAbs were reported.

CD22 antigen is a B-cell restricted 135 kDa transmembrane sialoglycoprotein located on chromosome 19q13.1 that plays a role in modulating B-cell function, survival and apoptosis (Walker *et al.*, 2008). B-cell malignancies express CD22 in up to 60-80% of cases and in more than 90% of the most common types of NHL, namely, follicular and diffuse large B-cell lymphoma (Derby *et al.*, 2011). Based on the potential for CD22 to become internalized upon antigen binding, it has emerged as an ideal target for mAb-based therapy of B-cell malignancies (Sullivan-Chang *et al.*, 2013). Antibody-drug conjugates and ITs were made with several anti CD22 antibodies. Inotuzumab ozogamicin is an anti-CD22 mAb conjugated with the antibiotic

calicheamicin that showed promising results in a phase I clinical trial in patients with relapsed or refractory NHL (Advani *et al.*, 2010). HB22.7 conjugated with the RIP saporin demonstrated antitumor efficacy in a murine xenograft model of human NHL (Kato *et al.*, 2012). Humanized mAb epratuzumab conjugated to a topoisomerase I inhibitor derived from irinotecan showed promising results both *in vitro* and in *in vivo* murine models of NHL (Sharkey *et al.*, 2012). A pre-treatment with HB22.7 was found to increase bortezomib cytotoxicity *in vitro* and *in vivo*, indicating that combined therapy with proteasome inhibitors could also increase anti-CD22 immunotargeted therapy (Martin *et al.*, 2011).

Saporin-S6 is a type 1 RIP purified from soapwort seeds (*Saponaria officinalis*, Caryophyllaceae family) showing an extremely high rRNA *N*-glycosylase activity in cell-free systems. Purified saporin-S6 is very stable and extremely resistant to high temperature, to denaturation by urea or guanidine and to attack by proteolytic enzymes. Saporin-S6 is also very stable in response to chemical modifications such as those necessary for derivatization and conjugation procedures (Polito *et al.*, 2013). Saporin-S6 was shown to induce apoptosis in intoxicated cells, but the exact mechanism of cell death involved is still not completely understood, as saporin-S6 seems to be able to induce different cell death pathways in lymphoma cells (Polito *et al.*, 2009), possibly involving protein synthesis inhibition, apoptosis, autophagy, necroptosis, oxidative stress and DNA damage (Polito *et al.*, 2013). Taken together, these properties make saporin-S6 an ideal candidate for the design and production of ITs.

Since different studies have shown that RIPs toxicity could be reduced due to proteasome degradation (Freudlsperger *et al.*, 2007; Battelli *et al.*, 2010), it is possible that pre-treatment of cells with proteasome inhibitors could lead to an increase of the amount of active enzyme inside the cell.

## AIM OF THE PROJECT

The vascular nature of the majority of lymphomas represents a favorable condition for the immunotherapy, since single malignant cells result very accessible to mAbs. Several mAbs targeting different CD markers have been developed to treat lymphoma, often with promising results either in preclinical models than in patients (Polito *et al.*, 2013b). Generally, mAbs eliminate target cells as a consequence of different possible cytotoxic pathways: CDC, ADCC and direct apoptosis induction. Cytotoxic efficacy of mAbs has been improved with several strategies, included the conjugation with toxic compounds such as radionuclides, drugs or toxins.

Rituximab is a genetically engineered chimeric anti-CD20 monoclonal antibody approved in 1997 by FDA for the treatment of NHL. Safety and clinical efficacy of rituximab have been investigated in more than 300 phase II/III clinical trials in aggressive, indolent NHL either as single agent than in combination with chemotherapeutics. However, despite its efficacy, adverse effect and development of resistance to rituximab treatments have been reported (Bonavida, 2014). Several attempts have been made to improve rituximab efficacy. Here, we tested the anti-tumor efficacy of RTX/S6, an IT produced by chemical conjugation of rituximab to plant toxic rRNA *N*-glycosylase saporin-S6, a type 1 ribosome-inactivating protein purified from seeds of *Saponaria officinalis*. This IT has been previously shown to have an enhanced *in vitro* cytotoxic activity compared to rituximab in CD20-positive cells. Since little is known about the mechanism of action of RTX/S6, the aim of this project is to evaluate the ability of RTX/S6 to induce apoptosis in target cells and compare its action to an anti-CD22 IT, OM124/S6, to understand if saporin-based ITs share a common cell death pathway independently from the carrier-moiety.

Since it has been described in literature that rituximab efficacy is improved by combination with proteasome inhibitor bortezomib (Smolewski *et al.*, 2006; Wang *et al.*, 2008; Alinari *et al.*, 2009, Yun *et al.*, 2015), and ribosome-inactivating proteins could be degraded by the proteasome following the ERAD pathway (Freudlsperger *et al.*, 2007; Battelli *et al.*, 2010), we designed our experiments to test the efficacy of a combined treatment of RTX/S6 and bortezomib on CD20-positive cells. Furthermore, proteasome inhibitor MG-132, that was shown to induce apoptosis in drug resistant

cancer cells (Zhang et al., 2008; Han et al., 2009; Guo e Peng, 2013; Li et al., 2013), was considered as a candidate to increase ITs anti-tumor efficacy.

In this research, we tested the cytotoxic effect of the immunoconjugate rituximab/saporin-S6 (RTX/S6) on CD20/CD22-positive cell line Raji and compared it to an anti-CD22 immunotoxin obtained by conjugating mAb OM124 to saporin-S6. We explored the possibility of combining RTX/S6 or OM124/S6 with proteasome inhibitors to augment the efficiency of killing target cells.

## RESULTS

Saporin-S6 was conjugated to rituximab through the insertion of an artificial disulphide bond as described by Polito *et al.*, 2004, to obtain RTX/S6 immunotoxin. Briefly, sulphhydryl groups (SH) were inserted by an imidoester reaction between 2-iminothiolane and the primary amino group of each protein. After conjugation, the composition of purified conjugate was analyzed by SDS-PAGE in a 4-15% gradient gel under non-reducing conditions. Reaction yielded three products, a 1:1 product containing 1 molecule of saporin conjugated to rituximab, a 2:1 product formed by 2 molecules of saporin conjugated to rituximab and a 3:1 product containing 3 molecules of saporin conjugated to rituximab. Densitometric analysis revealed that the 1:1 product represented the 36% of the total intensity, while 2:1 and 3:1 products represented the 39% and 25% respectively.

OM-124/S6 immunotoxin was produced in similar conditions as described in Bolognesi *et al.*, 1998. After purification the conjugate was composed by a mixture of three different products containing one molecule of mAb linked to 1-3 molecule of saporin. Densitometric analysis revealed that the 1:1 product represented the 42.8% of the total intensity, while 2:1 and 3:1 products represented the 36.2% and 21%, respectively.

The inhibitory activity of immunoconjugates on cell-free protein synthesis was evaluated *in vitro* using a rabbit reticulocyte lysate system. Characteristics of the two ITs are summarized in Table 1. After conjugation process, saporin retained its ability to inhibit protein synthesis by a rabbit reticulocytes lysate, with  $IC_{50}$  values in the picomolar range, moreover, the RIP/mAb molar ratio was in the optimum range. It is possible to conclude that derivatization and conjugation processes followed had low impact on RIP enzymatic activity.

**Table 1.** Immunotoxins properties

DERIVATIZATION			CONJUGATION	CELL-FREE PROTEIN SYNTHESIS INHIBITORY ACTIVITY	
Number of SH-group inserted per molecule			RIP/mAb (mol/mol)	IC <sub>50</sub> (M)	
	mAb	RIP	IT	IT	RIP
RTX/S6	3.70	0.81	1.89	7.0×10 <sup>-11</sup>	6.2×10 <sup>-11</sup>
OM-124/S6	1.30	1.20	1.43	8.1×10 <sup>-11</sup>	6.2×10 <sup>-11</sup>

### Cellular protein synthesis inhibition assays

To test the ability of saporin to inhibit cellular protein synthesis after the conjugation process, global cellular protein synthesis was assayed in CD20/CD22-positive Raji cells after 96 hours of treatment with RTX/S6 or OM124/S6 ITs (Fig. 1). Compared to a mixture of unconjugated rituximab and saporin-S6, RTX/S6 showed an enhanced efficacy, with IC<sub>50</sub> values of  $1.99 \times 10^{-9}$  M and  $> 10^{-7}$  M for the immunotoxin and the mixture, respectively. Protein synthesis was almost completely abolished at  $10^{-8}$  M concentration, expressed as RIP content (Fig. 1A). OM124/S6 showed a higher inhibitory activity. A complete inhibition of protein synthesis was observed at  $10^{-9}$  M concentration, while a mixture of unconjugated OM124 and saporin produced no effect on protein synthesis at the same concentration. OM124/S6 showed an IC<sub>50</sub> value of  $6.03 \times 10^{-11}$  M, about two logs lower than RTX/S6 (Table 2).

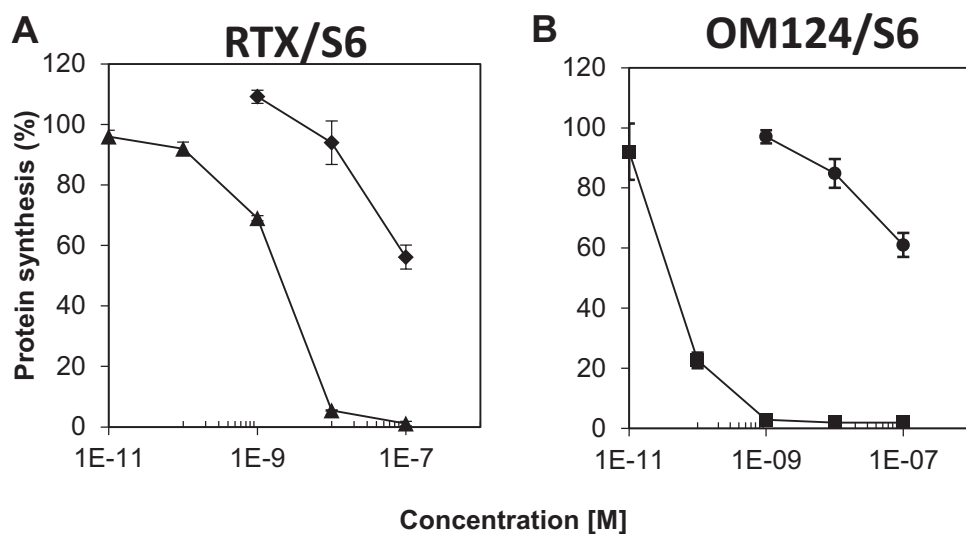


**Fig. 1** A) Protein synthesis inhibition assay on Raji cells treated for 96 hours with RTX/S6 IT (▲), a mixture of unconjugated rituximab and saporin-S6 (◆) or B) with OM124/S6 IT (■) or a mixture of unconjugated OM124 and saporin-S6 (●). A total of  $2 \times 10^4$  cells were seeded in 96-well plates in a final volume of 200  $\mu$ l of complete medium containing appropriate concentration of RTX/S6, OM124/S6 or a mixture of unconjugated mAb and saporin, expressed as RIP concentration. After 96 h of incubation and further 6 h with [ $^3$ H] leucine, the radioactivity incorporated was determined. Results are the means of three independent experiments each performed in triplicate. SD never exceeded 10%.

**Table 2.** Calculated  $IC_{50}$  values for RTX/S6 and OM124/S6 ITs in Raji cells.

	<b>RTX/S6</b>	<b>OM124/S6</b>	<b>FREE RIP + mAb</b>
<b><math>IC_{50}</math> (M)</b>	$1.99 \times 10^{-9}$	$6.03 \times 10^{-11}$	$> 10^{-7}$

### Cell viability assays

Cytotoxicity of the two ITs was evaluated after a 96 h treatment in Raji cells. Dose-response curves, shown in Fig. 2, appeared very similar to protein synthesis inhibition curves, being OM124/S6 the most toxic between the two immunoconjugates. No viable cells were observed after a 96 h treatment with RTX/S6 at  $10^{-7}$  M concentration, while no relevant effect on cell viability was achieved by a mixture of unconjugated rituximab and saporin at the same concentration. OM124/S6 was able to

completely inhibit cell viability at  $10^{-9}$  M concentration, being this IT 2 log more effective in killing Raji cells than RTX/S6. Again, a mixture of free-RIP and OM124 produced no relevant effect on Raji cells viability.  $EC_{50}$  values for the two ITs are reported in table 3.

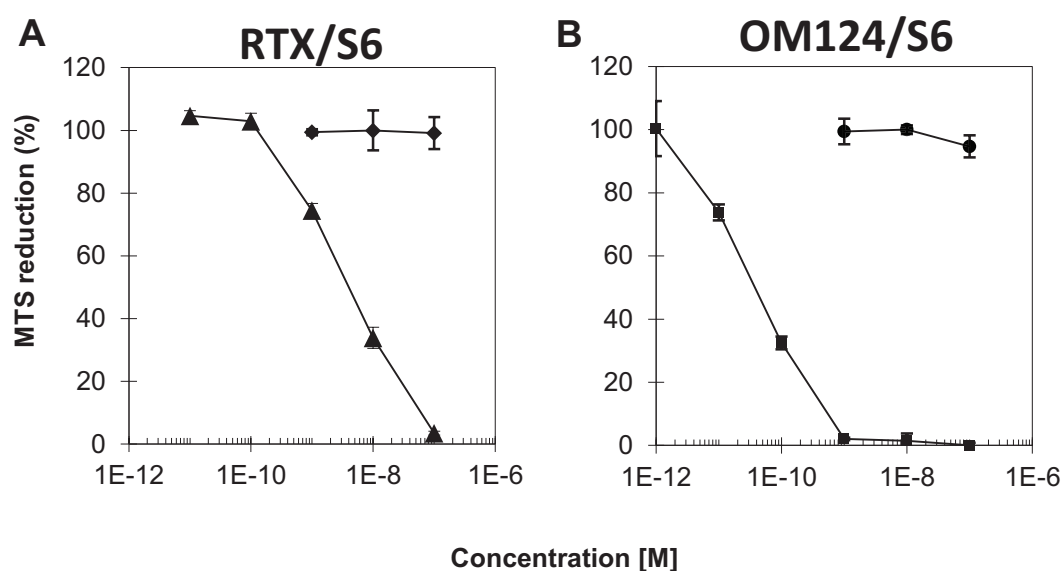


**Fig. 2 A)** Viability assay on Raji cells treated for 96 h with RTX/S6 IT (▲), a mixture of unconjugated rituximab and saporin-S6 (◆) or **B)** with OM124/S6 IT (■) or a mixture of unconjugated OM124 and saporin-S6 (●). A total of  $2 \times 10^4$  cells were seeded in 96-well plates in a final volume of 200  $\mu$ l of complete medium containing appropriate concentration of RTX/S6, OM124/S6 or a mixture of unconjugated mAbs and saporin. After 96 H, viability was evaluated using a colorimetric assay based on MTS reduction. Results are the means of three independent experiments each performed in triplicate. SD never exceeded 10%.

**Table 3.** Calculated  $EC_{50}$  values for RTX/S6 and OM124/S6 ITs in Raji cells.

	<b>RTX/S6</b>	<b>OM124/S6</b>	<b>FREE RIP + mAb</b>
<b><math>EC_{50}</math> (M)</b>	$4.06 \times 10^{-9}$	$4.81 \times 10^{-11}$	$> 10^{-7}$

Viability of Raji cells after IT exposure was also measured in a time-course experiment to evaluate the minimum time required to observe a cytotoxic effect. To this purpose, cells were exposed to different IT concentrations and viability assessed at 24, 48, 72 and 96 hours (Fig. 3). As expected, resulting curves showed that cytotoxicity of the ITs increased in prolonged incubation times and the maximum cytotoxic effect was observed only at the higher tested doses after 96 h. Dose-response curves showed a similar tendency for the two ITs.

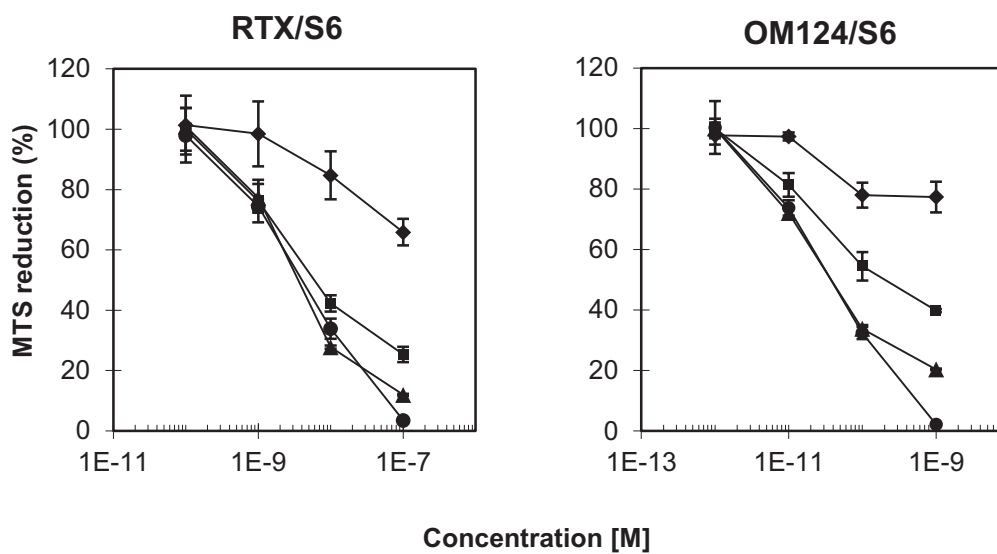


**Fig. 3** Viability assay on Raji cells treated for with **A)** RTX/S6 IT or **B)** with OM124/S6 IT for 24 h (♦), 48 h (■), 72 h (▲), and 96 h (●). Cells ( $2 \times 10^4$  / well) were seeded in 96-well plates in a final volume of 200  $\mu$ l of complete medium containing appropriate concentration of RTX/S6 or OM124/S6. Viability was evaluated using a colorimetric assay based on MTS reduction. Results are the means of three independent experiments each performed in triplicate. SD never exceeded 10%.

### Complement-dependent cytotoxicity (CDC) of RTX/S6 on Raji cells

Since rituximab is currently used in clinical practice to treat several forms of NHL, we compared the cell-killing efficacy of RTX/S6 to rituximab alone in the presence or absence of human complement. RTX/S6 IT significantly reduced cell viability at  $10^{-8}$  and  $10^{-7}$  M concentrations, whereas at the same concentrations, rituximab alone showed little effect even in the presence of 25% of human serum in the medium. Furthermore, the presence of human serum significantly increased RTX/S6 cytotoxicity compared to the same IT in the absence of a source of complement (Fig. 4).

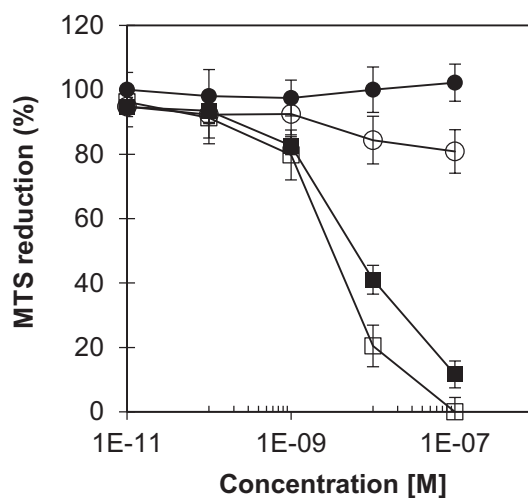


**Fig. 4** Complement-dependent and complement-independent cytotoxicity of rituximab and RTX/S6 on Raji cells. Cells were incubated in medium supplemented with 25% active human serum (white symbols) or in medium supplemented with 10% heat-inactivated FBS (black symbols) in the presence of rituximab (circles) or RTX/S6 (squares). After 96 h of incubation, cell viability was evaluated by a colorimetric assay based on MTS reduction. Results are the means of four independent experiments, each performed in triplicate. SD never exceeded 10%.

### Evaluation of RTX/S6 cytotoxicity in different CD20-positive cell lines

Potential anti-tumor activity of RTX/S6 was also evaluated on two other CD20-positive lymphoblastoid lines, namely D430B and Ramos cell lines. Viability was assessed after a 96 h incubation with scalar doses of the IT. D430B and Ramos cells were found to be more sensitive to RTX/S6 than Raji cells, showing a complete loss of viability when treated with a  $10^{-8}$  M concentration of IT, whereas a  $10^{-7}$  M concentration of the IT is necessary to achieve a complete depletion of Raji cells (Fig. 5). Estimated

EC<sub>50</sub> values at 96 hours for Raji, D430B and Ramos cells were  $4.1 \times 10^{-9}$  M;  $3.6 \times 10^{-10}$  M and  $2.7 \times 10^{-10}$  M, respectively. The cause of this difference in sensitivity was not investigated in the present work.

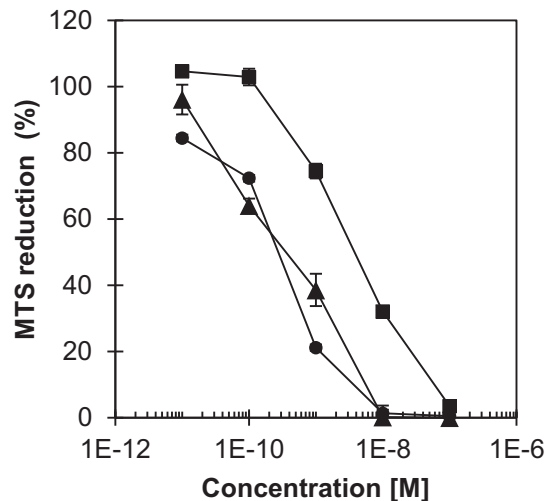


**Fig. 5** Viability assay on Raji (■), D430B (▲), and Ramos (●) cells treated for 96 h with RTX/S6 IT. Cells ( $2 \times 10^4$  / well) were seeded in 96-well plates in a final volume of 200  $\mu$ l of complete medium containing appropriate concentration of RTX/S6 or OM124/S6. Viability was evaluated using a colorimetric assay based on MTS reduction. Results are the means of three independent experiments each performed in triplicate. SD never exceeded 10%.

### **Evaluation of apoptotic membrane changes induced by RTX/S6 and OM124/S6 on Raji cells**

We evaluated the presence of membrane apoptotic changes in Raji cells treated for 96 h with RTX/S6 or OM124/S6 at EC<sub>50</sub> concentrations by a double staining with Annexin V-EGFP and propidium iodide. As shown in fig. 6 panel A, after exposure to RTX/S6 for 96 h almost 50% of the cells were positive for Annexin V and propidium iodide double staining localizing in Q2, indicating a late apoptosis. In panel B, almost 60% of the cells treated with EC<sub>50</sub> concentration of OM124/S6 for 96 h were positive for both Annexin V and propidium iodide.

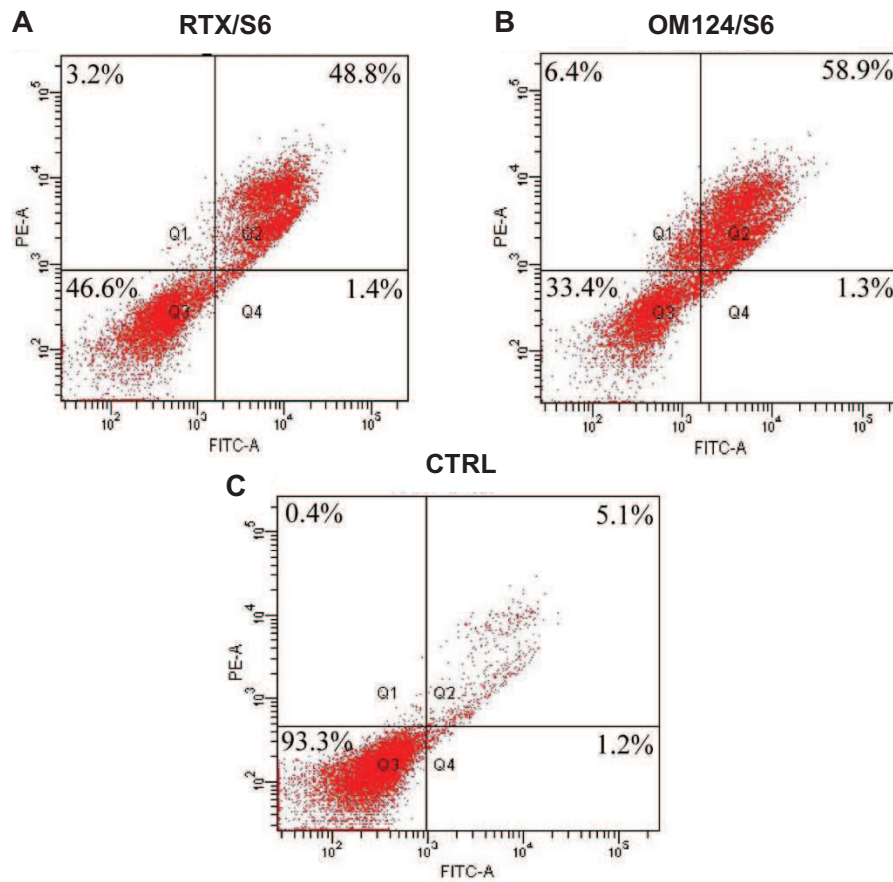


**Fig. 6** Cytofluorimetric analysis of Annexin V/propidium iodide double staining of Raji cells treated with  $EC_{50}$  concentrations of **A**) RTX/S6 or **B**) OM124/S6 for 96 h compared to **C**) untreated cells. FITC-A channel (x axis) is used for the detection of Annexin V-EGFP fluorescence. PE-A channel (y axis) is used for the detection of propidium iodide fluorescence.

### **Evaluation of caspase 3/7 activation in Raji cells treated with ITs**

Since it has been previously shown that saporin and saporin-based ITs are able to induce apoptosis in target cells (Bolognesi *et al.*, 1996; Polito *et al.*, 2013), activation of effector caspases 3/7 was measured in Raji cells after 48, 72 and 96 h of treatment with RTX/S6 and OM124/S6. Raji cells were treated with  $10^{-9}$  M concentration of RTX/S6. A significant activation of caspase 3/7 after 48 h was detected ( $p < 0.0001$ ). Intensity of caspase 3/7 activation was almost constant between 24, 48 and 96 h, reaching about 900% of controls after 96 h (Fig. 7 A). A concentration of  $10^{-11}$  M of OM124/S6 was able to significantly activate caspases 3/7 in Raji cells after 48 h ( $p < 0.0001$ ), but with less intensity compared to RTX/S6 at the same time-point. However, after 48 and 96 h of exposure to OM124/S6, caspases 3/7 activation augmented, reaching about 2300% of controls after 96 h (Fig. 7 B). Caspases 3/7 activation profiles were very different between the two ITs. RTX/S6 induced a rapid activation of caspases 3/7, reaching a plateau at 48 h that lasted until 96 h, while OM124/S6 induced a time-dependent gradient of caspases 3/7 activity, resulting in a greater activity of effector caspases at 72 h and 96 h. Both ITs were shown to efficiently induce activation of caspases 3/7 in target cells, but with different potency, being OM124/S6 the stronger, even if slower, inducer of caspases 3/7 activation. The difference in caspases 3/7 activity suggests a different intracellular fate of saporin. High level of caspases 3/7 activation measured were consistent with the idea that saporin-based ITs are able to induce caspase-dependent apoptosis in target cells.

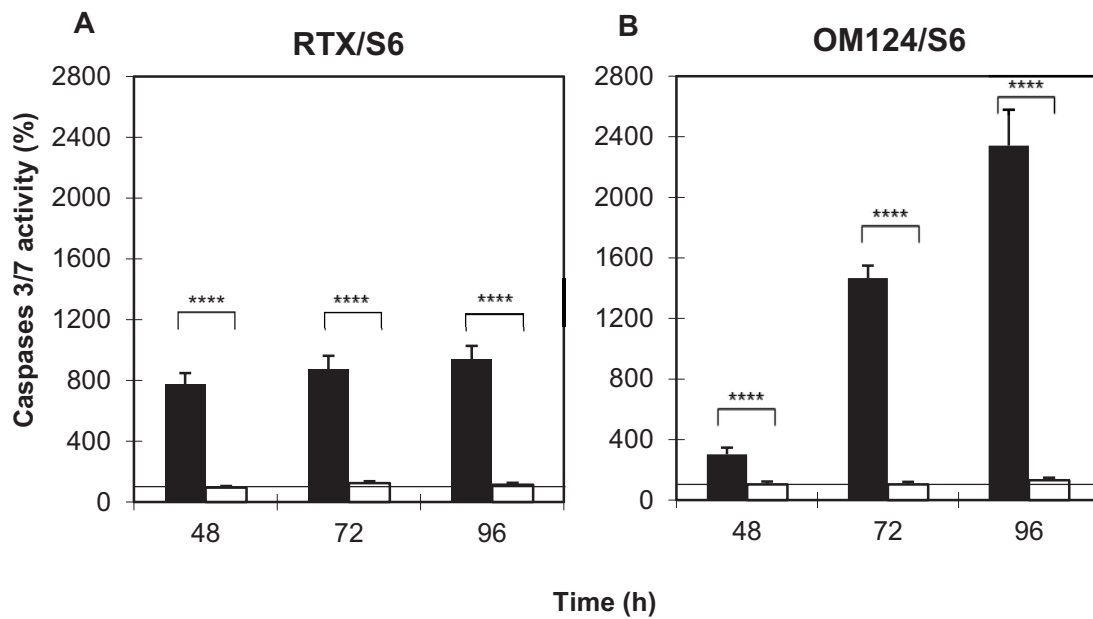


**Fig. 7** Caspases 3/7 activation in Raji cells exposed to RTX/S6 1 nM or OM124/S6 10 pM. Cells ( $2 \times 10^4$  / well) were seeded in 96-well plates in a final volume of 200  $\mu$ l of complete medium containing appropriate concentration of RTX/S6 or OM124/S6 (black columns) or a mixture of unconjugated mAb and saporin (white columns). Caspases activity was expressed as the percentage of control values. The results are the means of three independent experiments, each performed in triplicate. Asterisks indicate level of significance in ANOVA/Bonferroni followed by Dunnett's test (\*\*\*\* $p < 0.0001$ ).

### Effects of caspases inhibition on ITs cytotoxicity

To determine the role of caspase-dependent apoptosis in ITs-induced cell death, we designed further experiments including pan-caspase inhibitor Z-VAD. Raji cells were treated with RTX/S6 and OM124/S6 at  $10^{-8}$  and  $10^{-10}$  M concentrations, respectively. Those concentration were chosen to verify if caspase inhibition was effective in preventing apoptosis at IT doses causing almost 70% of reduction of viable cells. Raji cells viability was measured after 48, 72 and 96 h of exposure to ITs in the presence or absence of Z-VAD (10  $\mu$ M), added 3 h before ITs treatment (Fig. 8). Cell survival at 48 h increased significantly ( $p < 0.0001$ ) from  $40.5\% \pm 2.4\%$  for RTX/S6 alone at  $10^{-8}$  M concentration to  $72.2\% \pm 2\%$  in the presence of Z-VAD (Fig. 8, left). In Raji cells treated with OM124/S6 for 48 h, cell survival increased significantly ( $p = 0.039$ ) from  $54.5\% \pm 4.7\%$  to  $63.9\% \pm 4.2\%$  in the presence of Z-VAD (Fig. 8, right).

Z-VAD effect on cell survival was also assayed after 72 and 96 h of treatment with both ITs. As shown in fig. 10A, Z-VAD pre-treatment improved significantly cells survival treated with RTX/S6 after 72 h, even if the effect seems to be less prominent if compared to observed protective effect at 48 h; while a significant increase in cell viability is observed at 72 h only in OM124/S6-treated cells (fig. 8, right). Even after 96 h of treatment, the presence of Z-VAD resulted in a highly significant increase in RTX/S6-treated cells viability (Fig. 8, left), while a slight protective effect was observed with OM124/S6 (Fig. 8, right).

Taken together, these results suggest that caspase-dependent apoptosis may play a major role in RTX/S6-induced cell death, even if the lack of a complete protection following caspases inhibition may suggest other cell death pathways involved in RTX/S6 toxicity. OM124/S6 treatment induced a delayed strong activation of effector caspases in Raji cells, even if a little increase in cell survival was observed after caspases activity inhibition. These results may suggest that even if OM124/S6 is a strong activator of caspases 3/7, caspase-dependent apoptosis may not be the main cell death pathway involved in mediating OM124/S6 cell-killing activity.

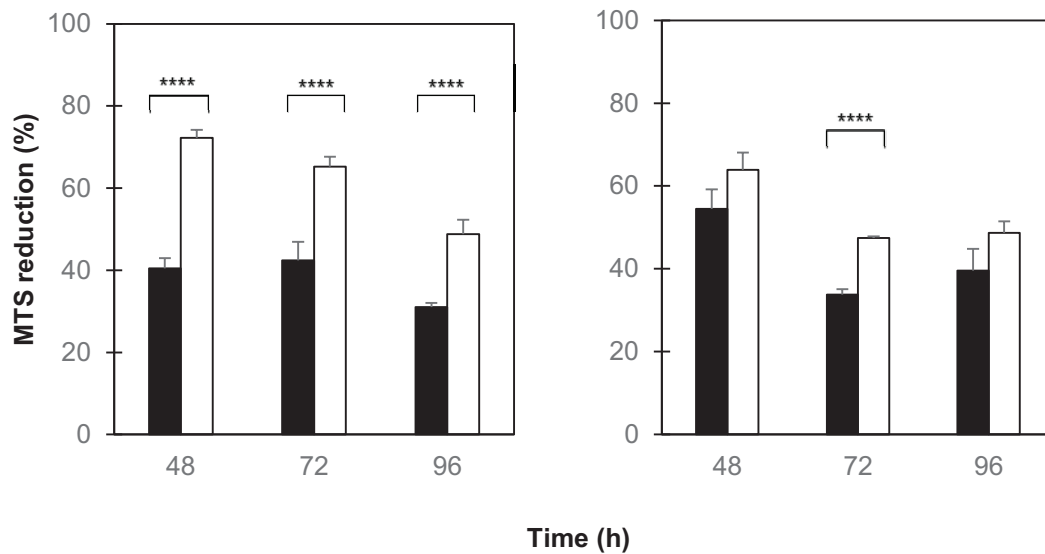


**Fig. 8** Viability of Raji cells ( $2 \times 10^4$  cells/well) treated for 48, 72, 96 h with RTX/S6 (left panel) or OM124/S6 (right panel) alone (black columns) or in the presence (white columns) of pan-caspase inhibitor Z-VAD 10  $\mu$ M. Z-VAD was added 3 h before the IT, and the viability was measured after 48 h. The results are the means of two independent experiments, each performed in triplicate, and are presented as the percentage of untreated control values. Asterisks indicate level of significance in ANOVA/Bonferroni followed by Dunnett's test (\*\*\*\* $p < 0.0001$ ). Only highly significant differences were reported.

### **Evaluation of the effect of catalase on ITs cytotoxicity**

Several studies in literature have reported that in some cell types treatment with RIPs induce the production of ROS, as reported for example in HeLa cells treated with ricin (Sutres *et al.*, 2005). To evaluate if ROS production may be involved in saporin-based ITs induction of apoptosis in Raji cells, we pre-treated cells with a ROS enzymatic scavenger, catalase. Viability was assessed after a 96 h treatment with minimum concentration of the ITs causing a complete inhibition of protein synthesis (fig. 9). Pre-treatment with catalase reduced significantly RTX/S6 cytotoxic effect, leading at a 50% of cell survival. An opposite effect was observed with OM124/S6, where no protective effect occurred at any concentration of catalase tested. This result suggests that production of hydrogen peroxide may have a role in RTX/S6- induced cell

death, while OM124/S6 exerts its cytotoxic effect following a pathway that is independent from hydrogen peroxide production.

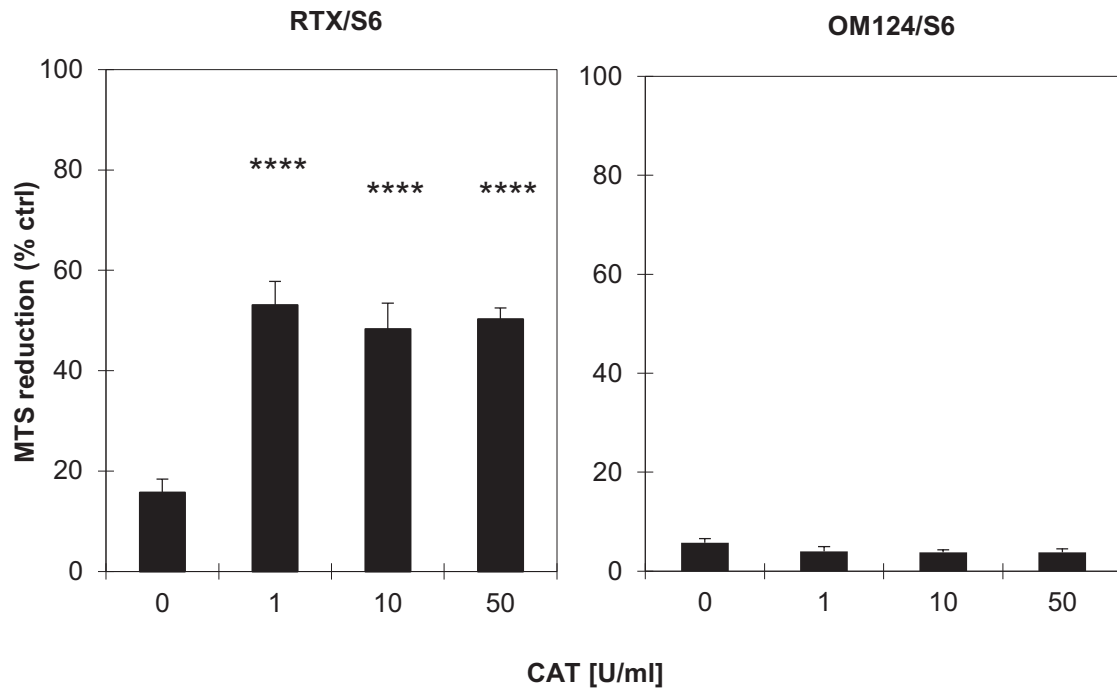


**Fig. 9** Viability of Raji cells ( $2 \times 10^4$  cells/well) treated with RTX/S6 ( $10^{-8}$  M) or OM124/S6 ( $10^{-9}$  M) in the presence of various concentrations of catalase added 3 h before ITs. Viability was evaluated after 96 h using a colorimetric assay based on MTS reduction. The results are the means of three independent experiments, each performed in triplicate, and are presented as the percentage of untreated control values. Asterisks indicate level of significance in ANOVA/Bonferroni followed by Dunnett's test (\*\*\*\* $p < 0.0001$ ).

### Combined cytotoxic effect of ITs with proteasome inhibitors

To test the possibility of enhancing ITs cytotoxic effect on Raji cells, we tested two proteasome inhibitors (MG-132 or PS-341, also known as bortezomib) given to Raji cells as single agent or in combination with the two ITs RTX/S6 and OM124/S6.

Sensitivity of Raji cells to either RTX/S6 and OM124/S6 was augmented when pre-treated for 3 h with  $10^{-7}$  M MG-132. ANOVA/Bonferroni test followed by Dunnett's test was utilized to compare toxicity by each IT and MG-132 alone or mixed. A combination of MG-132  $10^{-7}$  M + RTX/S6  $10^{-9}$  M produced a significant synergistic effect, showing an enhanced toxicity of 2.3 fold compared to MG-132 alone; and 2.8 fold compared to IT alone (fig. 10 A). A combination of MG-132  $10^{-7}$  M + RTX/S6  $10^{-10}$  M produced a significant synergistic effect, showing an enhanced toxicity of 2 fold compared to MG-132 alone; and 10 fold compared to IT alone (fig. 10 B).

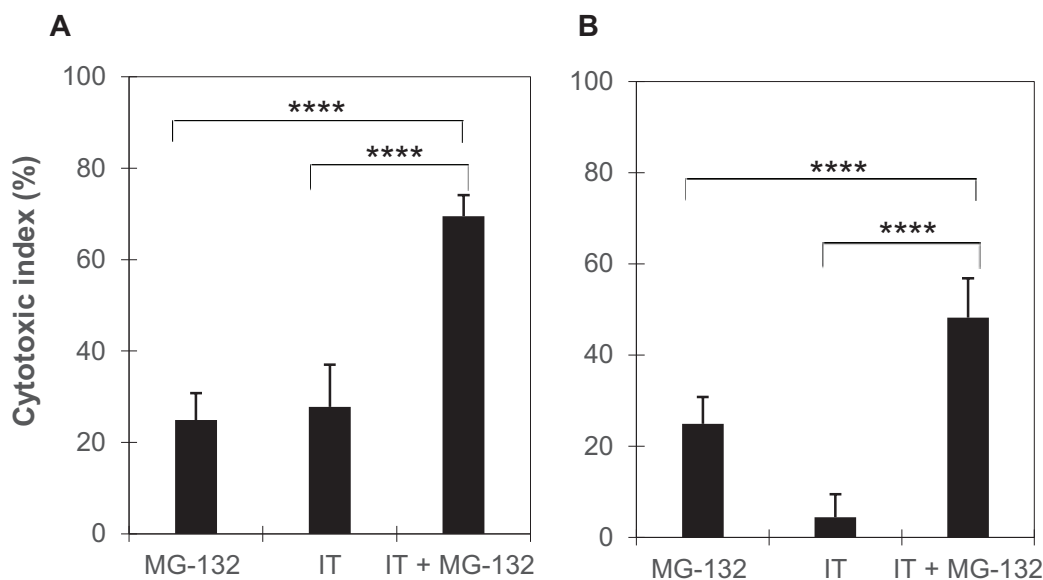


**Fig. 10** Combined cytotoxic effect of  $10^{-7}$  M MG-132 and **A)**  $10^{-9}$  M RTX/S6; or **B)**  $10^{-10}$  M RTX/S6 IT on Raji cells. Toxic effect is given as cytotoxic index, the percentage of non-viable cells. Viability was evaluated after 96 h using a colorimetric assay based on MTS reduction. The results are the means of three independent experiments, each performed in triplicate, and are presented as the percentage of untreated control values. Asterisks indicate level of significance in ANOVA/Bonferroni followed by Dunnett's test (\*\*\*\* $p < 0.0001$ ).

The combination of MG-132 with  $10^{-11}$  M OM124/S6 gave similar results, showing a significant increase in toxicity of 2 fold compared to MG-132 alone; and 2.5 fold compared to IT alone (fig. 11 A). A combination of MG-132 + OM124/S6  $10^{-12}$  M produced a non significant increase in toxicity of 1.6 fold compared to MG-132 alone (fig. 11 B), thus suggesting that either MG-132 and IT need to be administered at certain concentrations to produce a synergistic toxic effect on Raji cells.

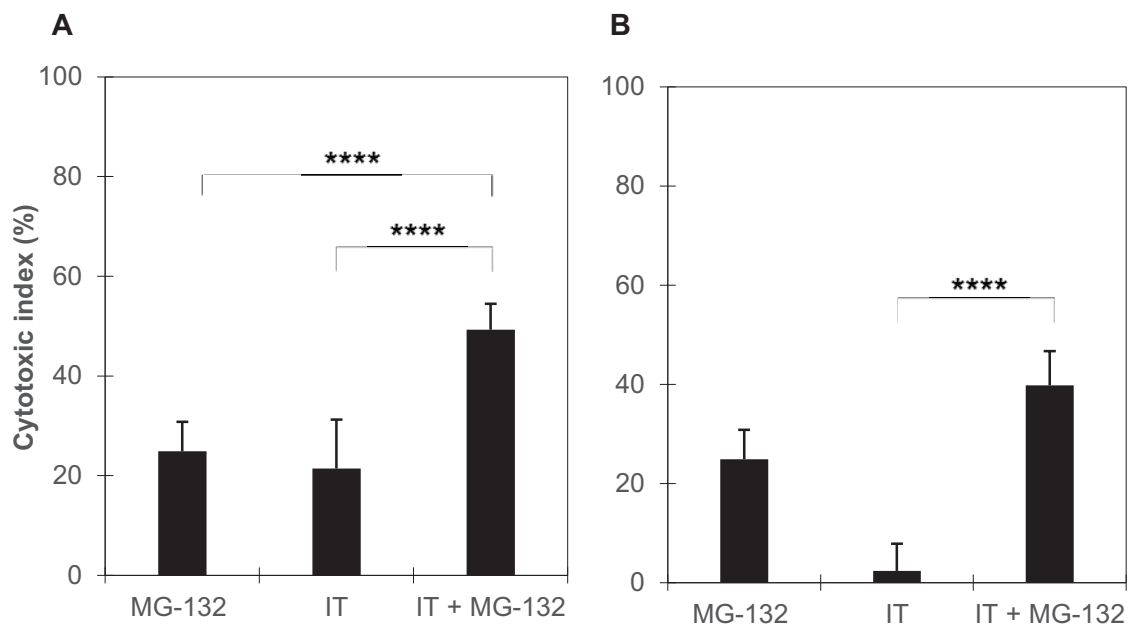


**Fig. 14** Combined cytotoxic effect of  $10^{-7}$  M MG-132 and **A)**  $10^{-11}$  M OM124/S6; or **B)**  $10^{-12}$  M OM124/S6 IT on Raji cells. Toxic effect is given as cytotoxic index, the percentage of non-viable cells. Viability was evaluated after 96 h using a colorimetric assay based on MTS reduction. The results are the means of three independent experiments, each performed in triplicate, and are presented as the percentage of untreated control values. Asterisks indicate level of significance in ANOVA/Bonferroni followed by Dunnett's test (\*\*\*\* $p < 0.0001$ ).

### **RTX/S6 produces a synergistic toxic effect with bortezomib (PS-341)**

Since additive cytotoxic effects have been reported in pre-clinical studies with the combination of PS-341 (bortezomib) and rituximab in the treatment of B-cell malignancies (Smolewski *et al.*, 2006; Alinari *et al.*, 2009), we tested the efficacy of a combined treatment with PS-341 and RTX/S6 IT. As expected, sensitivity to RTX/S6 was augmented when cells were coincubated with PS-341. The combination of  $10^{-9}$  M PS-341 and  $10^{-9}$  M RTX/S6 produced a significant increase in cytotoxic activity compared to single compounds ( $p < 0.0001$ ) (fig. 12).

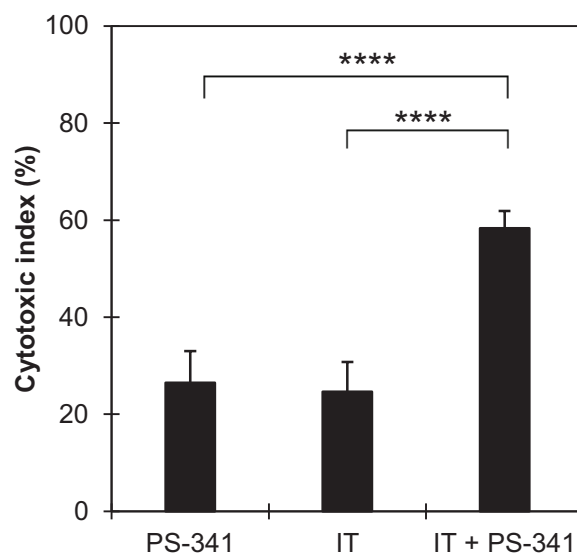


**Fig. 12** Combined cytotoxic effect of  $10^{-9}$  M PS-341 and  $10^{-9}$  M RTX/S6 IT on Raji cells. Toxic effect is given as cytotoxic index, the percentage of non-viable cells. Viability was evaluated after 96 h using a colorimetric assay based on MTS reduction. The results are the means of two independent experiments, each performed in triplicate, and are presented as the percentage of untreated control values. Asterisks indicate level of significance in ANOVA/Bonferroni followed by Dunnett's test (\*\*\*\* $p < 0.0001$ ).

### **Fludarabine acts synergistically with RTX/S6 and OM124/S6 in killing Raji cells**

Fludarabine (FLU) is a purine analog used in the treatment of hematological malignancies. It is employed in various combinations with cyclophosphamide, mitoxantrone, dexamethasone and rituximab in the treatment of indolent non-Hodgkin lymphomas (Cabanillas, 2000). In a previous work (Polito *et al.*, 2004) our group showed that a combination of RTX/S6 with FLU was successful to produce an enhanced cytotoxic effect in CD20-positive NHL cells. To test the hypothesis if the observed synergistic effect was not restricted to RTX/S6, we designed our experiments to verify if a combined treatment with OM124/S6 and FLU was able to produce similar results. To evaluate the possible combined effect of the drug and the IT, in our experiments FLU was tested at  $7.5 \times 10^{-7}$  M, the maxima concentration that in the previous experiments gave a limited cell toxicity.

FLU and RTX/S6 combinations were found to significantly reduce Raji cells viability compared to single compounds, resulting in a super additive effect. FLU alone showed an increase in the percentage of dead cells compared to untreated control of  $14.5\% \pm 9.1\%$ , while  $10^{-8}$  M RTX/S6 alone produced an increase of  $41.8\% \pm 5.3\%$ . Combination of the two compounds resulted in an almost complete depletion of Raji cells ( $95\% \pm 3.2\%$ ) (fig. 13 A, left).  $10^{-9}$  M RTX/S6 alone showed an increase in the percentage of dead cells compared to untreated control of  $23.8\% \pm 2.8\%$  and of  $65.5\% \pm 0.8\%$  in combination with FLU (fig. 13 A, right).

FLU was also tested in combination with two concentrations of OM124/S6, resulting in a significant increase in the cytotoxic effect compared to single drugs.  $10^{-10}$  M OM124/S6 showed an increase in the percentage of dead cells compared to untreated control of  $57.3\% \pm 6.1\%$  and of  $92.3\% \pm 0.5\%$  in combination with FLU (fig. 13 B, left);  $10^{-11}$  M OM124/S6 alone produced an increase of  $17.8\% \pm 6.3\%$  and of  $52.5\% \pm 1.6\%$  in combination with FLU (fig. 13 B, right).

Taken together, these results showed that FLU cytotoxic effect may be enhanced by contemporary administration of saporin-based ITs. The effect seems to be independent of the type of antibody used to target saporin to unwanted cells.

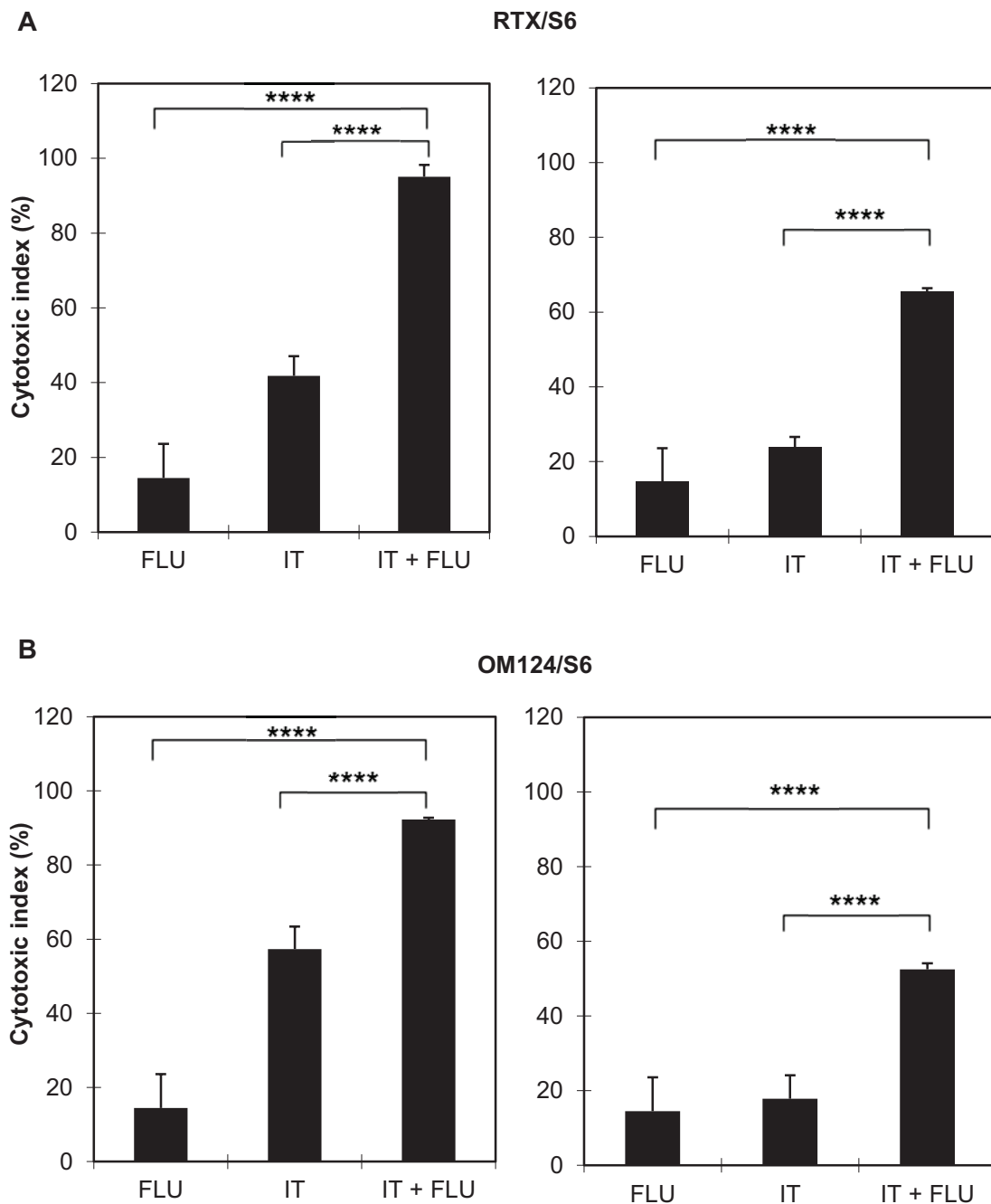


**Fig. 13** Combined cytotoxic effect of 0.75  $\mu$ M FLU and **A)** RTX/S6  $10^{-8}$ -M (left) or  $10^{-9}$  M (right); and **B)** OM124/S6  $10^{-10}$  M (left) or  $10^{-11}$  M (right) on Raji cells. Toxic effect is given as cytotoxic index, the percentage of non-viable cells. Viability was evaluated after 96 h using a colorimetric assay based on MTS reduction. The results are the means of three independent experiments, each performed in triplicate, and are presented as the percentage of untreated control values. Asterisks indicate level of significance in ANOVA/Bonferroni followed by Dunnett's test (\*\*\*\* $p < 0.0001$ ).

## DISCUSSION

Saporin-S6 is a highly toxic rRNA *N*-glycosylase with potential therapeutic application in a variety of human diseases as toxic moiety of immunotargeted conjugates. Saporin-S6 has been previously shown to be able to inhibit protein synthesis by removing an adenine in a well-conserved region of eukaryotic ribosomes and to induce multiple cell death pathways in lymphoma cells (Polito *et al.*, 2009). Those properties render saporin an attractive molecule for the production of immunotoxins for the treatment of NHLs, because its ability to induce cell death by more than one pathway may render more difficult to tumor cells to acquire a resistant phenotype to saporin-induced cell death. mAbs are currently used in cancer therapy both alone and conjugated to drugs or radioactive compounds, to selectively eliminate unwanted cells (Polito *et al.*, 2013b). Several mAbs have been conjugated to RIPs to take advantage of high toxicity of those enzymes with the selective targeting properties of mAbs (Polito *et al.*, 2011).

In our study, we tested and compared *in vitro* the anticancer properties and the cell death pathways of two saporin-based immunotoxins: RTX/S6, obtained by chemical coupling of saporin-S6 to anti-CD20 FDA approved mAb rituximab; and OM124/S6, produced coupling saporin-S6 to anti-CD22 mAb OM124 (Bolognesi *et al.*, 1998). Cell-killing activity of those immunotoxins was tested on CD20/CD22-positive cell line Raji.

Native saporin-S6 showed in a cell-free system the ability to inhibit protein synthesis by a rabbit reticulocytes lysate with an  $IC_{50}$  of  $6.2 \times 10^{-11}$  M. After conjugation processes, both RTX/S6 and OM124/S6 retained almost the same activity on cell-free protein synthesis, while the ability to inhibit protein synthesis in Raji cells was highly augmented, being RTX/S6 able to completely inhibit protein synthesis after 96 h at  $1.84 \times 10^{-7}$  M concentration and OM124/S6 at  $1.16 \times 10^{-9}$  M. RTX/S6  $IC_{50}$  value was almost 2 log lower than  $IC_{50}$  of native saporin-S6, while OM124/S6 showed an  $IC_{50}$  4 logs lower than saporin-S6. In both cases, the toxicity of ITs was time-dependent. OM124/S6 was shown to be more toxic than RTX/S6. The reason of this difference in cytotoxic activity may be represented by the efficiency of toxic payload internalization and intracellular routing of saporin, as the intracellular itinerary may modulate

cytotoxicity of ITs (Tortorella *et al.*, 2012). In fact, while it is known from literature that CD20 antigen is poorly internalized after ligand binding, CD22 undergoes a rapid internalization after binding (Countouriotis *et al.*, 2002; Sullivan-Chang *et al.*, 2013). In both cases, saporin-S6 internalization is demonstrated by the great increase in cellular protein synthesis inhibition and cytotoxicity observed compared to the mixture of unconjugated mAb and saporin-S6.

According to literature (Polito *et al.*, 2004; Polito *et al.*, 2009; Polito *et al.*, 2013) both ITs were found in our study to induce apoptosis in target cells, but a difference in timing and intensity was observed in caspases 3/7 activation. RTX/S6 showed a higher activity of caspases 3/7 after 48 h of treatment reaching a plateau of activity, while OM124/S6 showed a gradual activation of caspases 3/7 that became more intense in a time-dependent manner. Caspases 3/7 maximum activity induced by OM124/S6 was found to be slower, but 3 fold more intense than that induced by RTX/S6. Cells pre-treated with pan-caspase inhibitor Z-VAD resulted in a significant increase of survival in Raji cells treated with RTX/S6 suggesting that in cells treated with RTX/S6 caspase-dependent apoptosis may be the main cell death pathway activated, but the lack of a complete protection indicates that other pathways may contribute to cell death. Surprisingly, even if OM124/S6 was shown to strongly activate caspases, Z-VAD produced a poor reduction in OM124/S6 cytotoxicity, suggesting that inhibition of caspases was less efficient in improving cell survival. OM124/S6 may thus trigger also caspase-independent cell death pathways and possibly caspase-dependent cell death is not the main mechanism involved.

Several studies in literature reported an increase in intracellular ROS production in RIP-treated cells (Suntres *et al.*, 2005; Bhaskar *et al.*, 2008; Saxena *et al.*, 2014). We therefore investigated the role of hydrogen peroxide by treating cells with an enzymatic scavenger, catalase. RTX/S6 cytotoxic effect was significantly reduced by catalase, suggesting a role for hydrogen peroxide and ROS formation in RTX/S6 induced cell death. Conversely, catalase pre-treatment produced no effect in OM124/S6-treated cells.

Taken together with the differences in caspase activity induced by the two ITs, these results suggest that the two ITs might trigger different pathways of cell death, possibly due to differences in the intracellular routing followed. In fact, a saporin-based

IT might show a different anti-tumor activity depending on the targeted CD marker, showing different effects according to different CD marker properties.

The study of the mechanisms of action of ITs in target cells may help to design new immunoconjugates with higher cytotoxic potential and specificity to target cells, and to reduce IT related side-effects. Many studies in literature have reported new strategies to improve IT efficacy, often in combination with other chemotherapeutic agents (Alewine *et al.*, 2015). Since in a previous work by Battelli *et al.*, 2010 the possibility that RIP cytotoxic effect was reduced by proteasomal degradation was observed, we designed our experiments to verify if proteasome inhibition was effective in enhancing IT cytotoxic effect. To this purpose, we choose to test the cytotoxic efficacy of a combination of the proteasome inhibitor MG-132 and the ITs. MG-132 is an experimental compound showing antitumor efficacy (Han *et al.*, 2009; Guo e Peng, 2013; Li *et al.*, 2013). The combination of MG-132 with RTX/S6 showed a superadditive toxic effect ( $p < 0.0001$ ) at concentrations of IT that are suitable for an *in vivo* therapy. A superadditive effect was observed also with lower concentrations of OM124/S6, thus suggesting that in normal conditions the proteasome may be involved in the partial degradation of saporin. We then tested a combination of RTX/S6 with PS-341 (bortezomib), since in preclinical studies, additive cytotoxic effects was reported with the combination of bortezomib and rituximab in B-CLL and MCL. Again, a significant increase in RTX/S6 efficacy was observed. Bil *et al.*, 2010 showed that exposure of Raji cells to bortezomib at concentrations above 20 nM increase CD20 ubiquitination and reduce surface CD20 levels, possibly enhancing CD20 lysosomal or autophagic degradation. In our study, the enhanced cytotoxic effect was achieved with a concentration of bortezomib 20-fold lower, reducing the risk of the downregulation of CD20 due to treatment with the proteasome inhibitor.

In an attempt to improve the antitumor efficacy of the treatment, we also tried the simultaneous administration of RTX/S6 and fludarabine to target cells. Fludarabine is an adenine nucleoside analog used in clinic to treat several hematological malignancies, for example chronic lymphocytic leukemia (Lukenbill *et al.*, 2013). The combination of FLU with  $10^{-8}$  M RTX/S6 or  $10^{-10}$  M OM124 produced a synergistic toxic effect that led to an almost total elimination of target cells.

In conclusion, the low doses tested in our experiments strongly suggest that a combined IT/proteasome inhibitor or IT/FLU therapy should give synergistic cytotoxic effect also *in vivo*. Our study points out that it is possible to enhance ITs toxicity to target cells by an opportune combination with agents that not interfere with cell death pathways induced by ITs.

*Chapter IV*

**EVALUATION OF EARLY CHANGES  
INDUCED BY STENODACTYLIN IN  
AML CELLS**



## BACKGROUND

Stenodactylin is a 63.1 kDa highly toxic lectin belonging to type 2 RIPs purified from the caudex of *Adenia stenodactyla* (Stirpe *et al.*, 2007; Pelosi *et al.*, 2005). RIPs are family of RNA *N*-glycosylases (EC 3.2.2.22) widely expressed in the plant kingdom, which have been investigated for their anti-neoplastic potential. All RIPs are able to hydrolyze a specific adenine from the sarcin/ricin loop of the ribosomal 28S RNA, thus introducing an irreversible damage to ribosomes causing protein translation inhibition, finally resulting in cell death (Stirpe, 2013). Stenodactylin has been shown to possess a high enzymatic activity towards ribosomes and hsDNA substrates, but not on tRNA or poly(A). Stenodactylin separated A-chain was shown to inhibit protein synthesis by a rabbit reticulocytes lysate, with an IC<sub>50</sub> of  $4.4 \times 10^{-8}$  M, while the separated lectin B- chain showed no effect on protein synthesis at concentrations up to  $3 \times 10^{-5}$  M. (Stirpe *et al.*, 2007). Compared to ricin A chain, which was shown to be able to inhibit protein synthesis by a rabbit reticulocytes lysate with an IC<sub>50</sub> of  $1 \times 10^{-10}$  M (Hale, 2001), stenodactylin separated A chain possess a lower enzymatic activity, possibly due to reduction processes. In fact, native stenodactylin was found to be extremely toxic to several cell lines of different origin, with extremely low IC<sub>50</sub> values, often in the picomolar range. Furthermore, 48 h LD<sub>50</sub> for mice receiving stenodactylin by intraperitoneal injection is 2.76 µg/kg (2.12–3.58), a value very close to ricin toxin, whose LD<sub>50</sub> in mice is calculated to be 2.8–3.3 µg/kg when administered by injection (Schep *et al.*, 2009; Battelli *et al.*, 2010; Stirpe *et al.*, 2007). For these reasons, stenodactylin is considered to be amongst the most potent toxins of plant origin. Moreover, similarly to modeccin and volkensin, two other RIPs isolated from *Adenia* genus, (Wiley *et al.*, 2000), stenodactylin is retrogradely transported when injected into the central nervous system (Monti *et al.*, 2007).

Besides protein synthesis inhibition, a series of evidences suggest that RIPs are able to elicit alternative molecular mechanisms to trigger different cell death programs (Polito *et al.*, 2009; Bora *et al.*, 2010). The capability of RIPs, either type 1 than type 2, to induce cell death by apoptosis has extensively demonstrated using different models, both *in vitro* and *in vivo* (i.e. Rao *et al.*, 2005; Zhang *et al.*, 2012; Fang *et al.*, 2012).

However, the mechanisms involved in the regulation of RIP-induced apoptosis is still quite controversial and whether apoptosis is dependent on the inhibition of protein synthesis is not clear.

Very few informations are currently available in literature about how RIPs globally affect gene expression. It has been previously demonstrated *in vivo* that exposure of mice to ricin triggers the phosphorylation of JNK and p38 MAPK, whose activation is required for ricin-mediated expression of mRNAs encoding inflammatory cytokines and chemokines (Korcheva *et al.*, 2005). Macrophages appeared to be primary targets of ricin intoxication (Lindauer *et al.*, 2009), and exposure of macrophage cell lines to ricin resulted in apoptosis, activation of SAPKs and release of chemokines and cytokines (Higuchi *et al.*, 2003; Korcheva *et al.*, 2005; Gonzalez *et al.*, 2006; Gray *et al.*, 2008). A gene expression microarray analysis performed on ricin-treated airway cells showed after 24 h of exposure a significant increase in expression of transcription factors and DNA-binding proteins, such as c-Jun, c-Fos, early growth response-1 (EGR-1) and activating transcription factor 3 (ATF3), which are known to be associated with the transcriptional regulation of proinflammatory genes (Wong *et al.*, 2007). A similar inflammatory response was reported in response to ricin exposure in Balb/c mice (David *et al.*, 2009). A transcriptomic profile of host response in mouse brain after exposure to plant toxin abrin showed a similar tendency, with a number of differentially expressed genes responsible for various activities, such as immune response, cell adhesion, chemotaxis, inflammatory processes, transcription and signal transduction (Bhaskar *et al.*, 2012). Furthermore, an antibody-avidin fusion protein (ch128.1Av) conjugated to biotinylated saporin was shown to induce a transcriptional response consistent with oxidative stress and DNA damage, with differential expression of genes connected to apoptosis, regulation of cell cycle, immune response, signaling, stress response and transcription (Daniels-Wells *et al.*, 2013). An interesting finding was reported by Li *et al.*, 2011: a miRNA microarray assay on colorectal cancers cell lines treated with mistletoe lectin I reported a down-regulation of some miRNAs that was shown to be determined by direct degradation of miRNAs precursors. In fact, pre-miRNAs could represent a substrate for RIPs due to their characteristic stem-loop structures.

## AIM OF THE PROJECT

Firstly discovered and purified from the caudex of *Adenia stenodactyla* by Pelosi *et al.*, 2005; Stirpe *et al.*, 2007, stenodactylin has been shown to be among the most potent toxins of plant origin and an attractive candidate for the design of new ITs. To date, RIPs have been used alone or as toxic component of ITs for the experimental treatment of several diseases, such as cancer, immune disorders, graft-versus-host disease and as an antiviral agent for the treatment of AIDS, achieving the most promising results in the treatment of hematological cancers (Stirpe *et al.*, 2006). Despite several studies on RIP-induced cell death, a complete comprehension of the mechanism underlying induction of apoptosis is still missing. The knowledge of the cell death pathway(s) induced by RIPs in intoxicated cells, may be useful for the design of new specific immunotherapies and for clarifying the mechanism of damage, since some of this proteins represent a serious treat, as accidental or intentional contact may occur (for example ricin, which has been listed from the USA Centers for Disease Control and Prevention as a Category B Agent).

The aim of this project was to identify the early gene expression changes induced by stenodactylin in intoxicated cells following a whole-genome expression analysis approach, linking gene expression data to protein modification and to the activity of stenodactylin on host ribosomes. The identification of stenodactylin-induced cell death pathway(s) may provide new informations about RIP activity at cellular level, and could help to the design of new specific ITs or combination therapies with ITs to enhance RIP-based ITs cytotoxic activity.

In the present work, we evaluated early changes induced by stenodactylin treatment in acute monocytic leukemia cells MOLM-13. We performed a global gene expression microarray analysis to identify early gene expression changes, focusing on the shortest time needed to the toxin to produce a detectable change in cell viability and 28S rRNA integrity.

## RESULTS

### **MOLM-13 cells are more sensitive to stenodactylin than Raji and Ramos cells**

Stenodactylin is a highly toxic rRNA *N*-glycosylase whose activity could be potentially employed in the design and production of ITs against hematological malignancies. To evaluate the early response to stenodactylin-induced cell damage, we tested native stenodactylin on three cell lines of hematologic origin: lymphoblast Burkitt's lymphoma Raji and Ramos cells and acute monocytic leukemia cell line MOLM-13. Protein synthesis inhibition assays were performed after 48 h of exposure to the toxin, showing that stenodactylin was able to almost completely inhibit protein synthesis in all cell lines tested at  $10^{-9}$  M concentration. A marked difference in sensitivity to stenodactylin was observed at lower concentrations, being MOLM-13 cells the most sensitive, with an  $IC_{50}$  value almost 1 log lower than Raji and Ramos cells (fig.1, table 1).

Viability assays were also performed after 48 h of stenodactylin treatment. As shown in fig. 2, MOLM-13 were the most sensitive to the toxin among cell line tested. Despite the marked difference reported in the ability of stenodactylin to inhibit protein synthesis in the three cell lines, viability test showed that all tested cell lines were similarly sensitive to the toxin, showing very close  $EC_{50}$  values (fig 2, table 2). These results may partially support the idea that RIP-induced cell death is not fully dependent on the ability to inhibit cellular protein synthesis, but also other mechanisms participate (Das *et al.*, 2012).

Since MOLM-13 were found to be more sensitive to stenodactylin-induced inhibition of protein synthesis, this cell model was chosen for further analysis.

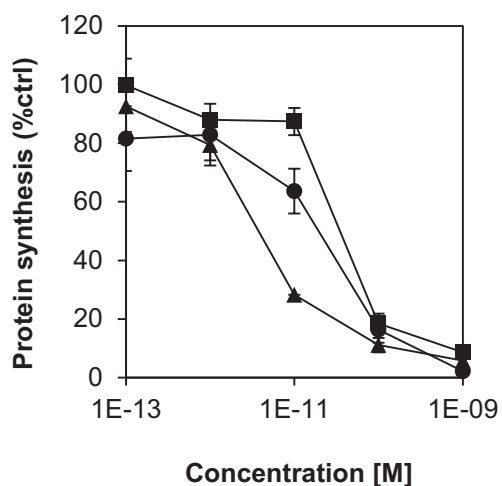


**Fig. 1** Protein synthesis inhibition assay on MOLM-13 (▲), Raji (●), and Ramos (■) cells treated for 48 hours with stenodactylin. A total of  $2 \times 10^4$  cells were seeded in 96-well plates in a final volume of 200  $\mu$ l of complete medium containing appropriate concentration of stenodactylin or control medium. After 48 hours of incubation and further 6 hours with [ $^3$ H] leucine, the radioactivity incorporated was determined. Results are the means of three independent experiments, each performed in triplicate. SD never exceeded 10%.

**Table 1** Calculated  $IC_{50}$  values for stenodactylin in MOLM-13, Raji and Ramos cells.

	<b>MOLM-13</b>	<b>RAJI</b>	<b>RAMOS</b>
<b><math>IC_{50}</math> (M)</b>	$3.75 \times 10^{-12}$	$1.95 \times 10^{-11}$	$3.49 \times 10^{-11}$

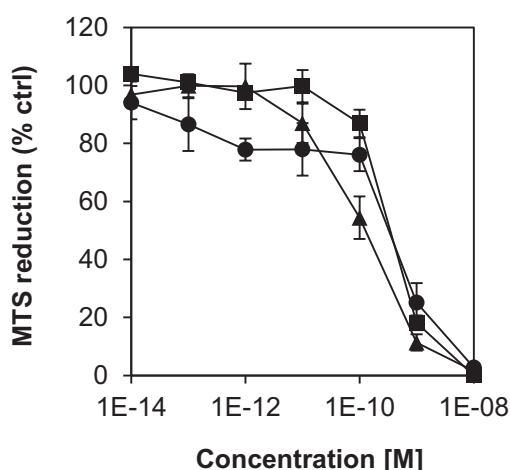


**Fig. 2** Viability assay on MOLM-13 (▲), Raji (●), and Ramos (■) cells treated for 48 hours with stenodactylin. A total of  $2 \times 10^4$  cells were seeded in 96-well plates in a final volume of 200  $\mu$ l of complete medium containing appropriate concentration of stenodactylin or control medium. After 48 hours, viability was measured using a colorimetric assay based on MTS reduction and expressed as percentage of untreated control value. Results are the means of three independent experiments each performed in triplicate. SD never exceeded 10%.

**Table 2** Calculated EC<sub>50</sub> values for stenodactylin in MOLM-13, Raji and Ramos cells.

	MOLM-13	RAJI	RAMOS
EC <sub>50</sub> (M)	$1.06 \times 10^{-10}$	$2.09 \times 10^{-10}$	$3.43 \times 10^{-10}$

### Ricin is more toxic than stenodactylin in MOLM-13 cells

Ricin from *Ricinus communis* seeds is the most known and studied type 2 RIP. Its modified A chain has been used to the design and production of immunotoxins for the experimental treatment of different hematological disorders achieving promising results, either *in vitro* than *in vivo* (Herrera *et al.*, 2009; Furman *et al.*, 2011; Schindler *et al.*, 2011; Liu *et al.*, 2012 ). We therefore compared ricin cytotoxicity to stenodactylin in MOLM-13 cells. After a 48 h exposure of cells to the toxin, viability was assessed. Ricin resulted to be more toxic than stenodactylin: a complete loss of

viability was observed at  $10^{-9}$  M concentration, whereas a complete loss in viability was observed at a concentration  $10^{-8}$  M of stenodactylin.  $EC_{50}$  value of ricin resulted of  $2.29 \times 10^{-11}$ , almost 1 log lower than what observed for stenodactylin (fig. 3).

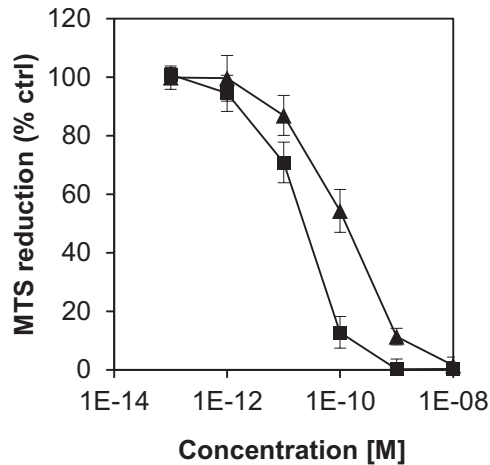


**Fig. 3** Viability assay on MOLM-13 cells treated for 48 hours with stenodactylin (▲) or ricin (■). A total of  $2 \times 10^4$  cells were seeded in 96-well plates in a final volume of 200  $\mu$ l of complete medium containing appropriate concentration of stenodactylin or control medium. After 48 hours, viability was measured using a colorimetric assay based on MTS reduction and expressed as percentage of untreated control value. Results are the means of three independent experiments each performed in triplicate. SD never exceeded 10%.

### Stenodactylin depurinates the 28S rRNA in a time-dependent manner

RIPs are known to remove a specific adenine from 28S rRNA, leading to translational arrest. To verify depurination induced by stenodactylin in MOLM-13 cells, we applied the method based on qRT-PCR developed by Melchior *et al.*, 2010, that allows the detection of apurinic sites in intact cells. Cells were treated with stenodactylin  $10^{-9}$  M, which has been shown to be the minimum concentration causing a complete inhibition of protein synthesis after 48 h. A time-dependent increase of apurinic sites in 28S rRNA was detected upon stenodactylin treatment. A significant increase in the relative amount of apurinic rRNA increased by  $12.1 \pm 3.2$  fold in response to stenodactylin after a 4 h exposure ( $p = 0,0003$ ) and by  $41.2 \pm 7.4$  fold after 6 h ( $p = 0,0001$ ), while no significant difference compared to control was observed after 2 h (fig. 4).

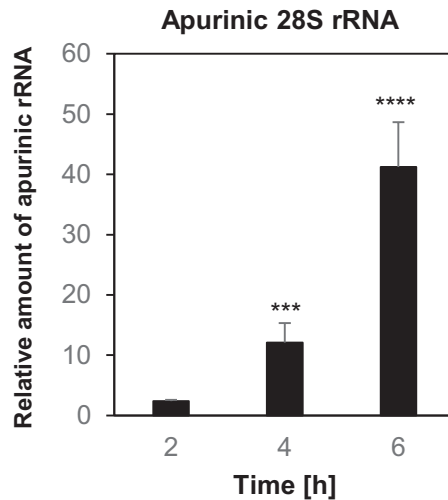


**Fig. 4** Depurination of the 28S rRNA by stenodactylin in MOLM-13 cells. Cells were incubated for indicated time with  $10^{-9}$  M stenodactylin. The resulting relative amount of apurinic sites in 28S rRNA compared to untreated control was determined by qRT-PCR. 28S rRNA aside from the depurination site was used for the normalization of the samples. Data are given as mean fold change  $\pm$  standard error of the mean (SEM) of three independent experiments, each performed in duplicate. \*\*\* $p = 0,0003$ ; \*\*\*\* $p = 0,0001$  (comparison between control and treatment).

#### Evaluation of apoptotic changes in stenodactylin-treated cells

Cell death induced by  $10^{-9}$  M stenodactylin was observed after 24 h and 48 h with phase contrast microscopy. As shown in fig. 5, cell morphology after 24 h and 48 h of exposure to the toxin appeared to become progressively compatible with apoptotic cell death, like nuclear condensation and membrane alterations.

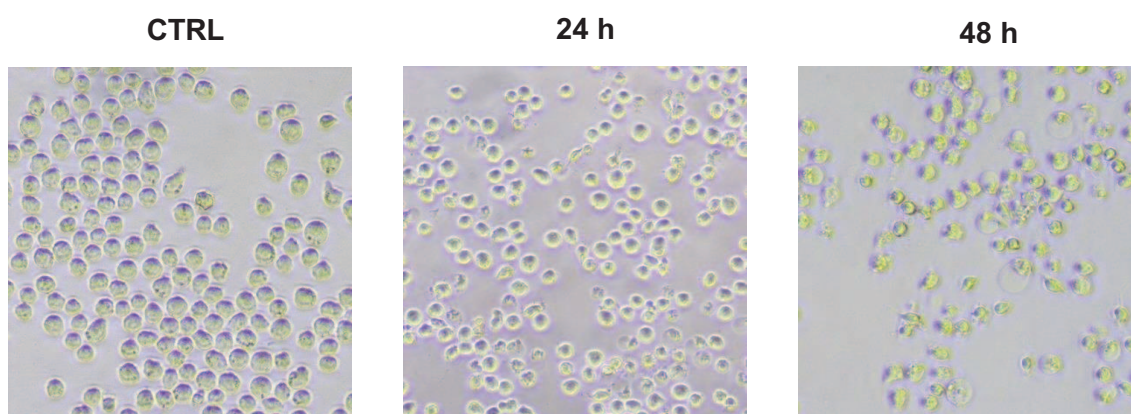


**Fig. 5** MOLM-13 cells untreated or treated with stenodactylin for 24 or 48 h. Cell morphology was assessed by phase contrast microscopy (20× magnification).

Apoptosis involvement was monitored by Annexin V/PI double staining and then analyzed by flow cytometry (fig. 6). Double staining with Annexin V/PI demonstrated that MOLM-13 cells treated with  $10^{-9}$  M stenodactylin showed a time-dependent increase in Annexin V positive cells. Quantitative analysis showed a significant increase in Annexin V positivity after 6 h compared to untreated control ( $11.5\% \pm 1.4\%$ ), and percentage of viable cells was  $84.2\% \pm 1.5\%$ . After a 24 h treatment with stenodactylin  $10^{-9}$  M, percentage of viable cells decreased to  $38.2\% \pm 3.2\%$ ; while after 48 h, only  $11.8\% \pm 1.7\%$  of viable cells were detectable. A small amount of necrotic cells appeared only after 48 h, suggesting that apoptosis is the main cell death pathway followed after stenodactylin intoxication (fig. 7).

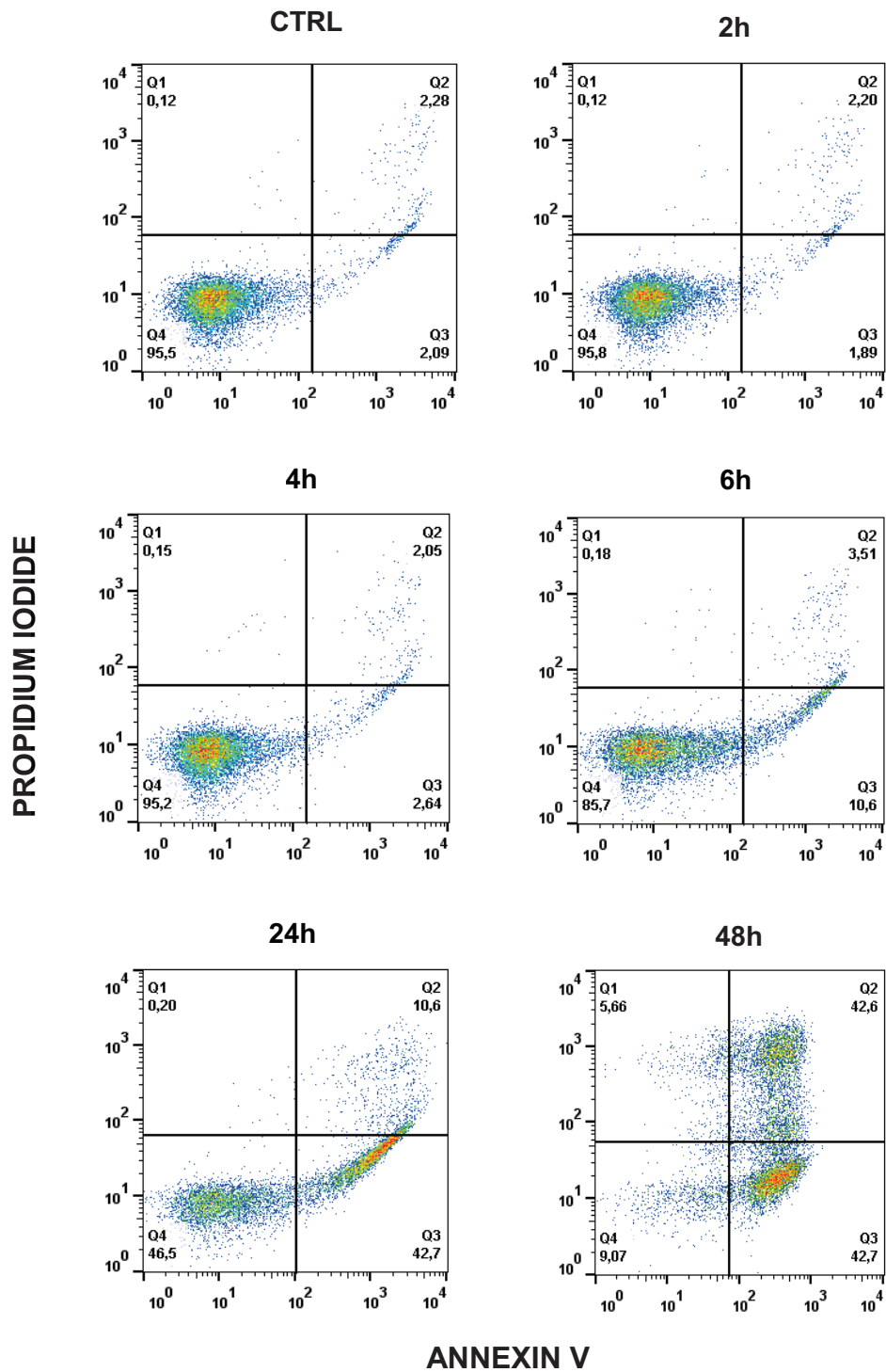


**Fig. 6** Flow cytometric analysis of apoptosis in MOLM-13 cells measured by using Annexin V – EGFP apoptosis detection Kit. Representative cytometric dot-plots images of MOLM-13 cells obtained after incubation with stenodactylin ( $10^{-9}$  M, 2-4-6-24-48 h). Each specimen presents: viable cells (left down corner Q3); early apoptotic cells (right down corner Q4); late apoptotic cells (right upper corner Q2); and necrotic cells (left upper corner Q1).

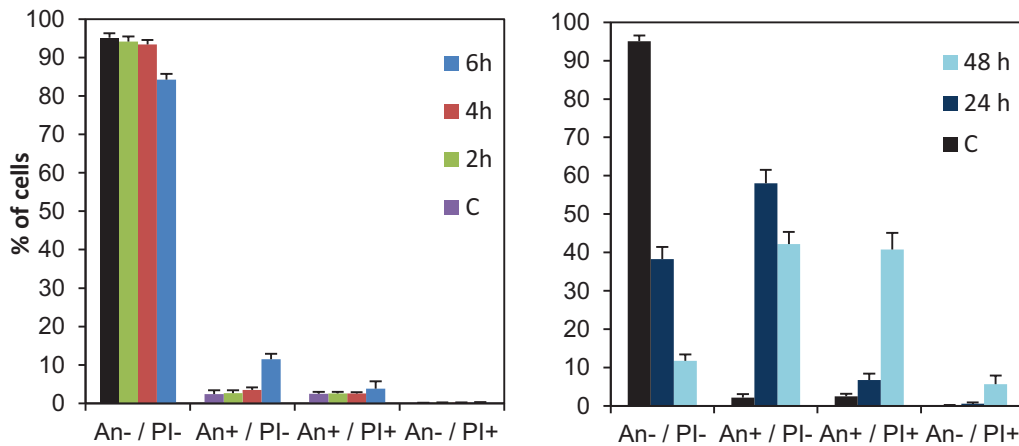


**Fig. 7** Flow cytometric analysis of MOLM-13 cells stained with Annexin V – EGFP apoptosis detection Kit. Cells were treated for indicated time with stenodactylin ( $10^{-9}$  M). Results are the means of six independent experiments. SD never exceeded 10%. Apoptosis induced by stenodactylin resulted significant by ANOVA/Bonferroni ( $P < 0.0001$ ) starting after 6 h of exposure to the toxin compared to untreated control.

### **Caspases activation in stenodactylin-treated MOLM-13**

Once we had established that the MOLM-13 cell line was responsive to stenodactylin in terms of depurination and protein synthesis inhibition, and that apoptotic membrane changes were observed in response to the treatment, we evaluated the involvement of caspases activation in apoptotic cell death induced by stenodactylin. As shown in fig. 8, stenodactylin treatment ( $10^{-9}$  M) caused a time-dependent increase in the activity of all tested caspases (fig. 8). All caspases were significantly activated after 6 h ( $p < 0.0001$ ). Despite a similar activity compared to caspase 8, only caspase 9 was found to be significantly activated after 4 h ( $p = 0.0001$ ). Effector caspases 3/7 also shown a significant activation after 4 h and a marked increase in activity after 6 h. The luminometric assay used to determine caspases activity cannot discriminate between

caspase 3 and caspase 7 as both have substrate specificity for the amino acid sequence Asp-Glu-Val-Asp. A further western blot analysis was performed to evaluate caspase 3 activation. As shown in fig. 9, caspase 3 cleavage appeared after 5 h. It is possible that the difference in activity observed with the luminometric assay may be due to a different sensitivity of the two assays, or to an early activation of caspase 7 before 5 h that cannot be excluded.

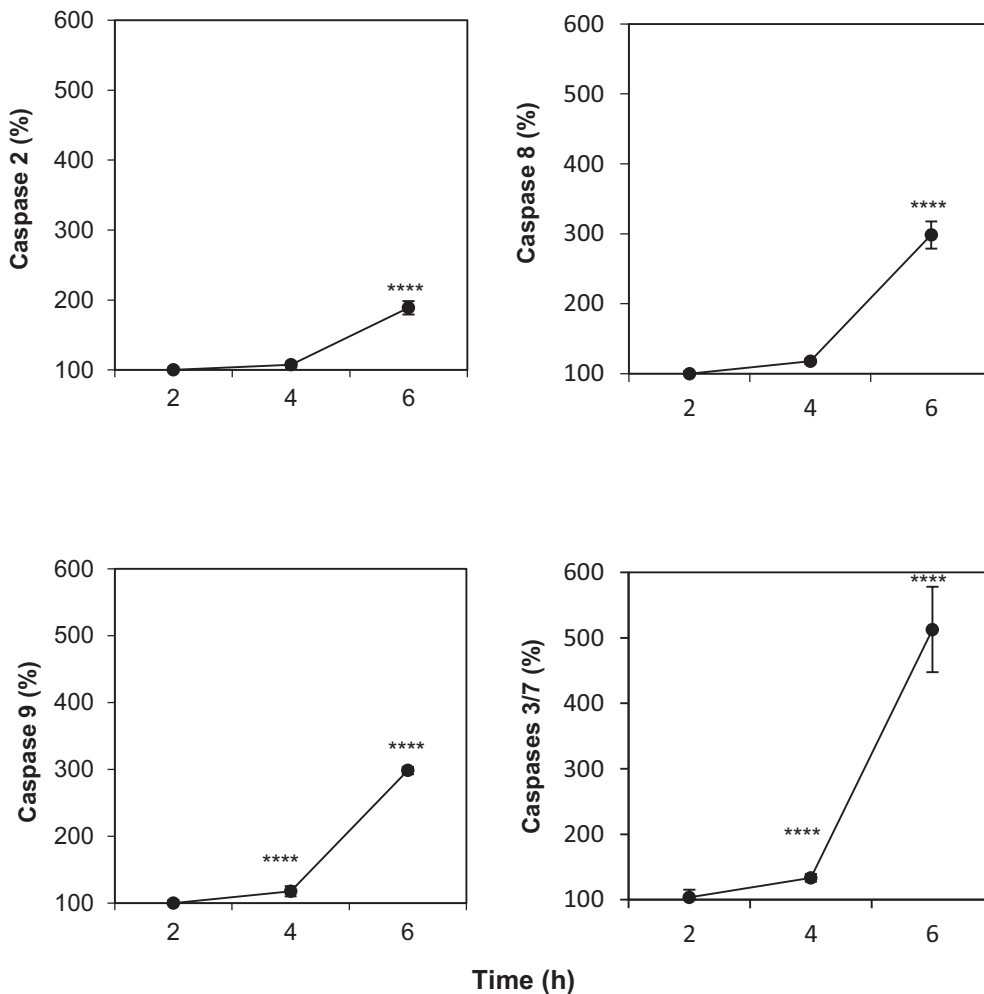


**Fig. 8** Caspase activation in MOLM-13 cells exposed to  $10^{-9}$  M stenodactylin. Caspase-2, -8, -9 and -3/7 activation were determined as described in materials and methods. Caspase activity is expressed as the percentage of control values obtained from cultures grown in the absence of the RIPs. All caspases were significantly activated after 6 h ( $p < 0.0001$ ). Despite a similar activity compared to caspase 8, only caspase 9 was found to be significantly activated after 4 h ( $p = 0.0001$ ). Mean results  $\pm$  SD are reported.

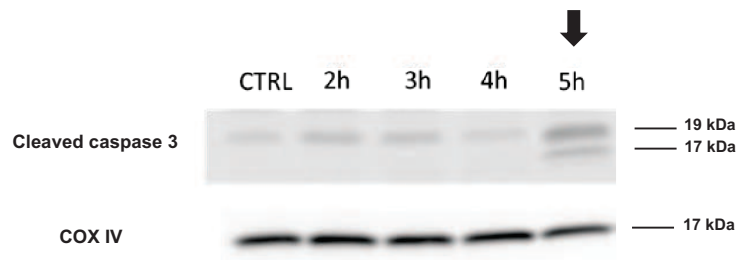


**Fig. 9** Western blot analysis of stenodactylin-induced caspase 3 cleavage. MOLM-13 cells were serum treated for the indicated time with  $10^{-9}$  M stenodactylin. Cell lysates (40  $\mu$ g total protein) were separated by SDS-PAGE and immunoblotted. Figure is representative of 3 separate experiments.

#### **Evaluation of early gene expression changes induced by stenodactylin in AML cells**

Early gene expression changes were evaluated in a time-course experiment considering 2-4-6 hours of treatment with stenodactylin  $10^{-9}$  M. RNA from MOLM-13 cells exposed to the toxin was used for the analysis of 47231 annotated RefSeq transcripts. After data quality control and pre-processing, significance analysis of microarrays (SAM) (Tusher *et al.*, 2001) was applied. SAM ranks the transcripts in a data set according to the regularized t-score that it calculates, providing also a q-value which is a measure of the statistical significance of the differences in expression levels between the compared groups. To select only interesting genes from the analysis, we set up a cut-off considering statistically interesting genes showing a q-value and a false discovery rate (FDR) = 0 and a fold change  $\pm 1.5$ .

After 2 hours of exposure to stenodactylin, no significant changes in gene expression were detectable, while after 4 hours, 6 transcripts were up-regulated. SAM analysis revealed stenodactylin-mediated increased expression of transcription factors such as c-Jun, early growth response-1 (EGR-1) and activating transcription factor 3 (ATF3), which are known to be associated with the transcriptional regulation of proinflammatory genes. Dual specificity protein phosphatase 1 (DUSP1) was also up-regulated. This enzyme is known to have a role in the inactivation of mitogen-activated protein (MAP) kinase and also an important role in the human cellular response to

environmental stress as well as in the negative regulation of cellular proliferation (RefSeq, Jul 2008). Proinflammatory cytokine interleukin-1B (IL1B) and chemokine interleukin-8 were also up-regulated (listed in table 3).

**Table 3** SAM ranked gene list after 4 h of exposure to stenodactylin

<b>Symbol</b>	<b>Definition</b>	<b>FDR</b>	<b>q-value</b>	<b>Fold Increase</b>
JUN	jun oncogene	0.0	0.0	5.3
EGR1	early growth response 1	0.0	0.0	2.5
ATF3	activating transcription factor 3	0.0	0.0	1.8
DUSP1	dual specificity phosphatase 1	0.0	0.0	1.5
IL1B	interleukin 1, beta	0.0	0.0	1.6
IL8	interleukin 8	0.0	0.0	1.7

After 6 hours, 65 transcripts were found to be up-regulated (listed in table 4). Correspondence analysis (CA) (Felleberg *et al.*, 2001) was applied to look for associations between the samples and expression levels of the transcripts in the data set. CA plot showed a tendency for samples to create a gradient, with control samples and samples treated with stenodactylin for 2 hours at one end, and samples treated with stenodactylin for 6 hours at the other end. Stenodactylin produced a time-dependent upregulation of selected genes (fig. 11).



**Table 4** SAM ranked gene list after 6 h of exposure to stenodactylin

<b>Symbol</b>	<b>Definition</b>	<b>FDR</b>	<b>q-value</b>	<b>Fold Increase</b>
JUN	jun oncogene	0.0	0.0	30.9
IL8	interleukin 8	0.0	0.0	11.7
ATF3	activating transcription factor 3	0.0	0.0	9.4
EGR1	early growth response 1	0.0	0.0	9.1
IL1B	interleukin 1, beta	0.0	0.0	5.9
DUSP1	dual specificity phosphatase 1	0.0	0.0	3.7
CCL3	chemokine (C-C motif) ligand 3	0.0	0.0	3.6
BTG2	BTG family, member 2	0.0	0.0	3.8
RNU6-15	U6 small nuclear 15 RNA	0.0	0.0	4.3
RNU6-1	U6 small nuclear 1 RNA	0.0	0.0	4.4
PPP1R15A	protein phosphatase 1, regulatory (inhibitor) subunit 15A	0.0	0.0	2.3
SLC25A24	solute carrier family 25 (mitochondrial carrier; phosphate carrier), member 24 nuclear gene encoding mitochondrial protein, transcript variant 1	0.0	0.0	4.0
ZFP36	zinc finger protein 36, C3H type, homolog (mouse)	0.0	0.0	3.0
CCL3L3	chemokine (C-C motif) ligand 3-like 3	0.0	0.0	3.2
CCL3L1	chemokine (C-C motif) ligand 3-like 1	0.0	0.0	2.8
CYP4B1	cytochrome P450, family 4, subfamily B, polypeptide 1	0.0	0.0	1.9
	Human small nuclear RNA U6atac, partial sequence	0.0	0.0	2.8
RPPH1	ribonuclease P RNA component H1	0.0	0.0	2.2

*Evaluation of early changes induced by stenodactylin in AML cells*

	RNase P RNA.			
IER2	immediate early response 2 (IER2)	0.0	0.0	2.1
RNU6ATAC	RNA, U6atac small nuclear (U12-dependent splicing) RNA	0.0	0.0	2.5
TRIB1	tribbles homolog 1 (Drosophila) (TRIB1)	0.0	0.0	2.0
RNU1A3	RNA, U1A3 small nuclear RNA	0.0	0.0	3.0
RNU1-3	RNA, U1 small nuclear 3 RNA	0.0	0.0	3.6
RNU1G2	RNA, U1G2 small nuclear RNA	0.0	0.0	3.4
TNFSF9	tumor necrosis factor (ligand) superfamily, member 9	0.0	0.0	1.9
CDKN1A	cyclin-dependent kinase inhibitor 1A (p21, Cip1) transcript variant 2	0.0	0.0	1.9
IER3	immediate early response 3	0.0	0.0	2.1
PLAU	plasminogen activator, urokinase	0.0	0.0	1.8
RNU1-5	RNA, U1 small nuclear 5 RNA.	0.0	0.0	3.6
RN7SK	RNA, 7SK small nuclear (RN7SK), non-coding RNA.	0.0	0.0	3.8
RNU1F1	RNA, U1F1 small nuclear RNA	0.0	0.0	2.7
NFKBIA	nuclear factor of kappa light polypeptide gene enhancer in B-cells inhibitor, alpha	0.0	0.0	2.2
ALB	albumin	0.0	0.0	2.0
MIR302C	microRNA 302c	0.0	0.0	1.9
CD83	CD83 molecule transcript variant 1	0.0	0.0	1.6
DUSP2	dual specificity phosphatase 2	0.0	0.0	1.7
RNU4ATAC	U4atac small nuclear (U12-dependent splicing) RNA	0.0	0.0	1.8

*Evaluation of early changes induced by stenodactylin in AML cells*

TIPARP	TCDD-inducible poly (ADP-ribose) polymerase	0.0	0.0	2.2
SNORD13	small nucleolar RNA, C/D box 13	0.0	0.0	2.0
FOS	v-fos FBJ murine osteosarcoma viral oncogene homolog	0.0	0.0	2.2
TNFAIP3	tumor necrosis factor, alpha-induced protein 3	0.0	0.0	1.7
HBEGF	heparin-binding EGF-like growth factor	0.0	0.0	1.6
MAFF	v-maf musculoaponeurotic fibrosarcoma oncogene homolog F (avian), transcript variant 1	0.0	0.0	1.8
LOC338758	PREDICTED: hypothetical protein LOC338758	0.0	0.0	2.1
OBFC2A	oligonucleotide/oligosaccharide-binding fold containing 2A	0.0	0.0	1.6
SNORD104	small nucleolar RNA, C/D box 104	0.0	0.0	2.0
RNU4-2	U4 small nuclear 2 RNA	0.0	0.0	2.8
RNU4-1	U4 small nuclear 1 RNA	0.0	0.0	1.6
OSM	oncostatin M (OSM)	0.0	0.0	1.9
PHLDA1	pleckstrin homology-like domain, family A, member 1	0.0	0.0	2.1
PTGER4	prostaglandin E receptor 4 (subtype EP4)	0.0	0.0	1.9
CD83	CD83 molecule transcript variant 2	0.0	0.0	1.5
SERTAD1	SERTA domain containing 1	0.0	0.0	1.7
KIAA1666	PREDICTED: Homo sapiens KIAA1666 protein	0.0	0.0	2.1
HIST2H2BE	histone cluster 2, H2be	0.0	0.0	1.7

ARL4A	ADP-ribosylation factor-like 4A transcript variant 1	0.0	0.0	1.5
PTGS2	prostaglandin-endoperoxide synthase 2 (prostaglandin G/H synthase and cyclooxygenase)	0.0	0.0	1.5
FAM53C	Homo sapiens family with sequence similarity 53, member C	0.0	0.0	1.6
SNORD3D	small nucleolar RNA, C/D box 3D	0.0	0.0	1.9
NFE2L2	nuclear factor (erythroid-derived 2)-like 2	0.0	0.0	1.5
KLF6	Kruppel-like factor 6 transcript variant 2	0.0	0.0	1.6
TXNIP	thioredoxin interacting protein	0.0	0.0	1.9
CDKN1A	cyclin-dependent kinase inhibitor 1A (p21, Cip1) transcript variant 1	0.0	0.0	1.8
HIST2H2AA3	Histone cluster 2, H2aa3	0.0	0.0	1.6

Hierarchical clustering of treatments *vs* control was performed considering genes showing q-values and FDR = 0 in SAM and a fold change of  $\pm 1.5$ . Hierarchical clustering showed a clear tendency to upregulation of selected gene in a time-dependent manner. Highest differences between treatment group and control are at the top of the plot (fig. 12).

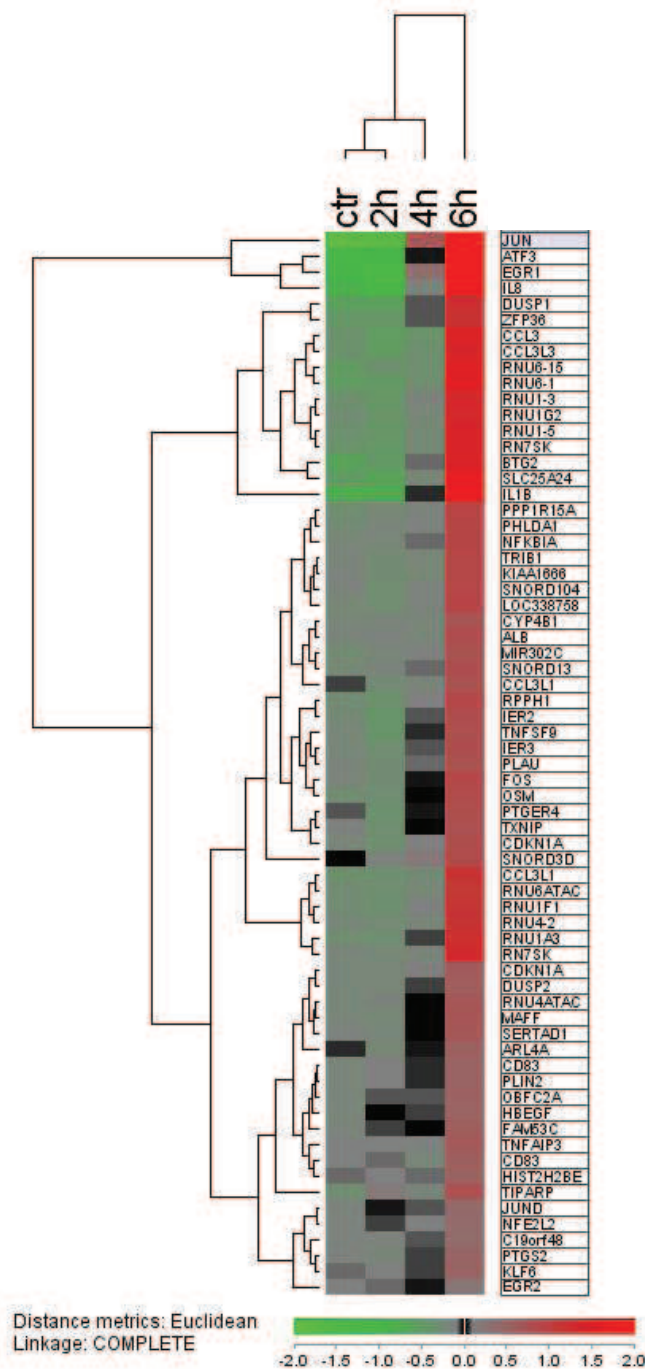


**Fig. 12** Hierarchical clustering of sample groups and transcripts. Sample groups are arranged in columns, while the transcripts are arranged in rows. Only the transcripts with q-value of 0, FDR = 0 and a fold change  $\pm 1.5$  fold were clustered. Negative log intensity ratios are shown in green and positive log ratios are shown in red in the heat map, as indicated by the color bar. Highest differences are at the top of the plot.

### Gene ontology and pathway analysis

To identify overrepresented gene-ontology groups (GO) and biological pathways associated with the genes upregulated by stenodactylin treatment, SAM gene list was imported into PANTHER (<http://www.pantherdb.org/>), and the binomial test (Cho *et al.*, 2000) was used to statistically determine overrepresentation of PANTHER classification categories. Bonferroni corrected  $p$ -values  $< 0.05$  and a fold enrichment  $> 5$  were considered as significant. As shown in table 5, pathway analysis by PANTHER tool showed that inflammation mediated by chemokine and cytokine signaling, apoptosis signaling, gonadotropin releasing hormone receptor and Toll receptor signaling pathways contained the largest number of upregulated genes. The most highly overrepresented genes activated following stenodactylin exposure were associated with cellular response to stress, intracellular signal transduction, regulation of cell death and apoptosis (in table 5, only biological processes showing  $\geq 15$  genes are reported). The molecular functions of these induced genes were associated with transcription, DNA-binding and chemokine and cytokine activity. molecular functions are linked to transcription factor, cytokine and chemokine activities.

**Table 5** PANTHER Overrepresentation Test

<b>PANTHER Pathway</b>	<b>No. of genes</b>	<b><math>p</math>-value</b>
Inflammation mediated by chemokine and cytokine signaling	8	1.76E-05
Apoptosis signaling	6	6.23E-05
Gonadotropin releasing hormone receptor	7	2.42E-04
Toll receptor signaling	4	2.34E-03
<b>GO Molecular Function</b>		
cytokine activity	7	2.44E-03
RNA polymerase II transcription regulatory region sequence-specific DNA binding transcription factor activity involved in positive regulation of transcription	7	5.18E-03
cytokine receptor binding	7	7.12E-03
chemokine activity	4	1.47E-02
transcription regulatory region DNA binding	9	2.74E-02
regulatory region nucleic acid binding	9	2.90E-02

regulatory region DNA binding	9	2.90E-02
chemokine receptor binding	4	3.13E-02
<b>GO Biological process</b>		
cellular response to stress	22	3.06E-09
response to external stimulus	24	6.16E-09
regulation of response to stress	17	8.61E-07
intracellular signal transduction	20	1.69E-06
regulation of cell death	19	2.67E-06
regulation of apoptotic process	18	8.62E-06
regulation of programmed cell death	18	9.72E-06
positive regulation of multicellular organismal process	17	1.01E-05
negative regulation of response to stimulus	17	1.31E-05
response to oxygen-containing compound	17	1.84E-05
regulation of cell proliferation	18	1.92E-05
immune response	17	2.16E-05
negative regulation of signaling	15	1.72E-04
negative regulation of cell communication	15	1.81E-04
regulation of protein modification process	16	2.76E-04

### **p38 and JNK MAPK signaling pathway is induced by stenodactylin**

Gene expression microarray profiling showed that early changes induced by stenodactylin converge on the activation of c-Jun transcription factor and proinflammatory cytokines. The JUN protein is a critical component of activator protein-1 (AP-1) transcription factor. JUN can stably associate with itself or FOS protein to form AP-1 complex. JUN can also interact with some activating transcription factor (ATF) members, such as ATF2, ATF3 and ATF4, to form heterodimers that bind to the cAMP-responsive element (CRE) DNA sequence, TGACGTCA. Members of the AP-1 family of transcription factors are activated by SAPKs, such as p38 and JNK, which are in turn activated by a cascade of upstream kinase further regulated by phosphatases (Wada *et al.*, 2004; Huang *et al.*, 2009) RIPs were previously shown to activate SAPKs eliciting a complex response termed the ribotoxic stress response (Iordanov *et al.*, 1997). We therefore investigated the involvement of p38, JNK and ERK signaling at early stages of stenodactylin intoxication. Flow cytometry was used to obtain a single-cell profiling of signal transduction using modification-specific antibodies and western blot was used to confirm observed changes.

As shown in fig. 13, stenodactylin induced a time-dependent increase in p38 phosphorylation (Thr180/Tyr182). Percentage of phospho-p38 cells increased significantly after 4 h of exposure to the toxin.

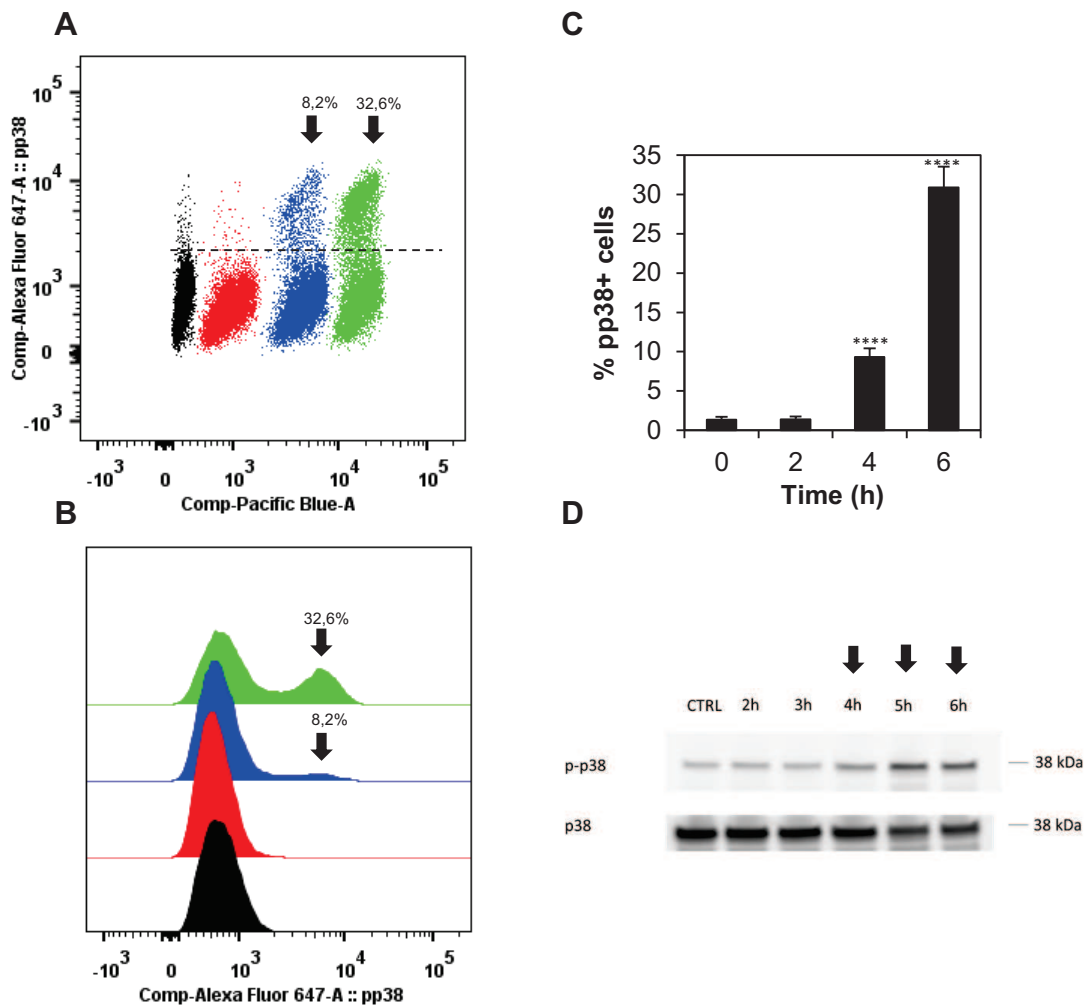


**Fig. 13** A) Phosflow analysis of MOLM-13 cells with Alexa-Fluor 647 anti-phospho-p38 antibody, representative plot out of six independent experiments. Cells were barcoded (see materials and methods) with Pacific Blue staining (x-axis). Control (black), 2 h (red), 4 h (blue) and 6 h (green) samples are represented in dot plot and **B**) histogram plot. **C**) Percentage of phospho-p38 positive cells increased significantly after 4 h and 6 h. Asterisks indicate level of significance in ANOVA/Bonferroni followed by Dunnett's test (\*\*\*\* $p < 0.0001$ ). **D**) Western blot analysis of phospho-p38. Cell lysates (40  $\mu$ g total protein) were separated by SDS-PAGE and immunoblotted. Figure is representative of 3 separate experiments.

A time-dependent increase in phosphorylation of JNK (Thr183/Tyr185) was also observed. Phosflow analysis showed a significant increase in phospho-JNK-positive cells after 6h, while western blot showed an increased band intensity for phospho-JNK at 2, 4 and 6 hours. The observed difference between two analysis may be due to differences in antibody sensitivity, or a poor accessibility of the epitope in intact cells.

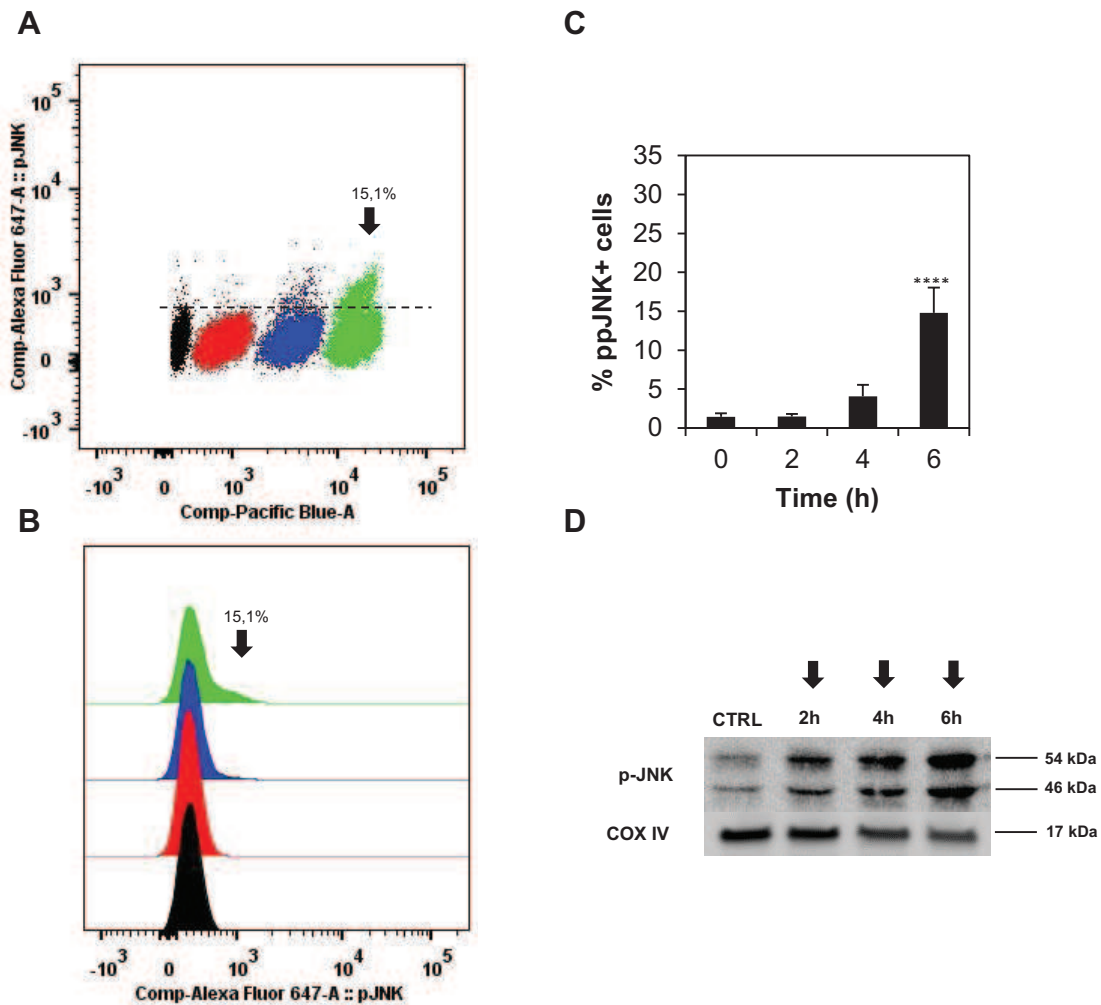


**Fig. 14** A) Phosflow analysis of MOLM-13 cells with Alexa-Fluor 647 anti-phospho-JNK antibody, representative plot out of six independent experiments. Cells were barcoded with Pacific Blue staining (x-axis). Control (black), 2 h (red), 4 h (blue) and 6 h (green) samples are represented in dot plot and **B**) histogram plot. **C**) Percentage of phospho-JNK positive cells increased significantly after 6 h. Asterisks indicate level of significance in ANOVA/Bonferroni followed by Dunnett's test (\*\*\*\* $p < 0.0001$ ). **D**) Western blot analysis of phospho-JNK. Cell lysates (40 μg total protein) were separated by SDS-PAGE and immunoblotted. Figure is representative of 2 separate experiments.

Both JNKs and p38 MAPK are known to be activated in response to a variety of cellular and environmental stresses, such as DNA damage, heat shock, inflammatory cytokines, UV irradiation or oxidative stress. ERK1 and ERK2 are well-characterized MAPKs, usually activated in response to growth stimuli. Phosflow analysis of phosphorylation of ERK1/2 (Thr202/Tyr204) showed no differences between stenodactylin-treated and control samples (fig. 15).

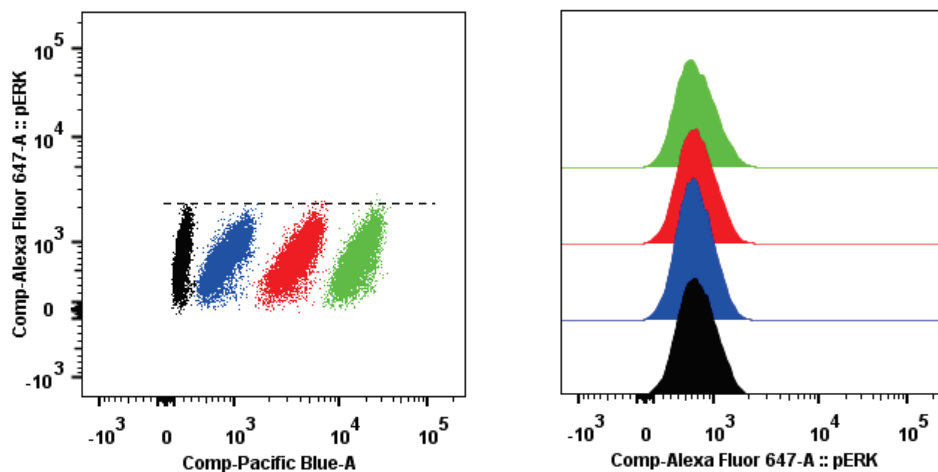


**Fig. 15** Phosflow analysis of MOLM-13 cells with Alexa-Fluor 647 anti-phospho-ERK1/2 antibody, representative plot out of six independent experiments. Cells were barcoded with Pacific Blue staining (x-axis). Control (black), 2 h (red), 4 h (blue) and 6 h (green) samples are represented in dot plot (left) and histogram plot (right).

## DISCUSSION

The enzymatic activity of RIPs was firstly postulated by Endo *et al.*, 1987, who discovered the *N*-glycosylase activity of ricin A-chain, which is able to remove a specific adenine (A<sub>4324</sub> in rat ribosomes, A<sub>4605</sub> in human ribosomes) located in a well-conserved stem-loop region in the 28S rRNA of the large ribosomal subunit. It was then proposed that the cytotoxic effects of type 2 RIPs were a direct consequence of ribosome damage causing an irreversible inhibition of protein synthesis, finally leading to apoptotic cell death. The question whether depurination is necessary for RIP-induced cell death has been controversially discussed (Battelli, 2004), and the mechanism linking depurination activity to the induction of programmed cell death is still not clear. Recently, a series of experimental evidences showed that several mechanisms contribute to RIP-induced cell death, often in a cell-type specific manner. Oxidative stress has been shown to significantly contribute to RIP cytotoxic activity. For example, a mutant form of abrin lacking *N*-glycosylase activity was found to induce apoptosis increasing intracellular ROS levels (Shih *et al.*, 2001), and treatment with antioxidant compounds was shown to confer significant protection in Jurkat cells by restoring antioxidant enzymes depleted by abrin treatment (Saxena *et al.*, 2014). Unfolded protein response was also shown to contribute to type 2 RIPs cytotoxicity (Lee *et al.*, 2008; Horrix *et al.*, 2011). RIPs are also able to activate MAPK pathway in response to the specific damage to 28S rRNA, inducing the so-called “ribotoxic stress response”. Signaling through the ribotoxic stress response has been linked to RIP-induced apoptosis, as the inhibition of components of this pathway resulted in a reduction of RIP-induced apoptotic features (Higuchi *et al.*, 2003; Smith *et al.*, 2003; Jetzt *et al.*, 2009, Wahome *et al.*, 2012). Taken together, those evidences suggest that RIPs might exert their toxicity not only by their *N*-glycosylase activity, but also by additional mechanisms, often involving multiple pathways of cell death (Polito *et al.*, 2009).

In the present work, we described the activity of stenodactylin, a recently identified type 2 RIP from *Adenia stenodactyla* showing a high cytotoxic potential. Stenodactylin was able to inhibit protein synthesis in the AML cell line MOLM-13 showing an IC<sub>50</sub> of  $3.75 \times 10^{-12}$  M. Compared to ricin, the most studied type 2 RIP, it showed to be almost 1 log less toxic in MOLM-13 cells, even if in other cellular models

it showed an extremely high toxicity, being more toxic than volkensin, the most toxic type 2 RIP known so far (Battelli *et al.*, 2010). Thus, stenodactylin can be considered among the most toxic RIPs from plant origin. At a concentration completely inhibiting cellular protein synthesis after 48 h of exposure, stenodactylin induce significant apoptotic membrane changes within 6 h. We therefore decided to evaluate early changes induced by stenodactylin treatment to identify the early response to toxin treatment. The qRT-PCR analysis of 28S rRNA revealed that stenodactylin-induced depurination of the ribosomal subunit occurred significantly after 4 h, and an increase in depurination was observed in a time-dependent manner. A significant time-dependent activation of caspases -2, -8, -9, 3/7 was observed after 6 h, while activation of caspases -9 was significant after 4 h. Caspases 3/7 showed a significant increase in activity at 4 h, even if western blot analysis showed activation of caspase 3 only after 5 h. As caspases 3/7 were evaluated using a luminometric assay, the difference observed may reflect a difference in sensitivity of the two methods. An earlier activation of caspase-7 over caspase-3 cannot be excluded, since the luminometric assay used to determine caspases activity cannot discriminate between caspase 3 and caspase 7 as both have substrate specificity for the amino acid sequence Asp-Glu-Val-Asp. In fact, although caspase-3 and caspase-7 can be activated in concert by the initiator proteases caspase-8 and caspase-9 in response to classical apoptotic triggers, the executioner caspases differ in their upstream activation mechanisms in response to inflammatory stimuli (Lamkanfi *et al.*, 2008). As ricin and other RIPs have been shown to induce inflammatory responses in intoxicated cells, further studies will be required to elucidate stenodactylin-induced caspase activation (Lindauer *et al.*, 2010; Jandhyala *et al.*, 2012).

MAPKs are serine/threonine kinases that can either positively or negatively regulate gene expression, mitosis, proliferation, motility, metabolism, cell survival and programmed cell death. Depurination of 28S rRNA by different ribotoxins, RIPs included, was shown to activate a MAPKs-mediated signaling pathway called the ribotoxic stress response (Iordanov *et al.*, 1997). Our treatment with stenodactylin resulted in an early increase in phosphorylation levels of p38 and JNK but not ERK1/2. JNK and p38 pathways are known to be involved in activating the proinflammatory response as well as apoptosis, two physiological responses that were shown to mediate RIPs toxicity (Korcheva *et al.*, 2005; Korcheva *et al.*, 2007; Lindauer *et al.*, 2010).

Mobilization of p38, JNK and ERK1/2 to the ribosome and subsequent phosphorylation was observed in monocytes and macrophages during ribotoxic stress response induced by trichothecene mycotoxin deoxynivalenol, suggesting a role for the ribosome as a scaffold to initiate the ribotoxic stress response (Bae *et al.*, 2008). JNK and p38 inhibition was found to decrease inflammation and apoptosis-induced by ricin, suggesting a major role of these MAPKs in mediating ricin toxicity (Wong *et al.*, 2007; Jetzt *et al.*, 2009).

Our microarray analysis provided a list of genes whose expression was increased following treatment with stenodactylin. Major pathways involved were inflammation mediated by chemokine and cytokine signaling, and apoptosis signaling. Early gene expression changes occurred after 4 h and involved upregulation of JUN, EGR1, ATF3, DUSP1, IL1B and IL8. Transcription factors and cytokine as well as chemokines were significantly overrepresented, regulating cellular processes like cellular response to stress and cell death. These findings were consistent with previous findings regarding RIPs-induced gene expression changes (Wong *et al.*, 2007; Bhaskar *et al.*, 2012; Daniels-Wells *et al.*, 2013 ).

In summary, stenodactylin treatment induces in MOLM-13 AML cells a stress response compatible with the previously described ribotoxic stress response, shared by different type 2 RIPs and also other ribotoxins targeting 28S rRNA. Further studies are required to elucidate p38 and JNK role in the regulation of inflammation and apoptotic processes induced by stenodactylin. For its elevated cytotoxicity, stenodactylin might represent a valuable option for the design and construction of a new immunotoxin for the experimental treatment of hematological malignancies.

*Chapter V*

**REFERENCES**



## REFERENCES

- Advani A, Coiffier B, Czuczman MS, Dreyling M, Foran J, Gine E, Gisselbrecht C, Ketterer N, Nasta S, Rohatiner A, Schmidt-Wolf IG, Schuler M, Sierra J, Smith MR, Verhoef G, Winter JN, Boni J, Vandendries E, Shapiro M, Fayad L. Safety, pharmacokinetics, and preliminary clinical activity of inotuzumab ozogamicin, a novel immunoconjugate for the treatment of B-cell non-Hodgkin's lymphoma: results of a phase I study. *J Clin Oncol*. 2010
- Alewine C, Hassan R, Pastan I. Advances in Anticancer Immunotoxin Therapy. *Oncologist*. 2015 Jan 5. pii: theoncologist.2014-0358.
- Alinari L, White VL, Earl CT, Ryan TP, Johnston JS, Dalton JT, Ferketich AK, Lai R, Lucas DM, Porcu P, Blum KA, Byrd JC, Baiocchi RA. Combination bortezomib and rituximab treatment affects multiple survival and death pathways to promote apoptosis in mantle cell lymphoma. *MAbs*. 2009;1:31–40.
- American Cancer Society. 2013. *Cancer Facts & Figures 2013*. American Cancer Society, Atlanta, GA.
- Bae HK, Pestka JJ. Deoxynivalenol induces p38 interaction with the ribosome in monocytes and macrophages. *Toxicol Sci*. 2008
- Bae H, Gray JS, Li M, Vines L, Kim J, Pestka JJ. Hematopoietic cell kinase associates with the 40S ribosomal subunit and mediates the ribotoxic stress response to deoxynivalenol in mononuclear phagocytes. *Toxicol Sci*. 2010 Jun;115(2):444-52.
- Baluna R, Rizo J, Gordon BE, Ghetie V, Vitetta ES. Evidence for a structural motif in toxins and interleukin-2 that may be responsible for binding to endothelial cells and initiating vascular leak syndrome. *Proc Natl Acad Sci U S A*. 1999 Mar 30;96(7):3957-62.

- Barbieri L, Stoppa C, Bolognesi A. Large scale chromatographic purification of ribosome-inactivating proteins. *J. Chromat. A.* 1987; 408: 235-243.
- Barbieri L, Valbonesi P, Bonora E, Gorini P, Bolognesi A, Stirpe F. Polynucleotide:adenosine glycosidase activity of ribosome-inactivating proteins: effect on DNA, RNA and poly(A). *Nucleic Acids Res.* 1997 Feb 1;25(3):518-22.
- Battelli MG. Cytotoxicity and toxicity to animals and humans of ribosome-inactivating proteins. *Mini Rev Med Chem.* 2004 Jun;4(5):513-21.
- Battelli MG, Scicchitano V, Polito L, Farini V, Barbieri L, Bolognesi A. Binding and intracellular routing of the plant-toxic lectins, lanceolin and stenodactylin. *Biochim Biophys Acta.* 2010 Dec;1800(12):1276-82
- Barnett BB, Smee DF, Malek SM, Sidwell RW. Selective cytotoxicity of ricin A chain immunotoxins towards murine cytomegalovirus-infected cells. *Antimicrob Agents Chemother.* 1996 Feb;40(2):470-2.
- Bhaskar AS, Deb U, Kumar O, Lakshmana Rao PV. Abrin induced oxidative stress mediated DNA damage in human leukemic cells and its reversal by N-acetylcysteine. *Toxicol In Vitro.* 2008 Dec;22(8):1902-8.
- Bhaskar AS, Gupta N, Rao PV. Transcriptomic profile of host response in mouse brain after exposure to plant toxin abrin. *Toxicology.* 2012 Sep 4;299(1):33-43.
- Bil J, Winiarska M, Nowis D, Bojarczuk K, Dabrowska-Iwanicka A, Basak GW, Sulek K, Jakobisiak M, Golab J. Bortezomib modulates surface CD20 in B-cell malignancies and affects rituximab-mediated complement-dependent cytotoxicity. *Blood.* 2010 May 6;115(18):3745-55.
- Bolognesi A, Tazzari PL, Olivieri F, Polito L, Falini B, Stirpe F. Induction of apoptosis by ribosome-inactivating proteins and related immunotoxins. *Int J Cancer.* 1996 Nov 4;68(3):349-55.
- Bolognesi A, Tazzari PL, Olivieri F, Polito L, Lemoli R, Terenzi A, Pasqualucci L, Falini B, Stirpe F. Evaluation of immunotoxins containing single-chain ribosome-inactivating proteins and an anti-CD22 monoclonal antibody (OM124): in vitro and in vivo studies. *Br J Haematol.* 1998 Apr;101(1):179-88.

- Bolognesi A, Polito L, Scicchitano V, Orrico C, Pasquinelli G, Musiani S, Santi S, Riccio M, Bortolotti M, Battelli MG. Endocytosis and intracellular localisation of type 1 ribosome-inactivating protein saporin-s6. *J. Biol. Regul. Homeost. Agents* 2012, 26, 97–109.
- Bolstad BM, Irizarry RA, Astrand M, Speed TP. A comparison of normalization methods for high density oligonucleotide array data based on variance and bias. *Bioinformatics*. 2003;19:185–193.
- Bonavida B. Postulated mechanisms of resistance of B-cell non-Hodgkin lymphoma to rituximab treatment regimens: strategies to overcome resistance. *Semin Oncol*. 2014 Oct;41(5):667-77.
- Bora N, Gadadhar S, Karande AA. Signaling different pathways of cell death: Abrin induced programmed necrosis in U266B1 cells. *Int J Biochem Cell Biol*. 2010 Dec;42(12):1993-2003.
- Borthakur G, Rosenblum MG, Talpaz M, Daver N, Ravandi F, Faderl S, Freireich EJ, Kadia T, Garcia-Manero G, Kantarjian H, Cortes JE. Phase 1 study of an anti-CD33 immunotoxin, humanized monoclonal antibody M195 conjugated to recombinant gelonin (HUM-195/rGEL), in patients with advanced myeloid malignancies. *Haematologica*. 2013 Feb;98(2):217-21.
- Cabanillas F. Purine nucleoside analogs in indolent non-Hodgkin's lymphoma. *Oncology (Williston Park)*. 2000 Jun;14(6 Suppl 2):13-5.
- Carzaniga R, Sinclair L, Fordham-Skelton AP, Harris N, Croy RRD. Cellular and subcellular distribution of saporins, type-1 ribosome-inactivating proteins in soapwort (*Saponaria officinalis* L.). *Planta*. 1994 ;194:461-470.
- Cho RJ, Campbell MJ. Transcription, genomes, function. *Trends Genet*. 16, 409–415 (2000).
- Countouriotis A, Moore TB, Sakamoto KM. Cell surface antigen and molecular targeting in the treatment of hematologic malignancies. *Stem Cells*.2002;20(3):215-29.

- Czuczman MS, Olejniczak S, Gowda A, Kotowski A, Binder A, Kaur H, Knight J, Starostik P, Deans J, Hernandez-Ilizaliturri FJ. Acquirement of rituximab resistance in lymphoma cell lines is associated with both global CD20 gene and protein down-regulation regulated at the pretranscriptional and posttranscriptional levels. *Clin Cancer Res.* 2008 Mar 1;14(5):1561-70.
- Daniels-Wells TR, Helguera G, Rodríguez JA, Leoh LS, Erb MA, Diamante G, Casero D, Pellegrini M, Martínez-Maza O, Penichet ML. Insights into the mechanism of cell death induced by saporin delivered into cancer cells by an antibody fusion protein targeting the transferrin receptor 1. *Toxicol In Vitro.* 2013 Feb;27(1):220-31.
- Das MK, Sharma RS, Mishra V. Induction of apoptosis by ribosome inactivating proteins: importance of N-glycosidase activity. *Appl Biochem Biotechnol.* 2012 Mar;166(6):1552-61.
- David J, Wilkinson LJ, Griffiths GD. Inflammatory gene expression in response to sub-lethal ricin exposure in Balb/c mice. *Toxicology.* 2009 Oct 1;264(1-2):119-30.
- Davis TA, Czerwinski DK, Levy R. Therapy of B-cell lymphoma with anti-CD20 antibodies can result in the loss of CD20 antigen expression. *Clin Cancer Res.* 1999 Mar;5(3):611-5.
- Derby L, Czuczman MS. Update on novel monoclonal antibodies and immunoconjugates for the treatment of lymphoproliferative disorders. *Future Oncol.* 2011 Aug;7(8):963-79.
- Dijoseph JF, Dougher MM, Armellino DC, Kalyandrug L, Kunz A, Boghaert ER, Hamann PR, Damle NK. CD20-specific antibody-targeted chemotherapy of non-Hodgkin's B-cell lymphoma using calicheamicin-conjugated rituximab. *Cancer Immunol Immunother.* 2007 Jul;56(7):1107-17.
- Endo Y, Mitsui K, Motizuki M, Tsurugi K. The mechanism of action of ricin and related toxic lectins on eukaryotic ribosomes. The site and the characteristics of the modification in 28 S ribosomal RNA caused by the toxins. *J Biol Chem.* 1987 Apr 25;262(12):5908-12.

European Cancer Observatory <http://eco.iarc.fr/EUCAN/>

- Fang EF, Zhang CZ, Wong JH, Shen JY, Li CH, Ng TB. The MAP30 protein from bitter melon (*Momordica charantia*) seeds promotes apoptosis in liver cancer cells in vitro and in vivo. *Cancer Lett.* 2012 Nov 1;324(1):66-74.
- Fellenberg K, Hauser NC, Brors B, Neutzner A, Hoheisel JD, et al. Correspondence analysis applied to microarray data. *Proc Natl Acad Sci U S A.* 2001;98:10781–10786.
- Ferreras JM, Citores L, Iglesias R, Jiménez P, Girbés T. Use of ribosome-inactivating proteins from sambucus for the construction of immunotoxins and conjugates for cancer therapy. *Toxins (Basel).* 2011 May;3(5):420-41.
- FitzGerald DJ, Wayne AS, Kreitman RJ, Pastan I. Treatment of hematologic malignancies with immunotoxins and antibody-drug conjugates. *Cancer Res.* 2011;71:6300–6309.
- Fracasso G, Stirpe F, Colombatti M. Ribosome-Inactivating Protein-Containing Conjugates for Therapeutic Use. In: Lord J.M., Hartley R.M., editors. *Toxic Plant Proteins, Plant Cell Monographs.* Springer-Verlag; Heidelberg, Berlin, German: 2010. pp. 225–263.
- Freudlsperger C, Thies A, Pfüller U, Schumacher U. The proteasome inhibitor bortezomib augments anti-proliferative effects of mistletoe lectin-I and the PPAR-gamma agonist rosiglitazone in human melanoma cells. *Anticancer Res.* 2007 Jan-Feb;27(1A):207-13.
- Furman RR, Grossbard ML, Johnson JL, Pecora AL, Cassileth PA, Jung SH, Peterson BA, Nadler LM, Freedman A, Bayer RL, Bartlett NL, Hurd DD, Cheson BD; Cancer Leukemia Group B; Eastern Cooperative Oncology Group. A phase III study of anti-B4-blocked ricin as adjuvant therapy post-autologous bone marrow transplant: CALGB 9254. *Leuk Lymphoma.* 2011 Apr;52(4):587-96.
- Garibal J, Hollville E, Renouf B, Tétaud C, Wiels J. Caspase-8-mediated cleavage of Bid and protein phosphatase 2A-mediated activation of Bax are necessary for Verotoxin-1-induced apoptosis in Burkitt's lymphoma cells. *Cell Signal.* 2010 Mar;22(3):467-75.

- Gilabert-Oriol R, Weng A, Mallinckrodt Bv, Melzig MF, Fuchs H, Thakur M. Immunotoxins constructed with ribosome-inactivating proteins and their enhancers: a lethal cocktail with tumor specific efficacy. *Curr Pharm Des.* 2014;20(42):6584-643.
- Girbés T, Ferreras JM, Arias FJ, Stirpe F. Description, distribution, activity and phylogenetic relationship of ribosome-inactivating proteins in plants, fungi and bacteria. *Mini Rev Med Chem.* 2004 Jun;4(5):461-76.
- Gonzalez TV, Farrant SA, Mantis NJ. Ricin induces IL-8 secretion from human monocyte/macrophages by activating the p38 MAP kinase pathway. *Mol Immunol.* 2006 Apr;43(11):1920-3.
- Gray JS, Bae HK, Li JC, Lau AS, Pestka JJ. Double-stranded RNA-activated protein kinase mediates induction of interleukin-8 expression by deoxynivalenol, Shiga toxin 1, and ricin in monocytes. *Toxicol Sci.* 2008 Oct;105(2):322-30.
- Guo N, Peng Z. (2013). MG132, a proteasome inhibitor, induces apoptosis in tumor cells. *Asia Pac. J. Clin. Oncol.* 9, 6-11.
- Han YH, Moon HJ, You BR, Park WH. (2009). The effect of MG132, a proteasome inhibitor on HeLa cells in relation to cell growth, reactive oxygen species and GSH. *Oncol. Rep.* 22, 215-221.
- Hale ML. Microtiter-based assay for evaluating the biological activity of ribosome-inactivating proteins. *Pharmacol Toxicol.* 2001 May;88(5):255-60.
- Hassan R, Miller AC, Sharon E, Thomas A, Reynolds JC, Ling A, Kreitman RJ, Miettinen MM, Steinberg SM, Fowler DH, Pastan I. Major cancer regressions in mesothelioma after treatment with an anti-mesothelin immunotoxin and immune suppression. *Sci Transl Med.* 2013 Oct 23;5(208):208ra147.
- Herrera L, Bostrom B, Gore L, Sandler E, Lew G, Schlegel PG, Aquino V, Ghetie V, Vitetta ES, Schindler J. A phase 1 study of Combotox in pediatric patients with refractory B-lineage acute lymphoblastic leukemia. *J Pediatr Hematol Oncol.* 2009 Dec;31(12):936-41.

- Higuchi S, Tamura T, Oda T. Cross-talk between the pathways leading to the induction of apoptosis and the secretion of tumor necrosis factor-alpha in ricin-treated RAW 264.7 cells. *J Biochem.* 2003 Dec;134(6):927-33.
- Horrix C, Raviv Z, Flescher E, Voss C, Berger MR. Plant ribosome-inactivating proteins type II induce the unfolded protein response in human cancer cells. *Cell Mol Life Sci.* 2011 Apr;68(7):1269-81.
- Hossann M, Li Z, Shi Y, Kreilinger U, Büttner J, Vogel PD, Yuan J, Wise JG, Trommer WE. Novel immunotoxin: a fusion protein consisting of gelonin and an acetylcholine receptor fragment as a potential immunotherapeutic agent for the treatment of Myasthenia gravis. *Protein Expr Purif.* 2006 Mar;46(1):73-84.
- Huang G, Shi LZ, Chi H. Regulation of JNK and p38 MAPK in the immune system: signal integration, propagation and termination. *Cytokine.* 2009 Dec;48(3):161-9.
- Hudak KA, Wang P, Tumer NE. A novel mechanism for inhibition of translation by pokeweed antiviral protein: depurination of the capped RNA template. *RNA.* 2000 Mar;6(3):369-80.
- Iordanov MS, Pribnow D, Magun JL, Dinh TH, Pearson JA, Chen SL, Magun BE. Ribotoxic stress response: activation of the stress-activated protein kinase JNK1 by inhibitors of the peptidyl transferase reaction and by sequence-specific RNA damage to the alpha-sarcin/ricin loop in the 28S rRNA. *Mol Cell Biol.* 1997 Jun;17(6):3373-81.
- Jandhyala DM, Ahluwalia A, Obrig T, Thorpe CM. ZAK: a MAP3Kinase that transduces Shiga toxin- and ricin-induced proinflammatory cytokine expression. *Cell Microbiol.* 2008 Jul;10(7):1468-77.
- Jandhyala DM, Thorpe CM, Magun B. Ricin and Shiga toxins: effects on host cell signal transduction. *Curr Top Microbiol Immunol.* 2012; 357:41-65.

- Jetzt AE, Cheng JS, Tumer NE, Cohick WS. Ricin A-chain requires c-Jun N-terminal kinase to induce apoptosis in nontransformed epithelial cells. *Int J Biochem Cell Biol.* 2009 Dec;41(12):2503-10.
- Johannes L, Popoff V. Tracing the retrograde route in protein trafficking. *Cell.* 2008 Dec 26;135(7):1175-87.
- Kato J, O'Donnell RT, Abuhay M, Tuscano JM. Efficacy and toxicity of a CD22-targeted antibody-saporin conjugate in a xenograft model of non-Hodgkin's lymphoma. *Oncoimmunology.* 2012 Dec 1;1(9):1469-1475.
- Kaur I, Gupta RC, Puri M. Ribosome inactivating proteins from plants inhibiting viruses. *Virol Sin.* 2011 Dec;26(6):357-65.
- Kim MS, Lee J, Lee KM, Yang SH, Choi S, Chung SY, Kim TY, Jeong WH, Park R. Involvement of hydrogen peroxide in mistletoe lectin-II-induced apoptosis of myeloleukemic U937 cells. *Life Sci.* 2003 Jul 25;73(10):1231-43.
- Korcheva V, Wong J, Corless C, Iordanov M, Magun B. Administration of ricin induces a severe inflammatory response via nonredundant stimulation of ERK, JNK, and P38 MAPK and provides a mouse model of hemolytic uremic syndrome. *Am. J. Pathol.* 2005;166:323–339.
- Korcheva V, Wong J, Lindauer M, Jacoby DB, Iordanov MS, Magun B. Role of apoptotic signaling pathways in regulation of inflammatory responses to ricin in primary murine macrophages.
- Krutzik PO, Nolan GP. Fluorescent cell barcoding in flow cytometry allows high-throughput drug screening and signaling profiling. *Nat Methods.* 2006;3(5):361–368.
- Lamkanfi M, Kanneganti TD, Van Damme P, Vanden Berghe T, Vanoverberghe I, Vandekerckhove J, Vandenabeele P, Gevaert K, Nunez G. Targeted peptide-centric proteomics reveals caspase-7 as a substrate of the caspase-1 inflammasomes. *Mol Cell Proteomics* 2008

- Leahy MF, Turner JH. Radioimmunotherapy of relapsed indolent non-Hodgkin lymphoma with 131I-rituximab in routine clinical practice: 10-year single-institution experience of 142 consecutive patients. *Blood*. 2011 Jan 6;117(1):45-52
- Lee SY, Lee MS, Cherla RP, Tesh VL. Shiga toxin 1 induces apoptosis through the endoplasmic reticulum stress response in human monocytic cells. *Cell Microbiol*. 2008 Mar;10(3):770-80.
- Li LN, Zhang HD, Zhi R, Yuan SJ. Down-regulation of some miRNAs by degrading their precursors contributes to anti-cancer effect of mistletoe lectin-I. *Br J Pharmacol*. 2011 Jan;162(2):349-64.
- Li X, Huang T, Jiang G, Gong W, Qian H, Zou C. (2013). Proteasome inhibitor MG132 enhances TRAIL-induced apoptosis and inhibits invasion of human osteosarcoma OS732 cells. *Biochem. Biophys. Res. Commun*. 439, 179-186.
- Lindauer M, Wong J, Magun B. Ricin Toxin Activates the NALP3 Inflammasome. *Toxins (Basel)*. 2010 Jun 1;2(6):1500-1514.
- Liu XY, Pop LM, Schindler J, Vitetta ES. Immunotoxins constructed with chimeric, short-lived anti-CD22 monoclonal antibodies induce less vascular leak without loss of cytotoxicity. *MAbs*. 2012 Jan-Feb;4(1):57-68.
- Lombardi A., Bursomanno S., Lopardo T., Traini R., Colombatti M., Ippoliti R., Flavell D.J., Flavell S.U., Ceriotti A., Fabbrini M.S. *Pichia. pastoris* as a host for secretion of toxic saporin chimeras. *FASEB J*. 2010;24:253–265.
- Lord JM, Roberts LM, Robertus JD. Ricin: structure, mode of action, and some current applications. *FASEB J*. 1994 Feb;8(2):201-8.
- Lukenbill J, Kalaycio M. Fludarabine: a review of the clear benefits and potential harms. *Leuk Res*. 2013 Sep;37(9):986-94.
- Madhumathi J, Verma RS. Therapeutic targets and recent advances in protein immunotoxins. *Curr Opin Microbiol*. 2012 Jun;15(3):300-9.

- Maloney DG. Anti-CD20 antibody therapy for B-cell lymphomas. *N Engl J Med.* 2012 May 24;366(21):2008-16
- Manoukian G, Hagemester F. Denileukin diftitox: a novel immunotoxin. *Expert Opin Biol Ther.* 2009 Nov;9(11):1445-51.
- Mansouri S, Choudhary G, Sarzala PM, Ratner L, Hudak KA. Suppression of human T-cell leukemia virus I gene expression by pokeweed antiviral protein. *J Biol Chem.* 2009 Nov 6;284(45):31453-62.
- Mariotti J, Taylor J, Massey PR, Ryan K, Foley J, Buxhoeveden N, Felizardo TC, Amarnath S, Mossoba ME, Fowler DH. The pentostatin plus cyclophosphamide nonmyeloablative regimen induces durable host T cell functional deficits and prevents murine marrow allograft rejection. *Biol Blood Marrow Transplant.* 2011 May;17(5):620-31.
- Martin SM, Churchill E, McKnight H, Mahaffey CM, Ma Y, O'Donnell RT, Tuscano JM. The HB22.7 Anti-CD22 monoclonal antibody enhances bortezomib-mediated lymphomacidal activity in a sequence dependent manner. *J Hematol Oncol.* 2011 Dec 1;4:49. doi: 10.1186/1756-8722-4-49.
- Mayfield S. Production of anti-cancer immunotoxins in algae: Ribosome inactivating proteins as fusion partners. *Biotechnol. Bioeng.* 2013;110:2826–2835.
- McGrath MS, Hwang KM, Caldwell SE, Gaston I, Luk KC, Wu P, Ng VL, Crowe S, Daniels J, Marsh J, et al. GLQ223: an inhibitor of human immunodeficiency virus replication in acutely and chronically infected cells of lymphocyte and mononuclear phagocyte lineage. *Proc Natl Acad Sci U S A.* 1989 Apr;86(8):2844-8.
- Melchior WB Jr, Tolleson WH. A functional quantitative polymerase chain reaction assay for ricin, Shiga toxin, and related ribosome-inactivating proteins. *Anal Biochem.* 2010 Jan 15;396(2):204-11.
- Mi H, Muruganujan A, Casagrande JT, Thomas PD. Large-scale gene function analysis with the PANTHER classification system. *Nat Protoc.* 2013 Aug;8(8):1551-66.

- Monti B, D'Alessandro C, Farini V, Bolognesi A, Polazzi E, Contestabile A, Stirpe F, Battelli MG. In vitro and in vivo toxicity of type 2 ribosome-inactivating proteins lanceolin and stenodactylin on glial and neuronal cells. *Neurotoxicology*. 2007 May;28(3):637-44.
- Mossoba ME, Onda M, Taylor J, Massey PR, Treadwell S, Sharon E, Hassan R, Pastan I, Fowler DH. Pentostatin plus cyclophosphamide safely and effectively prevents immunotoxin immunogenicity in murine hosts. *Clin Cancer Res*. 2011 Jun 1;17(11):3697-705.
- Nagai T, Tanaka M, Tsuneyoshi Y, Matsushita K, Sunahara N, Matsuda T, Yoshida H, Komiya S, Onda M, Matsuyama T. In vitro and in vivo efficacy of a recombinant immunotoxin against folate receptor beta on the activation and proliferation of rheumatoid arthritis synovial cells. *Arthritis Rheum*. 2006 Oct;54(10):3126-34.
- Nagai T, Kyo A, Hasui K, Takao S, Matsuyama T. Efficacy of an immunotoxin to folate receptor beta in the intra-articular treatment of antigen-induced arthritis. *Arthritis Res Ther*. 2012 May 2;14(3):R106.
- Narayanan S, Surendranath K, Bora N, Surolia A, Karande AA. Ribosome inactivating proteins and apoptosis. *FEBS Lett*. 2005 Feb 28;579(6):1324-31.
- Nicolson GL, Blaustein J, Etzler ME. Characterization of two plant lectins from *Ricinus communis* and their quantitative interaction with a murine lymphoma. *Biochemistry*. 1974 Jan 1;13(1):196-204.
- Nielsen K, Boston RS. RIBOSOME-INACTIVATING PROTEINS: A Plant Perspective. *Annu Rev Plant Physiol Plant Mol Biol*. 2001 Jun;52:785-816.
- Palanca-Wessels MC, Press OW. Advances in the treatment of hematologic malignancies using immunoconjugates. *Blood*. 2014 Apr 10;123(15):2293-301.
- Parikh BA, Tumer NE. Antiviral activity of ribosome inactivating proteins in medicine. *Mini Rev Med Chem*. 2004 Jun;4(5):523-43.

- Parikh BA, Baykal U, Di R, Tumer NE. Evidence for retro-translocation of pokeweed antiviral protein from endoplasmic reticulum into cytosol and separation of its activity on ribosomes from its activity on capped RNA. *Biochemistry*. 2005 Feb 22;44(7):2478-90.
- Pelosi E, Lubelli C, Polito L, Barbieri L, Bolognesi A, Stirpe F. Ribosome-inactivating proteins and other lectins from *Adenia* (Passifloraceae). *Toxicon*. 2005 Nov;46(6):658-63.
- Polito L, Bolognesi A, Tazzari PL, Farini V, Lubelli C, Zinzani PL, Ricci F, Stirpe F. The conjugate Rituximab/saporin-S6 completely inhibits clonogenic growth of CD20-expressing cells and produces a synergistic toxic effect with Fludarabine. *Leukemia*. 2004 Jul;18(7):1215-22.
- Polito L, Bortolotti M, Farini V, Battelli MG, Barbieri L, Bolognesi A. Saporin induces multiple death pathways in lymphoma cells with different intensity and timing as compared to ricin. *Int J Biochem Cell Biol*. 2009.
- Polito L, Bortolotti M, Farini V, Pedrazzi M, Tazzari PL, Bolognesi A. ATG-saporin-S6 immunotoxin: a new potent and selective drug to eliminate activated lymphocytes and lymphoma cells. *Br J Haematol*. 2009b Dec;147(5):710-8.
- Polito L, Bortolotti M, Pedrazzi M, Bolognesi A. Immunotoxins and other conjugates containing saporin-s6 for cancer therapy. *Toxins (Basel)*. 2011 Jun;3(6):697-720.
- Polito L, Bortolotti M, Mercatelli D, Battelli MG, Bolognesi A. Saporin-S6: a useful tool in cancer therapy. *Toxins (Basel)*. 2013 Oct 7;5(10):1698-722.
- Polito L, Bortolotti M, Mercatelli D, Mancuso R, Baruzzi G, Faedi W, Bolognesi A. Protein synthesis inhibition activity by strawberry tissue protein extracts during plant life cycle and under biotic and abiotic stresses. *Int J Mol Sci*. 2013b Jul 25;14(8):15532-45.
- Polito L, Mancuso R, Mercatelli D, Bortolotti M, Bolognesi A. mAbs targeting CD20 and other lymphocyte CD markers in lymphoma treatment. *Monoclonal*

- Antibodies in Oncology., London, Future Medicine, London, UK., 2013b, pp. 6-19
- Puri M, Kaur I, Perugini MA, Gupta RC. Ribosome-inactivating proteins: current status and biomedical applications. *Drug Discov Today*. 2012 Jul;17(13-14):774-83.
- Rao PV, Jayaraj R, Bhaskar AS, Kumar O, Bhattacharya R, Saxena P, Dash PK, Vijayaraghavan R. Mechanism of ricin-induced apoptosis in human cervical cancer cells. *Biochem Pharmacol*. 2005 Mar 1;69(5):855-65. Epub 2005 Jan 22.
- Ready MP, Brown DT, Robertus JD. Extracellular localization of pokeweed antiviral protein. *Proc Natl Acad Sci U S A*. 1986 Jul;83(14):5053-6.
- Sandvig K, van Deurs B. Delivery into cells: lessons learned from plant and bacterial toxins. *Gene Ther*. 2005 Jun;12(11):865-72.
- Saxena N, Rao PV, Bhaskar AS, Bhutia YD. Protective effects of certain pharmaceutical compounds against abrin induced cell death in Jurkat cell line. *Int Immunopharmacol*. 2014 Aug;21(2):412-25.
- Schep LJ, Temple WA, Butt GA, Beasley MD. Ricin as a weapon of mass terror-separating fact from fiction. *Environ Int*. 2009 Nov;35(8):1267-71.
- Schindler J, Gajavelli S, Ravandi F, Shen Y, Parekh S, Braunchweig I, Barta S, Ghetie V, Vitetta E, Verma A. A phase I study of a combination of anti-CD19 and anti-CD22 immunotoxins (Combotox) in adult patients with refractory B-lineage acute lymphoblastic leukaemia. *Br J Haematol*. 2011 Aug;154(4):471-6.
- Sharkey RM, Govindan SV, Cardillo TM, Goldenberg DM. Epratuzumab-SN-38: a new antibody-drug conjugate for the therapy of hematologic malignancies. *Mol Cancer Ther*. 2012 Jan;11(1):224-34.
- Shih SF, Wu YH, Hung CH, Yang HY, Lin JY. Abrin triggers cell death by inactivating a thiol-specific antioxidant protein. *J Biol Chem*. 2001 Jun 15;276(24):21870-7.

- Shi Y, Porter K, Parameswaran N, Bae HK, Pestka JJ. Role of GRP78/BiP degradation and ER stress in deoxynivalenol-induced interleukin-6 upregulation in the macrophage. *Toxicol Sci.* 2009 Jun;109(2):247-55.
- Siegel R, Ma J, Zou Z, Jemal A. Cancer statistics, 2014. *CA Cancer J Clin.* 2014 Jan-Feb;64(1):9-29.
- Sikriwal D, Batra JK. Ribosome inactivating proteins and apoptosis. In J. M. Lord & M. R. Hartley (Eds.), *Plant cell monographs 2010 (Toxic plant proteins, Vol. 18, pp. 107–132).*
- Smith WE, Kane AV, Campbell ST, Acheson DW, Cochran BH, Thorpe CM. Shiga toxin 1 triggers a ribotoxic stress response leading to p38 and JNK activation and induction of apoptosis in intestinal epithelial cells. *Infect Immun.* 2003 Mar;71(3):1497-504.
- Smolewski P, Duechler M, Linke A, Cebula B, Grzybowska-Izydorczyk O, Shehata M, Robak T. Additive cytotoxic effect of bortezomib in combination with anti-CD20 or anti-CD52 monoclonal antibodies on chronic lymphocytic leukemia cells. *Leuk Res.* 2006;30:1521–1529.
- Stirpe F. On the action of ribosome-inactivating proteins: are plant ribosomes species-specific? *Biochem J.* 1982 Jan 15;202(1):279-80.
- Stirpe F. Ribosome-inactivating proteins. *Toxicon.* 2004 Sep 15;44(4):371-83.
- Stirpe F. Ribosome-inactivating proteins: from toxins to useful proteins. *Toxicon.* 2013 Jun 1;67:12-6.
- Stirpe F, Bolognesi A, Bortolotti M, Farini V, Lubelli C, Pelosi E, Polito L, Dozza B, Strocchi P, Chambery A, Parente A, Barbieri L. Characterization of highly toxic type 2 ribosome-inactivating proteins from *Adenia lanceolata* and *Adenia stenodactyla* (Passifloraceae). *Toxicon.* 2007 Jul;50(1):94-105.
- Sullivan-Chang L, O'Donnell RT, Tuscano JM. Targeting CD22 in B-cell malignancies: current status and clinical outlook. *BioDrugs.* 2013 Aug;27(4):293-304.

- Suntres ZE, Stone WL, Smith MG. Ricin-induced toxicity: the role of oxidative stress. *J.MED. CBR.* 2005 Def/Volume 3.
- Tazzari PL, Polito L, Bolognesi A, Pistillo MP, Capanni P, Palmisano GL, Lemoli RM, Curti A, Biancone L, Camussi G, Conte R, Ferrara GB, Stirpe F. Immunotoxins containing recombinant anti-CTLA-4 single-chain fragment variable antibodies and saporin: in vitro results and in vivo effects in an acute rejection model. *J Immunol.* 2001 Oct 15;167(8):4222-9.
- Tortorella LL, Pipalia NH, Mukherjee S, Pastan I, Fitzgerald D, Maxfield FR. Efficiency of immunotoxin cytotoxicity is modulated by the intracellular itinerary. *PLoS One.* 2012;7(10):e47320.
- Tsai PC, Hernandez-Ilizaliturri FJ, Bangia N, Olejniczak SH, Czuczman MS. Regulation of CD20 in rituximab-resistant cell lines and B-cell non-Hodgkin lymphoma. *Clin Cancer Res.* 2012 Feb 15;18(4):1039-50.
- Tumer NE, Li XP. Interaction of ricin and Shiga toxins with ribosomes. *Curr Top Microbiol Immunol.* 2012;357:1-18. doi: 10.1007/82\_2011\_174.
- Tusher VG, Tibshirani R, Chu G. Significance analysis of microarrays applied to the ionizing radiation response. *Proc Natl Acad Sci U S A.* 2001;98:5116–5121.
- Uckun FM, Rajamohan F, Pendergrass S, Ozer Z, Waurzyniak B, Mao C. Structure-based design and engineering of a nontoxic recombinant pokeweed antiviral protein with potent anti-human immunodeficiency virus activity. *Antimicrob Agents Chemother.* 2003 Mar;47(3):1052-61.
- Vago R, Marsden CJ, Lord JM, Ippoliti R, Flavell DJ, Flavell SU, Ceriotti A, Fabbrini, MS. Saporin and ricin A chain follow different intracellular routes to enter the cytosol of intoxicated cells. *FEBS J.* 2005, 272, 4983–4995.
- Van Damme EJM, Hao Q, Chen Y, Barre A, Vandenbussche F, Desmyter S, Rougé P, Peumans WJ. Ribosome-inactivating proteins: a family of plant proteins that do more than inactivate ribosomes. *Crit Rev Palnt Sci.* 2001; 20:395-465.

- Wada T, Penninger JM. Mitogen-activated protein kinases in apoptosis regulation. *Oncogene*. 2004 Apr 12;23(16):2838-49.
- Wagner JY, Schwarz K, Schreiber S, Schmidt B, Wester HJ, Schwaiger M, Peschel C, von Schilling C, Scheidhauer K, Keller U. Myeloablative anti-CD20 radioimmunotherapy +/- high-dose chemotherapy followed by autologous stem cell support for relapsed/refractory B-cell lymphoma results in excellent long-term survival. *Oncotarget*. 2013 Jun;4(6):899-910.
- Wahome PG, Ahlawat S, Mantis NJ. Identification of small molecules that suppress ricin-induced stress-activated signaling pathways. *PLoS One*. 2012;7(11):e49075.
- Walker JA, Smith KGC. CD22: an inhibitory enigma. *Immunology*. 2008;123(3):314-25.
- Walsh MJ, Dodd JE, Hautbergue GM. Ribosome-inactivating proteins: potent poisons and molecular tools. *Virulence*. 2013 Nov 15;4(8):774-84.
- Wang D, Li Q, Hudson W, Berven E, Uckun F, Kersey JH. Generation and characterization of an anti-CD19 single-chain Fv immunotoxin composed of C-terminal disulfide-linked dgRTA. *Bioconj. Chem.* 1997;8:878-884.
- Wang H, Song S, Kou G, Li B, Zhang D, Hou S, Qian W, Dai J, Tian L, Zhao J, Guo Y. Treatment of hepatocellular carcinoma in a mouse xenograft model with an immunotoxin which is engineered to eliminate vascular leak syndrome. *Cancer Immunol Immunother.* 2007 Nov;56(11):1775-83.
- Wang H, Dai J, Li B, Fan K, Peng L, Zhang D, Cao Z, Qian W, Wang H, Zhao J, Guo Y. Expression, purification, and characterization of an immunotoxin containing a humanized anti-CD25 single-chain fragment variable antibody fused to a modified truncated *Pseudomonas* exotoxin A. *Protein Expr Purif.* 2008 Mar;58(1):140-7.
- Wang M, Han XH, Zhang L, Yang J, Qian JF, Shi YK, Kwak LW, Romaguera J, Yi Q. Bortezomib is synergistic with rituximab and cyclophosphamide in inducing

- apoptosis of mantle cell lymphoma cells in vitro and in vivo. *Leukemia*. 2008 Jan;22(1):179-85.
- Weldon JE, Xiang L, Zhang J, Beers R, Walker DA, Onda M, Hassan R, Pastan I. A recombinant immunotoxin against the tumor-associated antigen mesothelin reengineered for high activity, low off-target toxicity, and reduced antigenicity. *Mol Cancer Ther*. 2013 Jan;12(1):48-57.
- Weyergang A, Selbo PK, Berstad ME, Bostad M, Berg K. Photochemical internalization of tumor-targeted protein toxins. *Lasers Surg Med*. 2011 Sep;43(7):721-33.
- Wiley RG, Kline RH IV. Neuronal lesioning with axonally transported toxins. *J Neurosci Methods* 2000;103:73–82
- Wong J, Korcheva V, Jacoby DB, Magun BE. Proinflammatory responses of human airway cells to ricin involve stress-activated protein kinases and NF-kappaB. *Am J Physiol Lung Cell Mol Physiol*. 2007 Dec;293(6):L1385-94.
- Xu X, Yan H, Chen J, Zhang X. Bioactive proteins from mushrooms. *Biotechnol Adv*. 2011 Nov-Dec;29(6):667-74.
- Yadav RK, Chae SW, Kim HR, Chae HJ. Endoplasmic reticulum stress and cancer. *J Cancer Prev*. 2014 Jun;19(2):75-88.
- Yun H, Zhang HL, Wang HQ. Rituximab and bortezomib (RB): a new effective regimen for refractory or relapsed indolent lymphomas. *Med Oncol*. 2015 Jan;32(1):353.
- Zhang C, Gong Y, Ma H, An C, Chen D, Chen ZL. Reactive oxygen species involved in trichosanthin-induced apoptosis of human choriocarcinoma cells. *Biochem J*. 2001 May 1;355(Pt 3):653-61.
- Zhang B, Huang H, Xie J, Xu C, Chen M, Wang C, Yang A, Yin Q. Cucurmosin induces apoptosis of BxPC-3 human pancreatic cancer cells via inactivation of the EGFR signaling pathway. *Oncol Rep*. 2012 Mar;27(3):891-7.

Zhou HR, Lau AS, Pestka JJ. Role of double-stranded RNA-activated protein kinase R (PKR) in deoxynivalenol-induced ribotoxic stress response. *Toxicol Sci.* 2003 Aug;74(2):335-44.

Zhou HR, Jia Q, Pestka JJ. Ribotoxic stress response to the trichothecene deoxynivalenol in the macrophage involves the SRC family kinase Hck. *Toxicol Sci.* 2005 Jun;85(2):916-26.

Zhou HR, He K, Landgraf J, Pan X, Pestka JJ. Direct Activation of Ribosome-Associated Double-Stranded RNA-Dependent Protein Kinase (PKR) by Deoxynivalenol, Anisomycin and Ricin: A New Model for Ribotoxic Stress Response Induction. *Toxins (Basel).* 2014 Dec 16;6(12):340.

## ACKNOWLEDGEMENTS

My sincere gratitude goes to my supervisor Prof. Andrea Bolognesi for introducing me to the field of ribosome-inactivating proteins and antibody-based immunotargeted therapy. His expert scientific advice and knowledge has made the years in his lab very enjoyable. I am very grateful he let me join his group.

I would also like to thank Dr. Letizia Polito for all her help, support and for caring enough to take the time to mentor me and discuss scientific data.

A big thank you goes to my co-workers in Bologna, past and present, especially to Massimo for being a real friend and a valuable scientist.

Finally, I really want to thank Prof. Bjørn Tore Gjertsen for letting me participate to the activities of his amazing research group and for his enthusiasm, expert guidance and mentorship. All members of the Gjertsen-group are thanked for the making of a wonderful work environment and for being very good colleagues and friends.